ABSTRACT

Title of Document:	SELF-ASSEMBLY OF AMPHIPHILIC MOLECULES IN ORGANIC LIQUIDS
	Shih-Huang Tung, Doctor of Philosophy, 2007
Directed By:	Professor Srinivasa R. Raghavan, Department of Chemical and Biomolecular Engineering

Amphiphilic molecules are well-known for their ability to self-assemble in water to form structures such as micelles and vesicles. In comparison, much less is known about amphiphilic self-assembly in *nonpolar organic liquids*. Such "reverse" self-assembly can produce many of the counterparts to structures found in water. In this dissertation, we focus on the formation and dynamics of such reverse structures. We seek to obtain fundamental insight into the driving forces for reverse self-assembly processes. Three specific types of reverse structures are studied: (a) *reverse wormlike micelles*, i.e., long, flexible micellar chains; (b) *reverse vesicles*, i.e., hollow containers enclosed by reverse bilayers; and (c) *organogel networks*. While our focus is on the fundamentals, we note that reverse structures can be useful in a variety of applications ranging from drug delivery, controlled release, hosts for enzymatic reactions, and templates for nanomaterials synthesis.

In the first part of this study, we describe a new route for forming reverse wormlike micelles in nonpolar organic liquids. This route involves the addition of trace amounts of a *bile salt* to solutions of the phospholipid, lecithin. We show that bile salts, due to their unique "facially amphiphilic" structure, can promote the aggregation of

lecithin molecules into these reverse micellar chains. The resulting samples are viscoelastic and show interesting rheological properties. Unusual trends are seen in the temperature dependence of their rheology, which indicates the importance of hydrogen-bonding interactions in the formation of these micelles. Another remarkable feature of their rheology is the presence of strain-stiffening, where the material becomes stiffer at high deformations. Strain-stiffening has been seen before for elastic gels of biopolymers; here, we demonstrate the same properties for viscoelastic micellar solutions.

The second reverse aggregate we deal with is the reverse vesicle. We present a new route for forming stable unilamellar reverse vesicles, and this involves mixing short- and long-chain lipids (lecithins) with a trace of sodium chloride. The ratio of the short to long-chain lipid controls the type and size of self-assembled structure formed, and as this ratio is increased, a transition from reverse micelles to vesicles occurs. The structural changes can be explained in terms of molecular geometry, with the sodium chloride acting as a "glue" in binding lipid headgroups together through electrostatic interactions.

The final part of this dissertation focuses on organogels. The two-tailed anionic surfactant, AOT, is well-known to form spherical reverse micelles in organic solvents. We have found that trace amounts (e.g., less than 1 mM) of the dihydroxy bile salt, sodium deoxycholate (SDC) can transform these dilute micellar solutions into self-supporting, transparent organogels. The structure and rheology of these organogels is reminiscent of the self-assembled networks formed by proteins such as actin in water. The organogels are based on networks of long, rigid, cylindrical filaments, with SDC molecules stacked together in the filament core.

SELF-ASSEMBLY OF AMPHIPHILIC MOLECULES IN ORGANIC LIQUIDS

By

Shih-Huang Tung

Dissertation submitted to the Faculty of the Graduate School of the
University of Maryland, College Park, in partial fulfillment
of the requirements for the degree of
Doctor of Philosophy
2007

Advisory Committee:
Prof. Srinivasa R. Raghavan, Dept. of Chemical and Biomolecular Engineering, Chair
Prof. Sandra C. Greer, Dept. of Chemical and Biomolecular Engineering
Prof. Mikhail Anisimov, Dept. of Chemical and Biomolecular Engineering
Prof. Robert M. Briber, Dept. of Materials Science and Engineering
Prof. Douglas S. English, Dept. of Chemistry and Biochemistry

This dissertation is dedicated to my parents, Ching-Tzuen Tung and Shiau Shiou Tung, whose support and encouragement made this all possible…

ACKNOWLEDGEMENTS

I would first like to thank my advisor, Dr. Srinivasa Raghavan, for his unlimited advice and support. He led me into a fascinating scientific world and gave me a space that allowed me to devote myself to research without interference. The many improvements in my knowledge and in my writing and presentation skills can be attributed to his guidance.

I would also like to thank Dr. Greer, Dr. Anisimov, Dr. Briber, and Dr. English for serving on my committee and providing me with valuable suggestions and corrections that have greatly enhanced the quality of my dissertation. Illuminating discussions with Dr. Steve Kline (NIST) on SANS modeling and with Dr. Lionel Porcar (NIST) on strain-stiffening are acknowledged. I would like to thank Yi-En (Andy) Huang, an undergraduate student who has been working with me on this project throughout the past four years. Additionally, I would like to acknowledge Li-Chung Lai for his assistance in TEM experiments.

I am grateful to all of my group colleagues who have enriched my graduate experiences: Jae-Ho Lee, Bani Cipriano, Aimee Ketner, Hee-Young Lee, Rakesh Kumar, Matt Dowling, Chao Zhu, Oluwatosin Ogunsola, Peter Thomas, Kunshan Sun, George Chacko, Khyati Tiwari, Alex Nowodazkij, and Gabrielle Galvez. I would like to thank them for their many insightful discussions of my studies and the organization of various recreational activities that have brought my lab life lots of joy. I would also like to thanks several people for their support and encouragement, including Dr. I-Hsiang Tseng, Chi-

Wei Hung, Dr. Chen-Yu Tsao, Ta-I Yang, and Hsuan-Chen Wu. Their company has made my time in the USA delightful, and has given me the courage to overcome many difficulties. I could not have done this without them.

Finally, we would like to acknowledge NIST for facilitating the SANS experiments. This work was partially funded by grants from NIST BFRL, NIST EEEL and Du Pont.

TABLE OF CONTENTS

LIST OF TABLES

LIST OF FIGURES

Chapter 1

INTRODUCTION AND OVERVIEW

1.1. PROBLEM DESCRIPTION AND MOTIVATION

This dissertation is focused on the self-assembly of amphiphiles (molecules with both hydrophilic and hydrophobic parts) into reverse structures. The term "reverse" refers to the type of structure formed by amphiphiles in nonpolar organic solvents ("oils") in which the molecules are packed in a way opposite to that of "normal" aggregates found in water. Specifically, the hydrophilic heads of the amphiphiles are hidden in the core of reverse structures, while the hydrophobic tails are directed outward and thereby in contact with the nonpolar oil phase. The most common type of reverse aggregates is the reverse micelle, which tends to be either spherical or cylindrical in structure. Reverse micelles have been investigated for a variety of applications due to their unusual structure and properties. For example, hydrophilic drugs can be solubilized in the hydrophilic core of reverse micelles, and the micelles can thus be used as drug delivery vehicles.[1-3] Reverse micelles can also encapsulate enzymes, and these enzymes can efficiently catalyze reactions of oil-soluble substrates.[4-6]

Although reverse micelles have been studied for decades, much less is known about these systems compared to normal micelles. Most studies dealing with reverse micelles have focused on only two systems, lecithin/water/oil[7-12] and AOT/water/oil.[13-15] Lecithin is a zwitterionic phospholipid, while sodium bis(2-ethylhexyl) sulfo-succinate

(AOT) is a two-tailed anionic amphiphile (Figure 1.1). Both these molecules form reverse spherical micelles when added to oil. When a small quantity of water is added, the reverse micelles either transform their shape to cylindrical structures or form water-in-oil microemulsions. In the lecithin/oil system, the added water causes the reverse micelles to grow into very long and flexible cylindrical chains, which are referred to as reverse wormlike micelles.[8,11] These worms are very much like polymer chains, and they tend to entangle with each other and thereby impart high viscosity to the fluid.

Apart from the lecithin/water/oil and AOT/water/oil systems, there are few other examples of reverse micelles and especially reverse wormlike micelles or reverse vesicles in the literature.[16-19] This raises several important questions – for example, what role does water play in the growth of reverse micelles, i.e., what is so unique about water in this context? Are there other additives that are capable of inducing reverse micellar growth or reverse bilayer formation? What are the general rules that control the assembly of reverse aggregates? Can we formulate such general rules based on amphiphile geometry in much the same way as is possible with normal self-assembled structures? These are the questions that we will seek to answer in the present study. Our ultimate goal is to gain a better fundamental understanding of reverse self-assembly processes.

1.2. OUR APPROACH

In this dissertation, we report new routes for forming three types of reverse aggregates: reverse wormlike micelles, reverse vesicles, and organogels. The first two are lecithin-based systems while the third is AOT-based. These systems are depicted in

Figure 1.1 and briefly described below. In the process of discovering these new routes, we have used certain additives, such as *bile salts* and *short-chain lipids*, that have been previously studied in combination with lecithin in water, but never in organic solvents. Together our studies provide much new insight into reverse self-assembly processes. The principal techniques we have used are rheology to study the macroscopic flow properties and small-angle neutron scattering (SANS) to probe the nanostructure. Details on these techniques, including modeling of SANS data, are given in Chapter 2.

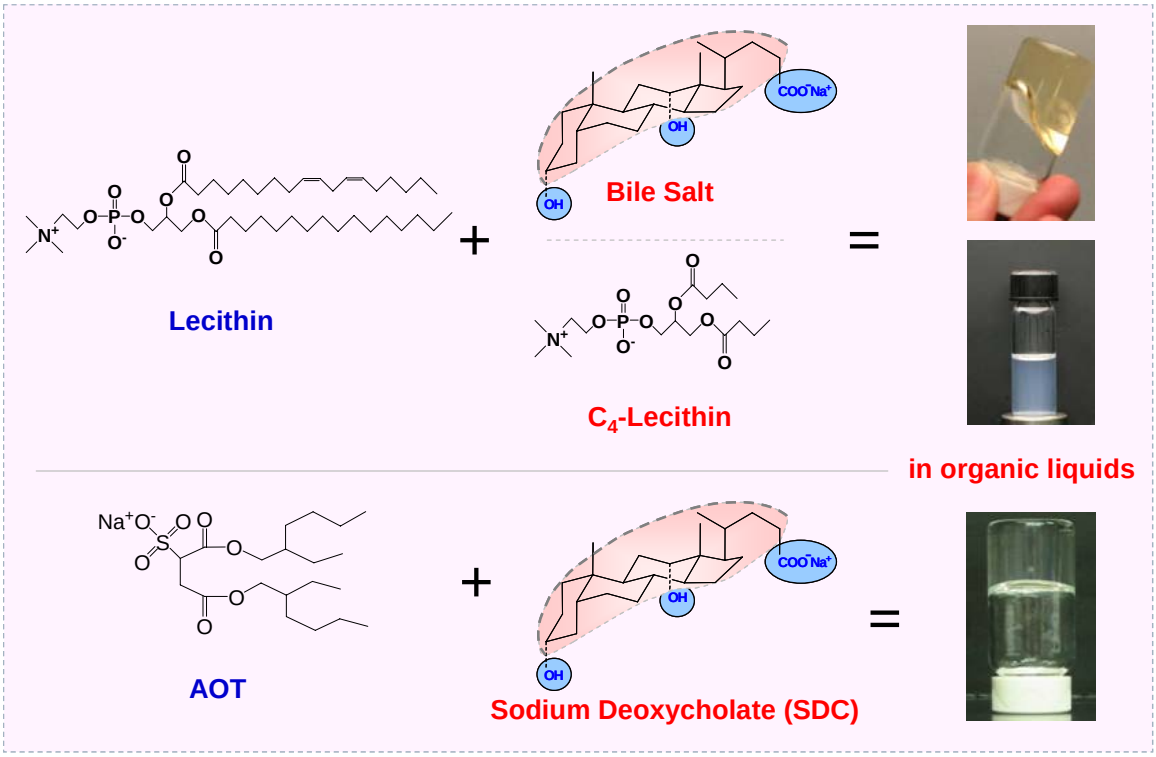

Figure 1.1. Amphiphilic systems investigated in this dissertation in the context of reverse self-assembly. A two-tailed amphiphile, such as lecithin or AOT is combined with a second amphiphilic additive, such as a *bile salt* or a short-chain lipid and added to a nonpolar organic liquid like cyclohexane. The result is to transform the sample into either a viscoelastic liquid containing **reverse wormlike micelles** (top vial), a solution of **reverse vesicles** that is bluish due to light scattering (middle vial) or an **organogel network** that can withstand its weight upon vial inversion (bottom vial).

1.2.1. Reverse Wormlike Micelles

The impetus for this work was provided by an unexpected discovery in our lab that *bile salts* can play a similar role to water in the growth of reverse wormlike micelles and can thus give rise to viscoelastic fluids (Figure 1.1). Bile salts are amphiphiles that are synthesized in the body within the liver. Unlike conventional amphiphiles that have a hydrophilic head and a hydrophobic tail or tails, bile salts are *facial amphiphiles* and have polar and non-polar faces (Figure 1.1).[20] Further details about bile salts are discussed in Chapter 2. In Chapter 3, we will present a detailed study on reverse wormlike micelles of lecithin and bile salt.

Reverse worms are very similar to "normal" worms that can be formed in water, and the rheological properties of the two types of worms are quite analogous. However, our studies indicate a key difference between normal and reverse worms with respect to how their rheological properties change upon heating. We believe that the different temperature effects gives crucial insight into the different mechanisms for the formation of these two structures, and this will be elaborated in Chapter 4.

The phenomenon of strain-stiffening or strain-hardening refers to an increase in the elastic modulus (stiffness) of a material with increasing strain amplitude. While this response is exhibited by many biological materials, including gels of biopolymers such as actin, it is rarely seen in other types of soft matter. In Chapter 5, we report an unusual strain-stiffening in the reverse wormlike micelles of lecithin and bile salt. We will

suggest a mechanism to explain the strain-stiffening that is different from the present theories for biopolymers.

1.2.2. Reverse Vesicles

Vesicles are liquid-filled containers formed in water by phospholipids and have been studied in great detail.[21] However, counterparts to these structures in oil, called "reverse vesicles" are still relatively unknown. Currently, there are no systematic rules or guidelines for the formation of reverse vesicles. We have discovered that it is possible for certain phospholipid mixtures to form reverse vesicles in organic solvents. In this case, one lipid must have a long tail while the second needs to be of a much shorter tail length. When these lipids are mixed into an organic solvent like cyclohexane, a variety of microstructures arise, starting with reverse spheres, then reverse cylinders, and finally reverse vesicles (bilayers). Interestingly, we have to add salts, such as sodium chloride, into the solution to stabilize the vesicles. This work will be detailed in Chapter 6.

1.2.3. Organogel Networks

In addition to lecithin-based systems, we have also performed experiments with a different type of double-tailed anionic surfactant, viz. AOT. In this case, we have discovered that the combination of AOT with a specific bile salt, sodium deoxycholate (SDC) results in organogels, i.e., samples that can support their weight in a vial (Figure 1.1). Interestingly, very low amounts of AOT and SDC are enough to form an organogel, e.g., 5 mM of AOT + 1 mM or less of SDC. The structure of the organogel consists of rather rigid filaments of AOT-SDC that are entangled into a network. This work is

described in Chapter 7. AOT-SDC organogels have many similarities with aqueous gels of biopolymers such as actin. We make this connection explicitly in Chapter 7, and this further underscores the importance of studying these organogel systems.

1.3. SIGNIFICANCE OF THIS WORK

The studies described in this dissertation are potentially significant from both scientific and practical standpoints. Firstly, from a scientific viewpoint, we provide useful, general guidelines for controlling reverse self-assembly processes. It is well known that the driving force for the self-assembly in water is the hydrophobic effect, which, however, is not a factor in non-polar liquids. Instead, our work suggests that hydrogen bonding and electrostatic interactions may be the important interactions in reverse self-assembly. Although the driving forces are different, the net geometry of amphiphiles is still the dominant factor controlling self-assembly in both aqueous and organic liquids. This knowledge could lead to new fundamental interest in this field.

Secondly, regarding the applications of the reverse systems we have discovered, the new reverse wormlike micelles based on bile salt could find application as hosts for enzymes or biomolecules. This system may offer some advantages for such applications because it does not involve the addition of water. As for the reverse vesicles, due to their ability to encapsulate hydrophobic solutes and release these in a slow manner, they can serve as controlled-release carriers, such as for drug delivery.

Thirdly, for the first time, we have studied certain molecules (e.g., bile salts) in non-aqueous media, even though these are insoluble in the media. The key to these studies has been our sample preparation using a co-precipitation method that pre-mixes soluble components (such as lecithin) and insoluble components (such as bile salt). This ensures that the insoluble components can be solubilized due to their affinity with the soluble components. We expect that others will use our method to explore new molecular combinations in nonpolar systems. In particular, nonpolar solvents may provide a platform to study certain interactions occurring in biological systems that may be disturbed by the presence of water (e.g., between lipids and metal ions).

Lastly, our studies could provide insight into biological materials or processes. Our synthetic organogels of AOT/SDC share many properties with biopolymer gels, and may prove to be a good model system for fundamental studies. Our investigations may also improve our understanding of strain-stiffening, a property hitherto associated with biological materials and believed to have physiological utility, such as to prevent the rupture of tissues from large deformation. Also, our studies of reverse aggregates based on bile salts could provide insight into self-assembly processes occurring in physiological fluids involving lecithin, bile salt, and non-polar substances such as fats or fatty acids.

Chapter 2

BACKGROUND

This proposal is concerned with "reverse" self-assembly in organic liquids. In this chapter, we discuss both "normal" and "reverse" self-assembly and we describe some of the structures that can be formed by self-assembly. We then describe the techniques that we will use to study these types of structures, such as rheology and small-angle neutron scattering (SANS).

2.1. SELF-ASSEMBLY OF AMPHIPHILES: NORMAL AND REVERSE

Amphiphilic molecules (also referred to as surfactants, detergents, or lipids) are molecules with distinct hydrophilic and hydrophobic portions. Figure 2.1 depicts these molecules with hydrophilic heads, shown in blue and hydrophobic tails, shown in red. Many kinds of amphiphilic molecules when added to water, can spontaneously organize into structures called micelles. The process of spontaneous organization is referred to as self-assembly and it is governed by thermodynamics, i.e., it occurs because the system minimizes its Gibbs free energy in the process. Micelle formation occurs only beyond a critical concentration of the amphiphile, referred to as the critical micelle concentration or CMC. The driving force for micellization is the gain in entropy of water molecules when surfactant hydrophobes are buried in a micelle; this aspect is referred to as the hydrophobic effect.

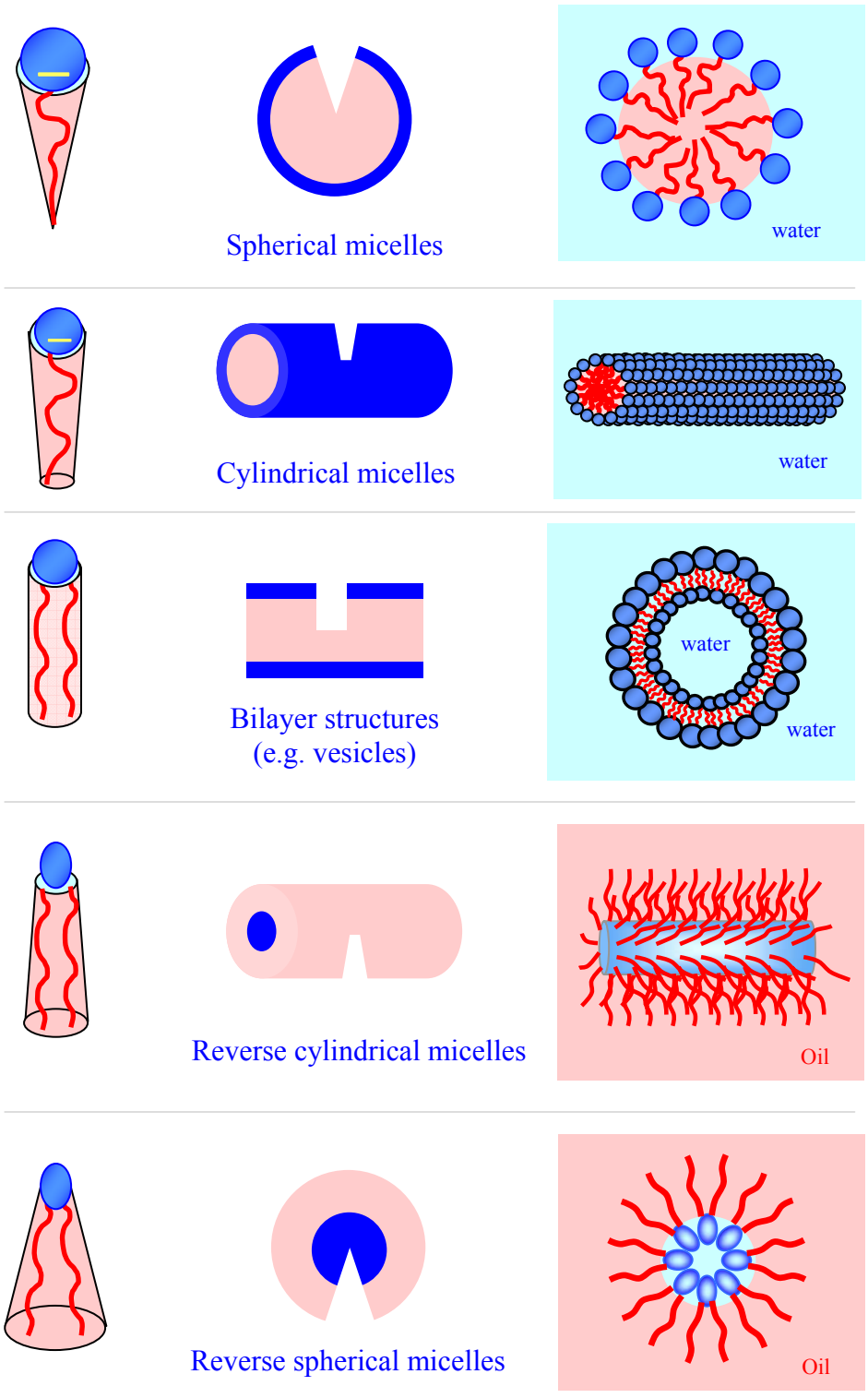

Figure 2.1. Schematics showing the connection between the self-assembled structures formed by amphiphiles in water and oil with the effective geometry of the amphiphilic molecules. The amphiphiles are depicted with hydrophilic heads, shown in blue and hydrophobic tails, shown in red.

Several different shapes are possible for micelles, including spheres, cylinders, and prolate or oblate ellipsoids. In the absence of any particular restrictions, spheres would always be favored thermodynamically over other shapes. Apart from micelles, a variety of other shapes are possible for self-assembled aggregates. Aggregate shape can be rationalized based on the net geometry of the amphiphilic molecules using a term called the critical packing parameter or CPP, which is defined as follows:[22]

$$\text{CPP} = \frac{a_{\text{tail}}}{a_{\text{hg}}} \tag{2.1}$$

where a_{hg} is the effective area of the amphiphile headgroup and a_{tail} is the average area of the amphiphilic tail. The larger the headgroup area compared to the tail area, the more curved the aggregate, as shown in Figure 2.1. Thus, a CPP of ⅓, corresponding to a cone shape, leads to spherical micelles in water while a CPP of ½ (truncated cone) corresponds to cylindrical micelles in water. Finally, molecules shaped like cylinders, i.e., having $a_{\text{tail}} \approx a_{\text{hg}}$ and CPP = 1, tend to assemble into bilayer structures (vesicles) in water.

Although self-assembly is commonly thought to be a process that occurs in water, it can also occur in a variety of other liquids. Generally, for amphiphilic molecules to self-assemble, the liquid must be either highly polar or highly non-polar. In highly polar liquids, micellar structures similar to those in water are formed. Self-assembly can also occur in highly non-polar liquids and this corresponds to CPP values greater than 1. Working from the bottom in Figure 2.1, we see that if the molecules have a large tail area and a small headgroup area, the CPP will be much greater than 1, and the molecules will form reverse spherical micelles. The term reverse refers to the different geometry of these

micelles compared to those in water. In a reverse micelle, the hydrophilic heads are buried in the interior and thus shielded from the oil phase, whereas the hydrophobic tails are extended into the oil. A slight reduction in CPP to values closer to 1 can drive a transition from reverse spherical micelles to reverse cylindrical micelles. Both normal and reverse cylinders are discussed in the next section.

2.2. WORMLIKE MICELLES: NORMAL AND REVERSE

Cylindrical micelles can grow to become very long, flexible chains and these are then called "wormlike" or "threadlike" or polymer-like micelles. The structure of normal wormlike micelles (in water) is shown in Figure 2.2. Such micelles can be formed by a variety of surfactants, including cationic, anionic, nonionic, and zwitterionic.[23] In the case of ionic surfactants, wormlike micelles are typically induced by adding salt to the solution. The added salt screens the ionic repulsions between the surfactant headgroups, reducing the headgroup area, and increasing the CPP from ⅓ to ½. This reduction in CPP promotes the growth of cylinders at the expense of spheres. In the case of cationic surfactants, which have been studied the most, the growth of worms can by induced by both simple salts (e.g., sodium chloride) as well as salts with aromatic counterions (e.g., sodium salicylate, NaSal).[23,24] The aromatic salts tend to be especially effective because their counterions bind to the surface of the micelles and thereby reduce the surface charge. As a result, these salts promote micellar growth at very low concentrations, i.e., at salt:surfactant molar ratios much less than one.

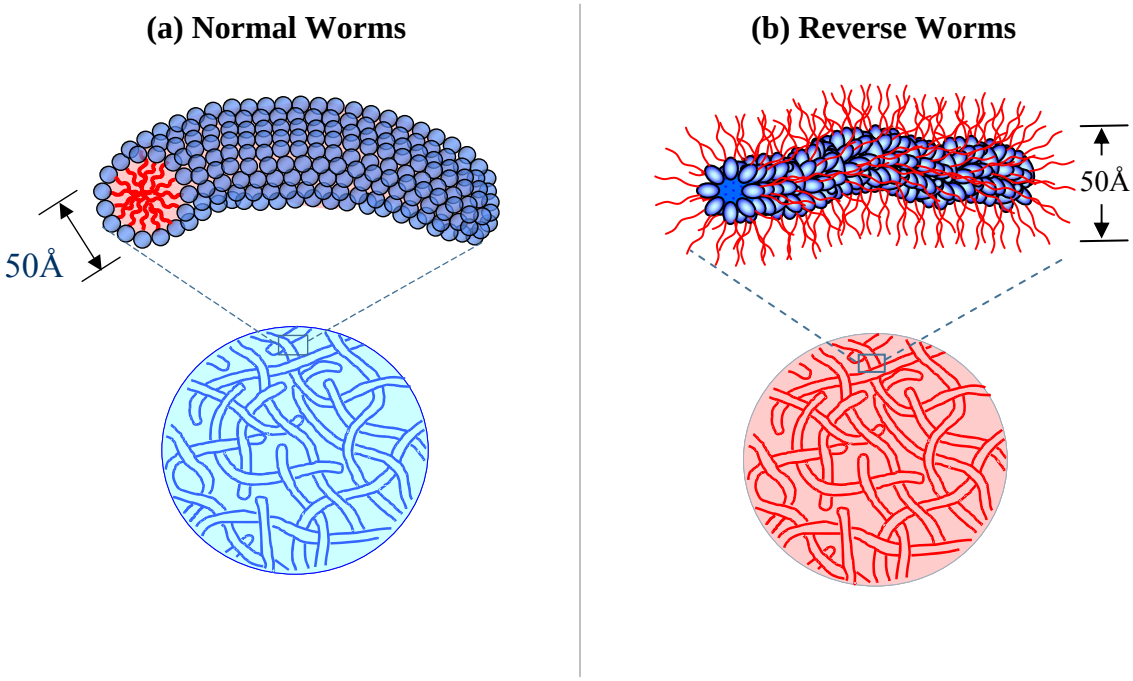

Figure 2.2. Structure of (a) normal wormlike micelles and (b) reverse wormlike micelles. In each case, the structure of an individual micelle as well as the entanglement of micellar chains into transient networks are shown.

Analagous to normal wormlike micelles in water, it is also possible to form reverse wormlike micelles in oil. Figure 2.2b shows the reverse structure of these micelles, with the red tails of the amphiphiles directed outward and the blue heads inward. While normal worms can be formed by a variety of surfactants, reverse worms have been reported only in a few systems,[8,16-19] most of which are based on the phospholipid, lecithin. When added to nonpolar solvents like alkanes or cycloalkanes, lecithin alone tends to form reverse spherical micelles, but when a small amount of water or a highly polar solvent is added, the spheres grow axially to become reverse worms.[8] Many studies have tried to elucidate the role of water in reverse micellar growth.[25,26] Water is believed to bridge the lecithin molecules by forming hydrogen bonds with the headgroup of lecithin. In other word, hydrogen bonds are the driving force for the formation of reverse

worms. From a geometric standpoint, the role of water is to expand the headgroup area of lecithin and thereby increase the CPP, which in turn causes the sphere to cylinder transition.

Wormlike micelles, both normal and reverse, are similar to polymeric chains and tend to become entangled in solution.[23] The entanglement leads to a transient network of chains (Figure 2.2) and this makes the micellar solution highly viscous and viscoelastic. However, unlike polymer chains that are held by strong covalent bonds, wormlike micelles are "equilibrium polymers", i.e., they break and recombine at a rapid rate. The competition between micellar breaking and chain reptation dictates the rheology of the fluid. If the breaking time τ_B is much lower than the reptation time τ_{rep}, the sample rheology becomes very simple and well-defined, with just a single relaxation time whose value is the geometric mean of τ_B and τ_{rep}.[27] The sample can then be described as a single-relaxation-time Maxwell fluid.

Another characteristic property of wormlike micellar fluids is their flow birefringence. That is, when a wormlike micellar solution placed in a vial is shaken lightly and observed under crossed polarizers, one observes bright streaks of light in the sample. These streaks emerge because the micellar chains tend to become aligned when sheared, thus making the sample anisotropic. Birefringence, which refers to a difference in refractive indices along mutually perpendicular directions, is a characteristic property of anisotropic materials like liquid crystals. Note that wormlike micelles do not exhibit birefringence at rest, but only when subjected to flow or shear.

2.3. VESICLES: NORMAL AND REVERSE

Vesicles are self-assembled capsules formed by amphiphilic molecules in water by lipids, surfactants, or block copolymers.[21,28] The shell of the vesicle can be considered to be the folding of amphiphilic bilayers, as shown in Figure 2.3a. The amphiphiles that tend to form bilayers have a CPP ~ 1, i.e. the shape of these molecules resembles that of a cylinder (Figure 2.2). The folding of bilayers into vesicles tends to occur only when the bilayers are present at low concentration; at high concentrations, bilayers form a lamellar phase.[29] The tendency for bilayers to fold is driven by a desire to minimize contact of the hydrophobes with water at the bilayer ends. Also, the formation of many vesicles from a single extended bilayer sheet increases the entropy of the system. Vesicles with only a single bilayer (or lamella) are called unilamellar vesicles (ULVs), while those with several concentric bilayers are called multilamellar vesicles (MLVs). The term "liposome" is sometimes used to refer to MLVs formed from lipids.

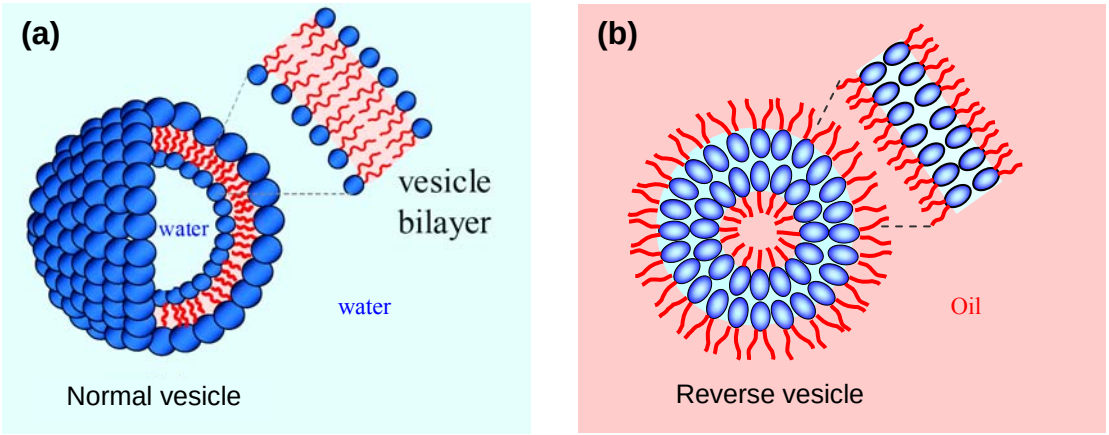

Figure 2.3. The structures of (a) normal vesicles and (b) reverse vesicles. The vesicles is formed by the folding of an amphiphilic bilayer that is about 2-5 nm in thickness.

In “normal” vesicles, i.e., vesicles formed in water, the hydrophilic heads of the amphiphiles are on both sides of the bilayer and thereby exposed to water, while the hydrophobic tails inside the bilayer are shielded from water (Figure 2.3). Analogous to the relationship between normal and reverse worms, the counterparts of normal vesicles in oil are also possible, and those are called reverse vesicles. Figure 2.3b shows the structures of reverse vesicles, with the red tails of the amphiphiles directed outward and inward to contact with the oil phase, while the blue (hydrophilic) heads are buried in the reverse bilayer. Only a few reverse vesicular systems have been reported, including those from polyoxyethylene ethers,[30] phospholipids,[31] amino acid derivatives,[32] sucrose esters,[33] and metallo-surfactans.[34] Most of these reverse vesicles are unstable, multilamellar and have a size in the micrometer range. In one study, reverse vesicles formed by sucrose esters in silicon oil have been shown to be effective for encapsulating *p*-aminobenzoic acid and cholesterol. However, reverse vesicles do not find wide use at the moment, and there is still a lack of a general framework for their formation.

2.4. SELF-ASSEMBLED ORGANOGELS

The term “gel” refers to a material with a network of subunits connected to each other by either chemical or physical bonds. Gels have the mechanical characteristics of solids, even though they are structurally disordered and may contain high volume fractions of liquid within their networks (the liquids are entrapped due to surface tension and capillary forces). Depending on the nature of the network bonds, one can distinguish between chemical gels (covalent bonds) and physical gels (weak, physical bonds). Our

interest in the context of this proposal is in physical gels that can be formed in organic solvents by the self-assembly of small molecules. Often, the bonds in these gel networks can be broken by heating and recovered by cooling, i.e., the gels are thermoreversible. The network in organogels often has a fibrillar nature (Figure 2.4), and the term "self-assembled fibrillar network" or SAFIN has been coined for such systems. Note that these networks are "permanent", meaning that the material will behave as a true solid and not relax with time; in contrast, a network of wormlike micelles is a transient one, so that the corresponding fluid will be viscoleastic, not elastic, and will relax at long timescales.

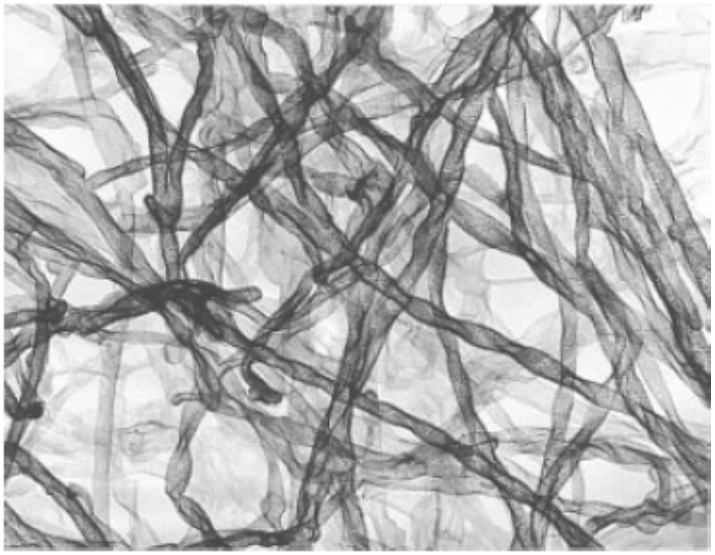

Figure 2.4. Electron micrograph of a gel of cholesteryl 4-(2-anthryloxy)butanoate (**CAB**) in 2-octanol. The fibrils in the gel each have a diameter of about 17 nm.[35]

A surprising variety of small, organic molecules can form organogels, including steroids, organometallic complexes, alkylamide derivatives, and fatty acids.[35] The diversity of such "organogelators" suggests that a wide range of physical interaction

forces may act as driving forces for gelation. Examples of such interactions are hydrogen bonds, metal coordination bonds, electrostatic bonds, van der Waals forces, and hydrophobic interactions.[35] Among the types of systems that give rise to fibrillar organogels are some that involve amphiphilic molecules such as AOT. While AOT alone forms reverse spherical micelles in organic liquids, the addition of molecules such as *p*-cresol or *p*-ethylphenol transforms the sample into an organogel.[36-38] It is believed that hydrogen bonds between the AOT and the additive lead to fibril formation, which in turn connect to form a network.

2.5. BIOMOLECULAR AMPHIPHILES: LIPIDS AND BILE SALTS

As mentioned in the Introduction, the reverse self-assembled systems we are studying involve two types of biological amphiphiles, viz. lipids and bile salts. Lipids are the constituents of biological membranes, a bilayer at the periphery of cells that regulates the passage of polar molecules and ions into the cell. Membrane lipids tend to have a CPP close to 1 due to their bulky hydrophobic tails, which is why these molecules self-organize into bilayer membranes. The most abundant membrane lipids are phospholipids, glycolipids and archaebacterial ether lipids. All of these have a glycerol or sphingosine as backbones that are attached by one or more long-chain alkyl tails and a hydrophilic headgroup. Lecithin, i.e. phosphatidylcholine (Figure 1.1), is a type of glycero-phospholipid that has a choline group joined to the glycerol backbone through a phosphodiester bond. Lecithin is electrically neutral but has a positive charge on the

choline group and a negative charge on the phosphate, thus forming a zwitterion. Lecithin is usually isolated from either egg yolk or soy beans.

Bile salts are physiological surfactants that are involved in the digestion of fat in the intestine and also facilitate the excretion of cholesterol.[20,39] The common feature in the chemical structure of bile salts is a characteristic steroid structure with a rigid, nonplanar, fused-ring and a carboxylic acid group that may be conjugated with amino acids such as taurine and glycine. Different bile salts contain different numbers (one to three) and positions of hydroxyl groups attached to these rings. Since the hydroxyl groups lie on the same side of the ring, bile salts are an unusual class of "facial amphiphiles" with hydrophilic and hydrophobic faces (Figure 1.1) that are different from regular surfactants with hydrophilic heads and hydrophobic tails.[20] Due to this facial structure, bile salts alone in aqueous solution form unusual micelles in which molecules are packed back-to-back with a small aggregation number (4-10).[40]

The average composition of normal human gallbladder bile is about 84% water, 11.5% bile salts, 3% lecithin, 0.5% cholesterol and 1% of other components.[39] Since bile salts and lecithin are the main components involved in the physiological function of bile, much effort has focused on the mixed micelles of bile salt and lecithin, and their function in the digestive process. Evidence from light,[41] small-angle neutron scattering,[42] and HPLC[43] techniques have shown that bile salts and lecithin tend to aggregate into rodlike micelles in water at certain lecithin/bile salt ratio and concentration.

2.6. CHARACTERIZATION TECHNIQUES

2.6.1. Rheology

Rheology is formally defined as the study of flow and deformation in materials.[44] Rheological measurements provide important information on soft materials, specifically on the relation between microstructure and macroscopic properties. These measurements are typically performed under steady or dynamic shear. In steady shear, the sample is subjected to a constant shear-rate $\dot{\gamma}$ (e.g. by applying a continuous rotation at a fixed rate on a rotational instrument), and the response is measured as a shear-stress σ. The ratio of shear-stress σ to shear-rate $\dot{\gamma}$ is the (apparent) viscosity η. A plot of the viscosity vs. shear-rate $\dot{\gamma}$ is called the flow curve of the material.

Rheological experiments can also be conducted in dynamic or oscillatory shear, where a sinusoidal strain $\gamma = \gamma_0 \sin(\omega t)$ is applied to the sample. Here γ_0 is the strain-amplitude (i.e. the maximum applied deformation) and ω is the frequency of the oscillations. The sample response will be in the form of a sinusoidal stress $\sigma = \sigma_0 \sin(\omega t + \delta)$ which will be shifted by a phase angle δ with respect to the strain waveform. Using trigonometric identities, the stress waveform can be decomposed into two components, one in-phase with the strain and the other out-of-phase by 90°:

$$\sigma = G'\gamma_0 \sin(\omega t) + G''\gamma_0 \cos(\omega t) \tag{2.2}$$

where G' is the **Elastic** or **Storage Modulus** and G'' is the **Viscous** or **Loss Modulus**.

The physical interpretation of the two moduli are as follows. The elastic modulus G' is the in-phase component of the stress and provides information about the elastic nature of the material. Since elastic behavior implies the storage of deformational energy, this parameter is also called the storage modulus. The viscous modulus G'', on the other hand, is the out-of-phase component of the stress and characterizes the viscous nature of the material. Since viscous deformation results in the dissipation of energy, G'' is also called the loss modulus. For these properties to be meaningful, the dynamic rheological measurements must be made in the "*linear viscoelastic*" (LVE) regime of the sample. This means that the stress must be linearly proportional to the imposed strain (i.e., moduli independent of strain amplitude). In that case, the elastic and viscous moduli are only functions of the frequency of oscillations ω, and are true material functions. A log-log plot of the moduli vs. frequency, i.e. $G'(\omega)$ and $G''(\omega)$, is called the frequency spectrum of the material and represents a signature of the material microstructure.

The important advantage of dynamic shear measurements is that they allow us to characterize microstructures without disrupting them in the process. The net deformation imposed on the sample is minimal because the experiments are restricted to small strain amplitudes within the LVE regime of the sample. As a result, the linear viscoelastic moduli reflect the microstructures present in the sample at rest. This is to be contrasted with steady shear, where the material functions are always obtained under flow conditions corresponding to relatively drastic deformations. We can therefore correlate dynamic rheological parameters to static microstructures, and parameters under steady shear to flow-induced changes in microstructure.

2.6.2. Small-Angle Neutron Scattering (SANS)

Scattering techniques are invaluable probes of micro- and nanostructure in soft materials.[45] The basic principle underlying all scattering techniques is that the intensity of scattered radiation is a function of the size, shape, and interactions of the "particles" present. Small-angle neutron scattering (SANS) is the technique of choice in this study because contrast between the "particles" and the solvent can be easily achieved by substituting deuterium for hydrogen in solvent molecules: for example, replacing cyclohexane, C_6H_{12} with deuterated cyclohexane, C_6D_{12}. Also, the incident radiation in SANS is composed of neutrons having a wavelength ~ 7 Å, and as a result, SANS is useful in probing size scales on the order of a few nm. SANS experiments require a nuclear reactor to generate neutrons and we are fortunate to have one of the premier SANS facilities close by at NIST in Gaithersburg, MD.

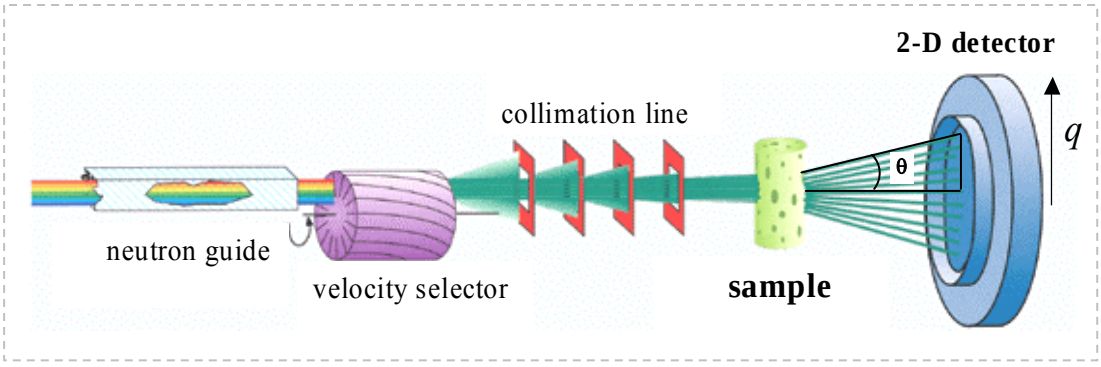

Figure 2.5. Schematic of a SANS experiment (adapted from www.gkss.de).

The basic geometry of a SANS experiment is illustrated in Figure 2.5. Neutrons emitted from a nuclear reactor are selected at a particular wavelength and wavelength

spread using a velocity selector, collimated by several lenses, and passed through a sample chamber. The neutrons scattered by the sample are collected on a 2-D detector. These 2-D data are corrected and placed on an absolute scale using calibration standards. They are then converted into a plot of scattered intensity I vs. scattering vector q by spherical averaging. The scattering vector q is related to the scattering angle and wavelength by:[45]

$$q = \frac{4\pi}{\lambda} \sin\left(\frac{\theta}{2}\right) \tag{2.3}$$

Here, λ is the wavelength of the incident radiation and θ is the scattering angle. Thus, q can be considered an inverse length scale, with high q corresponding to small structures, and vice versa.

The SANS intensity $I(q)$ from a structured fluid containing n_p particles per unit volume can be expressed in the following manner:

$$I(q) = n_p \cdot P(q) \cdot S(q) \tag{2.4}$$

where $P(q)$ is called the form factor and $S(q)$ the structure factor. $P(q)$ is the scattering that arises from intraparticle interference, which is a function of the particle size and shape. $S(q)$ arises from interparticle interactions and thereby reflects the spatial arrangement of particles in solution. When the particles are in dilute solution or are non-interacting, the structure factor $S(q) \rightarrow 1$ and the SANS intensity $I(q)$ can then be modeled purely in terms of the form factor $P(q)$. Form factors for different particle geometries are known and these can be fitted to the data to obtain structural information about the particles.

We describe below some form factor models for different micellar shapes: ellipsoids, rigid cylinders, and flexible cylinders. In these expressions, ($\Delta\rho$) is the difference in scattering length density between the micelle and the solvent, so that $(\Delta\rho)^2$ is the scattering contrast.

Spheres. The form factor $P(q)$ for spheres with radius R_s is given by:[46,47]

$$P_{sphere}(q) = (\Delta\rho)^2 \left(\tfrac{4}{3}\pi R_s^{\,3}\right)^2 \left[\frac{3\left(\sin(qR_s) - qR_s\cos(qR_s)\right)}{(qR_s)^3}\right]^2 \tag{2.5}$$

Rigid Cylinders. The form factor $P(q)$ for rigid cylindrical rods of radius R and length L is given by:[46,47]

$$P(q) = (\Delta\rho)^2 \left(\pi R^2 L\right)^2 \int_0^{\pi/2} [F(q,\alpha)]^2 \sin\alpha \, d\alpha \tag{2.6}$$

where
$$F(q,\alpha) = \frac{J_1(qR\sin\alpha)}{(qR\sin\alpha)} \cdot \frac{\sin(qL\cos\alpha/2)}{(qL\cos\alpha/2)} \tag{2.7}$$

Here α is the angle between the cylinder axis and the scattering vector q and J_1(x) is the first-order Bessel function of the first kind.

Coexistence of Spheres and Rigid Cylinders. For the coexisting spheres and cylinders, the overall intensity of scattering would be the sum of contributions from spheres and cylinders. If solutions are sufficiently dilute, the relation can be simply given by:

$$I_{overall}(q) = c\left[\phi_s P_{sphere}(q) + (1-\phi_s) P_{cylinder}(q)\right] \tag{2.8}$$

Here c is overall concentration and ϕ_s is the volume fraction of spheres.

Ellipsoids. The form factor $P(q)$ for ellipsoids of revolution with minor and major axes R_a and R_b is given by:[46,47]

$$P(q) = (\Delta\rho)^2 \left(\tfrac{4}{3}\pi R_a R_b^2\right)^2 \int_0^1 \left[3\frac{(\sin z - z\cos z)}{z^3}\right]^2 d\mu \tag{2.9}$$

where $$z = q\sqrt{\mu^2 R_b^2 + R_a^2(1-\mu^2)} \tag{2.10}$$

Here μ is the cosine of the angle between the scattering vector q and the symmetry axis of the ellipsoid.

Flexible Cylinders. The form factor for semiflexible chains of contour length L, persistence length l_p and cross-sectional radius R can be represented as the product of a cross-sectional form factor P_{CS} and wormlike-chain form factor P_{WC}:[47,48]

$$P(q) = P_{CS}(q,R) \cdot P_{WC}(q,L,l_p) \tag{2.11}$$

The cross section form factor P_{CS} can be approximated by the following expression, which is valid for cylindrical chains:

$$P_{CS}(q,R) = \left[\frac{2J_1(qR)}{qR}\right]^2 \tag{2.12}$$

The form factor P_{WC} for a wormlike chain with excluded-volume interactions is detailed in the paper by Pedersen and Schurtenberger,[48] where it was originally derived, and then modified by Chen et al.[49]

Unilamellar Vesicles. The form factor $P(q)$ for unilamellar vesicles of radius R and bilayer thickness t is given by the following expression:[45,50]

$$P(q) = (\Delta\rho)^2 \left\{ \frac{4}{3}\pi R^3 \frac{3J_1(qR)}{qR} - \frac{4}{3}\pi (R+t)^3 \frac{3J_1[q(R+t)]}{q(R+t)} \right\}^2 \tag{2.13}$$

where $J_1(x)$ is the first-order Bessel function, given by:

$$J_1(x) = \frac{\sin x - x\cos x}{x^2} \tag{2.14}$$

For thin bilayers ($t << R$), or equivalently for large vesicles, $P(q)$ reduces to the following expression:

$$P(q) = (\Delta\rho)^2 \cdot (4\pi R)^2 \cdot \frac{t^2}{q^2} \sin^2(qR) \tag{2.15}$$

Eq 2.15 indicates that for large, non-interacting vesicles, $I(q)$ should show a q^{-2} decay in the low q range. If the vesicles are polydisperse, the form factor has to be averaged over the vesicle distribution in the following manner: [45,50]

$$P(q) = \int f(R) \cdot P(q,R)\ dR \tag{2.16}$$

where $P(q, R)$ is the form factor for a vesicle of radius R (eq 2.13). The polydispersity in vesicle radius $f(R)$ can be accounted for by a Schulz distribution equation:

$$f(R) = \left(\frac{p+1}{R_0} \right)^{z+1} \frac{R^z}{\Gamma(z+1)} \exp\left(-(z+1)\frac{R}{R_0} \right) \tag{2.17}$$

In the above expression, R_0 is the average vesicle radius and Γ is gamma function. The polydispersity p_d is given by:

$$p_d = \frac{1}{\sqrt{z+1}} \tag{2.18}$$

Indirect Fourier Transform (IFT) of SANS Data. SANS data were also analyzed by IFT method, which yields particle shape and size without the need for any *a priori* assumptions. To use IFT, first the incoherent background is estimated from the asymptotic slope of a Porod plot (Iq^4 vs. q^4) at high q. The scattering intensity $I(q)$ (with incoherent background subtracted) is then Fourier-transformed to obtain the pair distance distribution function $p(r)$ in real space. For non-interacting scatterers, $I(q)$ and $p(r)$ are related by:[51]

$$I(q) = 4\pi \int_0^\infty p(r) \frac{\sin(qr)}{qr} dr \tag{2.19}$$

The $p(r)$ provides information on the shape and size of the scattering entities. In particular, the largest dimension of the scatterers can be estimated, corresponding to the value of r beyond which $p(r) = 0$. IFT analysis was implemented using the commercial PCG software package.

2.6.3. Dynamic Light Scattering (DLS)

Static scattering techniques such as SANS provide important information about the quiescent structure in complex fluids. Dynamic scattering techniques have a complementary role in that they probe structural relaxations and dynamics. In particular,

dynamic light scattering (DLS) probes the Brownian motion of particles in the fluid. This method can give a reliable estimate of particle size under certain limiting conditions. In a DLS experiment, the fluctuating intensity of light scattered from the sample is recorded at a certain angle θ. The fluctuations are then correlated to yield the intensity autocorrelation function $g^{(2)}(q,\tau)$ vs. the correlation time τ.[52]

$$g^{(2)}(q,\tau) = \frac{\langle I(q,t)I(q,t+\tau)\rangle}{\langle I(q,t)^2\rangle} \tag{2.20}$$

Note that in light scattering, the definition of the wave vector is slightly modified as:

$$q = \frac{4\pi n}{\lambda}\sin\left(\frac{\theta}{2}\right) \tag{2.21}$$

where n is the refractive index of the medium (the wavelength of light through the medium is thus λ/n). Thus, in DLS, relaxation is measured at length scales of q^{-1}.

The measured intensity autocorrelation function $g^{(2)}(q, \tau)$ can be converted into an electric field autocorrelation function $g^{(1)}(q, \tau)$ through the Siegert relation:

$$g^{(2)}(q,\tau) = 1 + f\left|g^{(1)}(q,\tau)\right|^2 \tag{2.22}$$

Here, f is an adjustable parameter called the coherence factor that depends on the instrument geometry. For a dilute solution of monodisperse spherical particles, the electric-field autocorrelation function is a single exponential whose time decay is determined by the translational diffusion coefficient of the particle D:

$$g^{(1)}(q,\tau) = \exp\left(-Dq^2\tau\right) \tag{2.23}$$

From the measured diffusion coefficient, the particle size can be obtained by the Stokes-Einstein equation:

$$D = \frac{k_B T}{6\pi\eta R_h} \tag{2.24}$$

where k_B is the Boltzmann constant, T the absolute temperature and η the viscosity of the solvent (assumed to be a Newtonian liquid). The size obtained from DLS is the *hydrodynamic radius* R_h. The hydrodynamic size is the bare particle size along with any solvation layer.

Chapter 3

REVERSE WORMLIKE MICELLES OF BILE SALTS AND LECITHIN

The results presented in this chapter have been published in the following journal article: Shih-Huang Tung, Yi-En Huang and Srinivasa R. Raghavan, "*A New Reverse Wormlike Micellar System: Mixtures of Bile Salt and Lecithin in Organic Liquids*." J. Am. Chem. Soc. 128, 5751-5756 (**2006**).

3.1. INTRODUCTION

In this chapter, we describe our first study, which puts forward a new route to forming reverse wormlike micelles in organic liquids ("oils"). The self-assembly of reverse wormlike micelles has been studied for more than two decades, following the work of Luisi and co-workers.[7-12] The first examples of such micellar systems were ternary mixtures of the type lecithin/water/oil.[8] Lecithin is a zwitterionic phospholipid with two alkyl tails (Figure 1.1), which when added alone to oil gives rise to reverse spherical or ellipsoidal micelles. When a small quantity of water is added to these fluids, the micelles grow axially into flexible cylinders. Thus, the crucial component is water, and the molar ratio of water to lecithin (denoted by w_0) is the key parameter in dictating reverse micellar growth. The growth of these micellar chains and their subsequent entanglement into a transient network transforms the sample into a highly viscous and viscoelastic one.[10,12] In turn, the viscosity in the limit of low shear rates, i.e., the zero-

shear viscosity η_0, is enhanced by several orders of magnitude relative to that of neat lecithin solutions.

Here, we report that an entirely different class of additives – *bile salts* – can induce lecithin to form reverse worms in organic solvents. Bile salts are *facial* amphiphiles, with a polar and a non-polar face (Figure 1.1).[20] We suggest that this "facially amphiphilic" structure of bile salts is critical to their ability to induce the growth of lecithin reverse worms – indeed, the role of bile salt is potentially quite analogous to that of water in this regard. Interestingly also, we find that micellar growth is induced by very small concentrations of bile salt – i.e., at molar ratios of bile salt to lecithin much less than one. In this regard, the action of bile salts on reverse micelles is similar to the action of aromatic "binding" salts like sodium salicylate on cationic micelles in water. This similarity implies a strong binding of bile salts with the reverse micelles, and we will elaborate on this point later in this chapter.

Apart from their scientific peculiarity, there are other reasons for studying bile salt-lecithin reverse micelles. Currently, there is much interest in using reverse micelles as hosts for enzymes[1-3] and also in drug delivery.[4-6] Studies have found that biomolecules or drugs encapsulated in reverse micelles can show good biological activity; however, the stability of these molecules is often inversely related to the amount of water present in the formulation. The reverse micelles described here are formed without any added water and could thereby offer some advantages for the encapsulation of biological or organic molecules. In addition, the study of these reverse micelles could also provide insights into

physiological processes involving lecithin, bile salt, and non-polar substances such as fats or fatty acids.

3.2. EXPERIMENTAL SECTION

Materials. Soybean lecithin (95% purity) was purchased from Avanti Polar Lipids, Inc. The bile salts, sodium deoxycholate (SDC, > 97% purity), sodium cholate (SC, > 99%), sodium tauro-deoxycholate (STDC, > 97%), and sodium taurocholate (STC, > 97%) were purchased from Sigma-Aldrich. Cyclohexane, iso-octane, and isopropyl palmitate were purchased from EM Sciences, Fisher and TCI, respectively. *N*-hexane, 1-hexene, and *n*-decane were purchased from Sigma-Aldrich. Deuterated cyclohexane (99.5% D) was obtained from Cambridge Isotopes.

Sample Preparation. Mixed solutions containing bile salt and lecithin were prepared as follows. Lecithin and bile salt were dissolved in methanol to form 200 mM and 100 mM stock solutions, respectively. Samples of desired composition were prepared by mixing the stock solutions. Methanol was removed by drying the samples in a vacuum oven at 50°C for 48 hours. The final samples with desired concentrations were obtained by adding the organic solvent, followed by stirring till the solutions became transparent and homogeneous. The above procedure ensured the removal of any residual water from the sample, and thereby facilitated reproducible sample preparation.

Residual Water Content. Residual water content in the dried bile salt samples was studied using $_1$H NMR on a Bruker 400 MHz spectrometer. The studies revealed the

presence of residual water at a 0.9:1 molar ratio in these samples. This aspect is further elaborated in the Discussion section of the paper.

Rheology. Steady and dynamic rheological experiments were performed on a Rheometrics RDA-III strain-controlled rheometer. A parallel-plate geometry of 25 mm radius was used for all samples. The plates were equipped with Peltier-based temperature control and all samples were studied at 25 $\pm$ 0.1°C. A solvent trap was used to minimize cyclohexane evaporation. Frequency spectra were conducted in the linear viscoelastic regime of the samples, as determined from dynamic strain sweep measurements. For the steady shear experiments, sufficient time was allowed before data collection at each shear rate so as to ensure that the viscosity reached its steady-state value.

Small Angle Neutron Scattering (SANS). SANS measurements were made on the NG-7 (30 m) beamline at NIST in Gaithersburg, MD. Neutrons with a wavelength of 6 Å were selected. The distances between sample chamber and detector were 1.2 m and 15 m. The range of scattering vector q was 0.004~0.4 $Å^{-1}$. Samples were prepared with deuterated cyclohexane and studied in 1 mm quartz cells at 25°C. The scattering spectra were corrected and placed on an absolute scale using calibration standards provided by NIST. The data are shown for the radially averaged intensity I versus the scattering vector $q = (4\pi/\lambda) \sin(\theta/2)$, where λ is the wavelength of incident neutrons and θ is the scattering angle. Modeling of SANS data was done using software modules provided by NIST to be used with the IGOR graphing package.[53] Details of these models have been discussed earlier in Section 2.6.2.

3.3. RESULTS

3.3.1. Lecithin/SDC/Cyclohexane: Phase Behavior and Rheology

We first focus on mixtures of lecithin and the bile salt, sodium deoxycholate (SDC) in cyclohexane. Results with other bile salts and in other nonpolar solvents will be discussed later. We chose cyclohexane because our results could be compared with those for lecithin/water/cyclohexane mixtures from the literature. In cyclohexane, lecithin forms reverse spherical or ellipsoidal micelles and the resulting solutions have a low viscosity, essentially identical to that of the solvent.[12] Adding SDC to these solutions increases the viscosity dramatically. This is evident even by visual observation – for example, the sample barely flows when the vial is tilted, and bubbles remain trapped in the fluid for long periods of time. To quantify the effect of SDC, we conducted rheological experiments at a fixed lecithin concentration of 100 mM and with increasing concentrations of SDC. The results are expressed as a function of B_0, the molar ratio of bile salt to lecithin.

Figure 3.1 shows the zero-shear viscosity η_0 of 100 mM lecithin solutions as a function of B_0. The values of η_0 were obtained from steady-shear rheological experiments in the limit of low shear rates, where the viscosity asymptotically approached a plateau. We note that η_0 increases by five orders of magnitude as B_0 increases from 0.2 to 0.45. All these solutions are transparent and isotropic at rest, with the more viscous samples showing a weak birefringence under flow (e.g., on shaking a vial). Photographs of sample

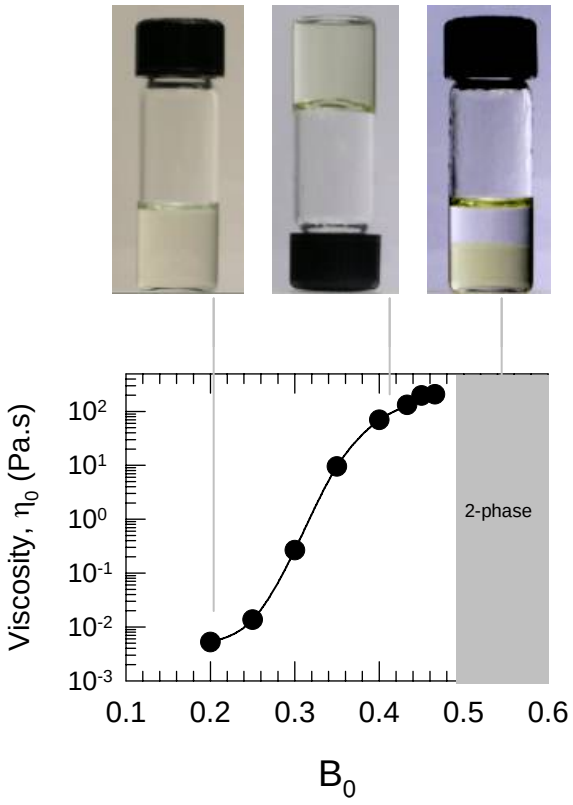

Figure 3.1. Zero shear viscosity η_0 of lecithin + bile salt (SDC) in cyclohexane at 25°C as a function of B_0, the molar ratio of bile salt to lecithin, with the lecithin concentration held constant at 100 mM. Photographs of three samples corresponding to different B_0 values are also shown. At low B_0, the sample is a solution of low viscosity. At a B_0 around 0.4, the sample viscosity is a factor of 10^5 higher and the sample flows very slowly in the overturned vial. Finally, when B_0 exceeds ca. 0.5, the sample phase-separates into two co-existing liquid phases.

vials for B_0 = 0.2 and 0.4 are also shown in Figure 3.1. The B_0 = 0.4 sample is shown in an inverted vial to highlight how slowly the sample flows under gravity because of its high viscosity. Note that, because this sample does flow, albeit slowly, it cannot be termed a "gel" – the dynamic rheological data (Figure 3.2) confirm this point. A further interesting observation is that, above a B_0 of 0.45, lecithin-SDC samples in cyclohexane phase-separate into two isotropic liquid phases, one nonviscous and the other viscous (see photograph of typical sample on the top right in Figure 3.1). The lower phase, which is

similar in viscosity to the one-phase samples at lower B_0, contains most of the lecithin and SDC. The upper, nonviscous phase is a very dilute reverse micellar solution. A similar phase separation occurs for the lecithin-water-cyclohexane system at higher water:lecithin molar ratios.[12]

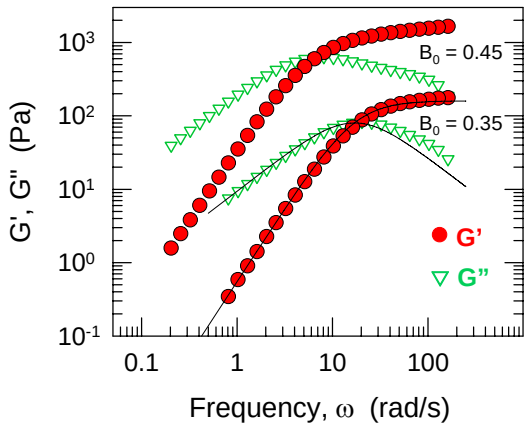

Figure 3.2. Dynamic rheology at 25°C of two lecithin-SDC mixtures in cyclohexane. The samples contain 100 mM lecithin and the SDC:lecithin molar ratios are B_0 = 0.35 and 0.45. The plot shows the elastic modulus G' (filled circles) and the viscous modulus G'' (unfilled triangles) as functions of frequency ω. Fits to a single-relaxation-time Maxwell model are shown as solid lines for the B_0 = 0.35 sample.

To characterize the viscoelasticity of lecithin-SDC reverse worms, we turned to dynamic rheology. Figure 3.2 shows representative dynamic rheological data (elastic modulus G' and the viscous modulus G'' as functions of frequency ω) for two samples containing 100 mM lecithin with B_0 = 0.35 and 0.45. The data clearly reveal the viscoelastic response of these samples. That is, at high ω or short timescales, the samples show elastic behavior, with G' tending to a plateau and dominating over G''. On the other hand, at low ω or long timescales, the samples show viscous behavior, with G'' exceeding G' and the slopes of G' and G'' being close to 2 and 1 respectively on the log-log plot.

The dominant relaxation time t_R of these viscoelastic samples can be estimated as $1/\omega_c$, where ω_c is the frequency at which G' and G'' cross. In Figure 3.2, we also show fits to $G'(\omega)$ and $G''(\omega)$ for the 0.35 sample using a Maxwell model with a single relaxation time. The predictions of this model are:[27]

$$G'(\omega) = \frac{G_p \omega^2 t_R^2}{1 + \omega^2 t_R^2} \tag{3.1}$$

$$G''(\omega) = \frac{G_p \omega t_R}{1 + \omega^2 t_R^2} \tag{3.2}$$

Here, G_p is the plateau modulus, i.e., the value of G' in the high-frequency limit. We note that the Maxwell model fits the data reasonably well, especially at low and intermediate frequencies, while there is a slight discrepancy at high frequencies. This confirms that a single relaxation time (or a narrow spectrum of relaxation times) dominates the rheological response of this sample. Maxwell fluid-like behavior is indicative of entangled wormlike micelles, both normal and reversed.[27]

Figure 3.3 shows the variation of dynamic rheological parameters with bile salt concentration. Here, the plateau modulus G_p and the relaxation time t_R (= $1/\omega_c$) are plotted as a function of B_0 for a fixed lecithin concentration of 100 mM. Both G_p and t_R are seen to increase steeply with B_0. The increase of relaxation time t_R with B_0 is related to the growth of reverse micellar chains upon addition of bile salt. A similar increase in t_R is seen for cationic worms in water as they grow upon addition of aromatic salts.[23,24] However, the sharp increase in plateau modulus G_p is unexpected. For comparison, the G_p of cationic worms is generally independent of salt for a fixed surfactant content.[24] An increase in G_p generally implies an increase in the volume fraction of entangled

micelles.[27] One can thereby consider the bile salt to have a dual rule: not only does it induce the growth of lecithin reverse micelles, but also it induces a greater number of such micelles to form. A mechanism where bile salt molecules are incorporated into the body of the reverse micelle can explain these results, and is discussed later in this paper.

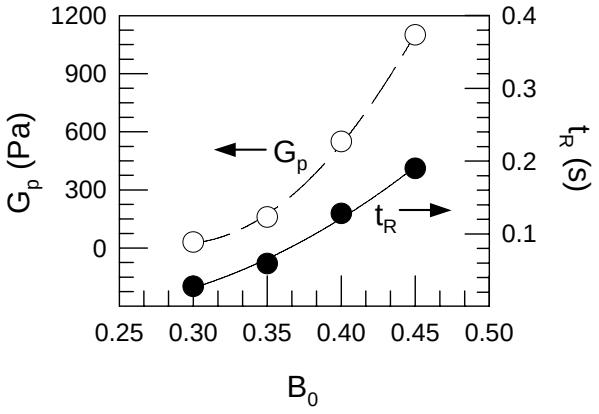

Figure 3.3. Plateau modulus G_p and relaxation time t_R for lecithin-SDC mixtures in cyclohexane as a function of the SDC:lecithin molar ratio B_0. The lecithin concentration in these samples is 100 mM. The parameters were extracted from dynamic rheological spectra such as those shown in Figure 3.2.

We now describe the variation of rheological parameters with lecithin volume fraction ϕ at fixed values of the bile salt-to-lecithin molar ratio B_0. The scaling of the plateau modulus G_p vs. ϕ is shown in Figure 3.4a for two different B_0 (0.35 and 0.45), and similar data for the zero-shear viscosity η_0 vs. ϕ are shown in Figure 3.4b. As expected, both G_p and η_0 increase steeply with ϕ, with the data following power laws. However, the power law exponents are unexpectedly large. Taking the case of G_p first, the reptation theory of De Gennes predicts $G_p \sim \phi^{2.25}$ for semidilute entangled polymers.[54] The same exponent of 2.25 is predicted in the semidilute regime for entangled linear

worms as well, and this has been verified experimentally for many aqueous and reverse wormlike micellar systems.[23,24,27] Here, on the other hand, the power-law exponents from Figure 3.4a for G_p are 3.4 ± 0.2 for B_0 = 0.35 and 3.0 ± 0.1 for B_0 = 0.45. These values are considerably larger than the theoretical exponent of 2.25, and the discrepancy arises possibly because the bile salt induces an increase in the volume fraction of reverse wormlike micelles. A similar scenario occurs with the η_0 vs. ϕ data in Figure 3.4b, where the power-law exponents are 4.4 ± 0.2 and 4.0 ± 0.2 for B_0 = 0.35 and B_0 = 0.45, respectively. These exponents are larger than those typically reported for nonionic or charge-screened wormlike micelles in water.[23,24,27]

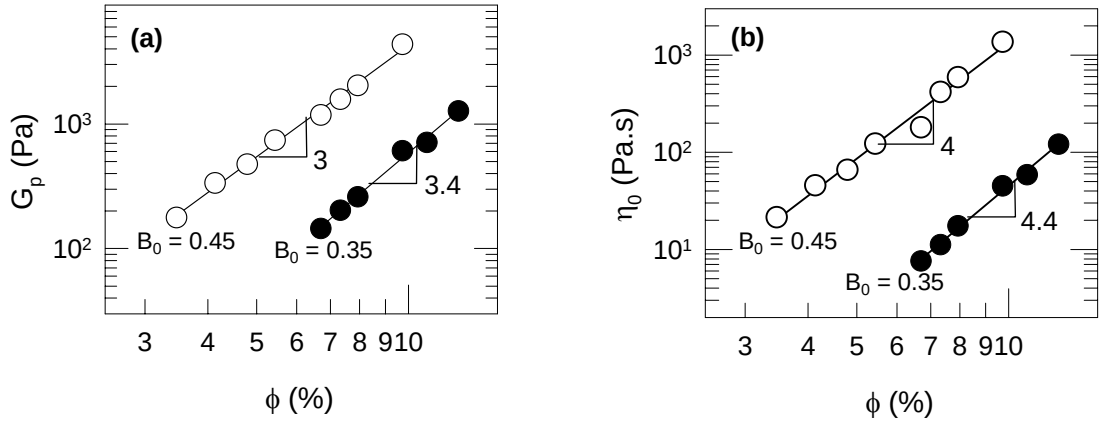

Figure 3.4. Rheological parameters for lecithin-SDC mixtures as a function of the lecithin volume fraction ϕ. Data are provided for two values of the SDC:lecithin molar ratio B_0. Figure 3.4a shows the plateau modulus G_p and Figure 3.4b the zero-shear viscosity η_0.

3.3.2. Lecithin/SDC/Cyclohexane: Small-Angle Neutron Scattering (SANS)

Having characterized the rheology, we now turn to SANS to elucidate the underlying microstructure in lecithin-bile salt samples. For these experiments, samples

were made in deuterated cyclohexane (these samples were rheologically identical to those made in cyclohexane). We fixed the lecithin concentration at a relatively low value of 20 mM for the SANS experiments so as to keep the micellar volume fraction low and thereby minimize intermicellar interactions (structure factor contributions). SANS spectra (I vs. q) for 20 mM lecithin solutions containing varying amounts of bile salt (B_0 ranging from 0 to 0.4) are shown in Figure 3.5. Clearly, the addition of bile salt causes a dramatic increase in the low-q scattering while the intensity at higher q remains practically unchanged. The increase in low-q scattering is consistent with the growth of elongated structures.[47] Thus, the SANS data immediately provide a qualitative confirmation of reverse micellar growth induced by the bile salt.

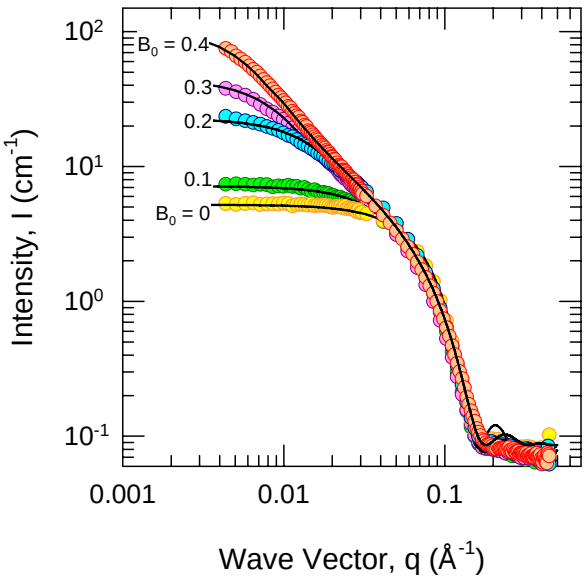

Figure 3.5. SANS data from samples in deuterated cyclohexane containing 20 mM lecithin and different SDC:lecithin molar ratios B_0. The solid curves through the data are fits to appropriate models (see text for details).

To obtain a more quantitative picture of micellar sizes, we model these SANS data using appropriate form factors. The fits are shown as solid curves through the data in Figure 3.5. First, for the case of lecithin in cyclohexane (B_0 = 0), the micelles are modeled as ellipsoids of revolution (eq 2.9 and 2.10) with radii of 22 Å and 33 Å, respectively, for their minor and major axes. From the parameters, these micelles are found to be slightly oblate ellipsoids (incidentally, a model for polydisperse spheres does not fit the data as well). Upon the addition of bile salt, the micelles grow axially. For B_0 = 0.1 and 0.2, the micelles can be modeled as rigid cylinders (eq 2.6 and 2.7). The cylinder radius in each case is about 22 Å, while the contour length increases from ca. 96 Å for B_0 = 0.1 to ca. 289 Å for B_0 = 0.2. With further increase in bile salt content, the micelles become even longer and their flexibility must be taken into account in modeling the SANS data. Thus, for B_0 = 0.3 and 0.4, the micelles are modeled as semiflexible cylindrical chains (eq 2.11 and 2.12).[48] For these cases, the cylinder radius is around 22 Å, the persistence length is ca. 190 Å, and the contour length of the chains increases from ca. 700 Å for B_0 = 0.3 to ca. 1440 Å for B_0 = 0.4. In sum, the SANS data confirm that adding bile salt causes the rapid growth of reverse wormlike micelles. Our analysis also shows that the cross-sectional radius of the mixed lecithin-bile salt micelles is nearly the same as that of pure lecithin micelles. Thus, bile salts induce longitudinal micellar growth without expanding the micellar cross-section.

3.3.3. Lecithin/SDC Micelles: Growth in Different Organic Solvents

We have studied the bile salt-induced growth of reverse wormlike micelles in a range of organic solvents. In terms of reverse micelle growing ability, bile salts are very

similar to water, and Figure 3.6 presents a comparison between the two in terms of their worm-inducing abilities in different solvents. As stated in the Introduction, water is

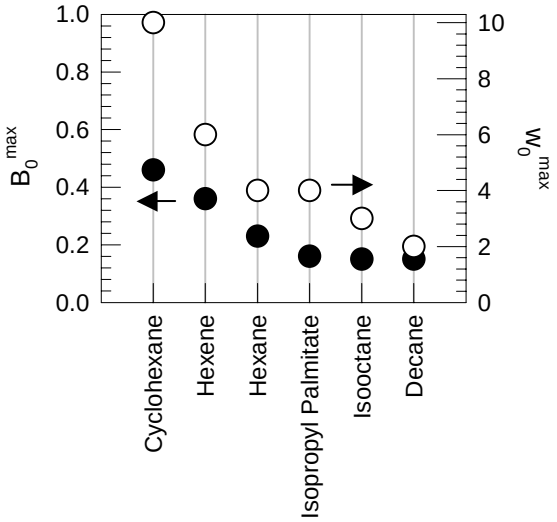

Figure 3.6. Comparison of bile salt (SDC) and water in terms of their ability to induce viscoelastic reverse micelles of lecithin in six different solvents. The lecithin concentration is fixed at 100 mM. The parameters plotted are the molar ratios of bile salt:lecithin (B_0^{max}) and water:lecithin (w_0^{max}) at which the zero-shear viscosities of the respective mixtures reaches a maximum.

well-known for its ability to induce growth of lecithin reverse worms. Interestingly, when water is added to a lecithin organosol, the viscosity increases to a maximum at a certain water:lecithin molar ratio w_0^{max}, while further addition of water typically causes a decrease in viscosity, followed by phase separation.[10,12] The behavior with bile salts is qualitatively different (Figure 3.1) – the viscosity increases with bile salt content monotonically until the phase boundary (the highest viscosities attained with bile salt and water are quite similar). For comparison, we focus on the molar ratio of bile salt:lecithin at which the viscosity is the highest, i.e., just prior to phase separation, and we denote this value by B_0^{max}. Figure 3.6 thereby compares B_0^{max} (for the bile salt, SDC) and w_0^{max} for

six different organic solvents, with the lecithin concentration fixed at 100 mM. While the differences from solvent to solvent presumably lie in their interactions with the lecithin head group,[12] the important point from Figure 3.6 is that B_0^{max} and w_0^{max} generally *track each other*. For example, w_0^{max} is ca. 10 for cyclohexane and ca. 4 for hexane, while B_0^{max} is 0.45 for cyclohexane and 0.2 for hexane. Note that the B_0^{max} values are much lower than the w_0^{max} values – indeed, very small (less than equimolar) amounts of bile salt are sufficient to substantially increase viscosity. The low values of B_0^{max} imply a strong binding of the bile salt to the lecithin reverse micelle, and this is elaborated further in the Discussion section.

3.3.4. Lecithin Micelles in Cyclohexane: Induced by Different Bile Salts

In addition to SDC, we have studied other bile salts, and a number of these are capable of inducing lecithin to form reverse worms in organic liquids. Figure 3.7 shows the structures of four such bile salts and a comparison of their worm-inducing abilities based on their B_0^{max} values in cyclohexane (i.e., the bile salt:lecithin molar ratio at which the viscosity of 100 mM lecithin solutions reaches a maximum). All four bile salts induced highly viscoelastic reverse micellar solutions at less than equimolar ratios relative to the lecithin (the viscosities at the maximum point were comparable). From Figure 3.7, we note that the B_0^{max} values are quite similar (~ 0.4) for SDC and sodium cholate (SC), both of which have a carboxylate functionality. The corresponding values for the bile salts with a taurine functionality, i.e., sodium taurodeoxycholate (STDC) and sodium taurocholate (STC), are about twice as high (~ 0.8), although these values are still lower than equimolar. Based on these results, it appears that the ability to induce growth

of reverse micelles is mainly related to the unusual "facially amphiphilic" structure of the bile salt amphiphile. The presence or absence of an extra hydroxyl group, or the nature of the headgroup itself, are relatively minor factors in terms of the ability of bile salts to induce growth of reverse worms.

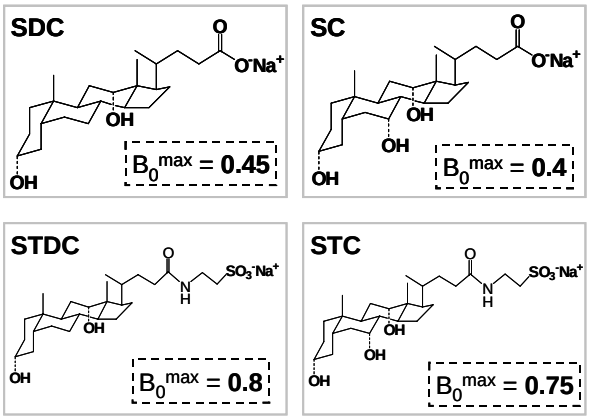

Figure 3.7. Comparison of four different bile salts in terms of their ability to induce viscoelastic reverse micelles of lecithin in cyclohexane. The lecithin concentration is fixed at 100 mM and B_0^{max} is the molar ratio of the respective bile salt:lecithin mixture at which the zero-shear viscosity reaches a maximum.

3.4. DISCUSSION

In the preceding section, we have shown that bile salts can induce a dramatic growth of lecithin reverse micelles in organic solvents. The presence of long wormlike reverse micelles, in turn, imparts a strong viscoelastic character to the samples. Why are bile salts effective at inducing reverse micellar growth? This is the question that we will address in the current section.

First, it is important to state that the micellar growth is indeed caused by the bile salt and is not an artifact due to residual water in the sample. To underscore this point, we have exhaustively dried both the lecithin and bile salt prior to use, as described in the Experimental section. Still, it is well-known that both soybean lecithin as well as the bile salts have a residual layer of bound water (ca. equimolar), which cannot be removed by drying.[11] We have confirmed the presence of residual water at a 0.9:1 molar ratio by ^{1}H NMR studies on dried bile salt samples. However, this residual water content is too small to explain our results. Consider our data for cyclohexane (Figure 3.6), where w_0^{max}, i.e., the water:lecithin molar ratio at the viscosity maximum, is about 10. This means that we must add a significant amount of water to induce a high viscosity. For comparison, the value of B_0^{max}, i.e., the bile salt (SDC):lecithin molar ratio at the viscosity maximum, is 0.45. Clearly, we require a *much lower* amount of bile salt to induce a similar viscosity, and the difference is too large to attribute to residual water. Also, as indicated earlier, the progression in viscosity upon adding water and bile salt are quite different – with water, the viscosity goes through a peak, whereas with bile salt, the viscosity rises monotonically. Thus, our results clearly show that bile salts have a distinct influence on reverse micellar growth, and we offer below a mechanism to explain their effect.

The type of self-assembled structure formed by amphiphiles is known to be governed by molecular geometry, and this relationship is usually expressed in terms of the critical packing parameter $p = a_{tail}/a_{hg}$ where a_{tail} and a_{hg} are the cross-sectional areas of the tail and headgroup respectively.[55] In water, ionic surfactants in the absence of salt have a p around 1/3 (i.e., a "cone" shape), which implies the formation of spherical

micelles. When salt is added, the effective headgroup area is reduced due to a reduction in the electrostatic screening length.[27] In turn, the packing parameter *p* increases to around 1/2 (the molecule adopts a "truncated cone" shape) and the micelles consequently transform from spheres to rods.

In the case of organic solvents, the formation of reverse micelles requires a packing parameter *p* well in excess of 1, and *spherical* reverse micelles evidently correspond to an inverse cone shape (Figure 3.8). For these spheres to grow into rods or worms, the packing parameter *p* must *decrease*. We believe that such a decrease is caused in the present lecithin-bile salt system by the binding of bile salt to the lecithin headgroups.[42,43,56] In other words, the bile salt increases the headgroup area a_{hg} while maintaining about the same tail area. The net effect is to decrease *p* and transform the effective geometry into a truncated cone (Figure 3.8), thereby driving a transition to long, cylindrical micelles. Note that in the proposed scenario, the bile salt orients its hydrophobic face outward into the organic solvent while its hydrophilic face is directed towards the interior of the micelle (the –OH groups of the bile salt possibly form hydrogen bonds with the lecithin headgroup).[42] Thus, we believe the facially-amphiphilic structure of the bile salt is the key to its ability to induce lecithin reverse worms.

The above mechanism is supported by previous work on lecithin-bile salt mixtures in water.[42,43,56-58] While lecithin alone tends to form vesicles in water, the addition of bile salt transforms these vesicles into cylindrical micelles.[57,58] Such a transition implies a reduction in packing parameter from ca. 1 to ca. 1/2. This, in turn, has

been attributed to an increase in headgroup area due to the binding of bile salt with lecithin head groups. We hypothesize a similar binding of bile salt to lecithin in the context of our reverse micellar system.

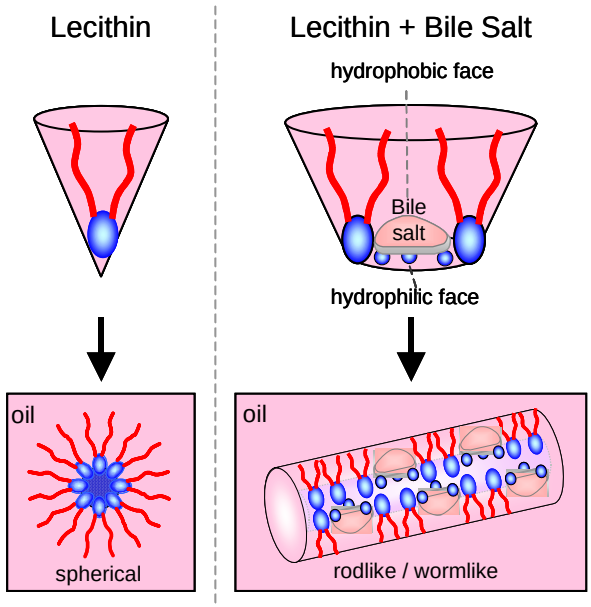

Figure 3.8. Schematic of the reverse micellar structures formed by lecithin with and without bile salt. Lecithin is shown as a molecule with a blue head and two red tails, while the bile salt is schematically represented following Figure 1.1. Lecithin alone tends to form approximately spherical reverse micelles in a nonpolar solvent (oil). When bile salt is added, its hydrophilic moieties bind to the lecithin headgroups, thus expanding the headgroup area. This alters the net geometry from a cone to a truncated cone, and thereby induces the spherical micelles to grow into flexible cylinders (worms). Note the orientation of bile salt molecules in the cylindrical micelles – their hydrophilic faces are turned inward while the hydrophobic faces are exposed to the external oil phase.

Finally, we should point out that bile salts appear to have an analogous effect as water in inducing the formation of lecithin reverse worms. A number of studies have suggested that water is distributed in the headgroup region of lecithin reverse micelles, and that water molecules form hydrogen bonds with the phosphate groups of neighboring lecithin moieties.[11,25,26] (Such a scenario can also explain why other hydrogen-bonding

solvents have a similar effect as water on reverse micellar growth.[25]) We believe that bile salt molecules, due to their planar structure, are distributed in a similar fashion between the lecithin headgroups. This explains why water and bile salts have similar effects on micellar growth. Note that the volume of a bile salt molecule is much larger than that of water, and therefore, a few molecules of bile salt can have the same effect on headgroup size as a much larger number of water molecules. This aspect can help explain why a larger molar ratio of water compared to bile salt is necessary to reach the viscosity maximum, i.e., why w_0^{max} is always larger than B_0^{max} in Figure 3.6.

3.5. CONCLUSIONS

We have shown that the addition of bile salt to lecithin organosols induces a transition from discrete spherical reverse micelles to entangled networks of wormlike reverse micelles. In turn, the zero-shear viscosity rises by more than five orders of magnitude and the fluid shows a viscoelastic response with a single dominant relaxation time (Maxwell-fluid-like behavior). SANS measurements further confirm the presence of flexible wormlike cylinders in these samples. Micellar growth has been demonstrated with four different bile salts, and in each case, the molar ratio of bile salt to lecithin is the controlling parameter. We attribute the micellar growth to a change in molecular geometry caused by the binding of bile salt molecules to lecithin headgroups (and the resulting expansion of the headgroup area). The unique "facially amphiphilic" structure of bile salts allows them to get sequestered between lecithin headgroups in a manner similar to water, which explains why bile salts and water have analogous effects on reverse micellar growth.

Chapter 4

TEMPERATURE EFFECTS ON REVERSE AND NORMAL WORMLIKE MICELLES

The results presented in this chapter have been published in the following journal article: Shih-Huang Tung, Yi-En Huang and Srinivasa R. Raghavan, "*Contrasting Effects of Temperature on the Rheology of Normal and Reverse Wormlike Micelles*." Langmuir, 23, 372-376 (**2007**).

4.1. INTRODUCTION

In this chapter, we describe the different rheological responses to temperature of normal and reverse wormlike micelles. The self-assembly of amphiphilic molecules results in a variety of remarkable structures of diverse shapes and sizes.[29] Among the most intriguing of these are the "wormlike micelles," which are flexible cylindrical chains with radii of a few nanometers and contour lengths up to several microns.[23,27,59] These structures have fascinated scientists because they are similar to polymer chains in their ability to entangle into viscoelastic networks.[27] At the same time, the micellar chains are held by weak, physical bonds unlike the covalent bonds in polymers – consequently, the chains can break and recombine, and their contour length is not fixed by chemical synthesis but by solution thermodynamics. From a rheological standpoint, wormlike micellar samples are interesting because they can behave as Maxwell fluids, i.e., as model viscoelastic fluids having just a single relaxation time.[23,59]

Wormlike micelles can be formed both in water as well as in nonpolar organic solvents ("oils").[59] In water, a variety of surfactants (cationic, anionic, zwitterionic) can give rise to these structures, although academic studies have largely focused on cationic surfactants combined with salt.[23] The salt is necessary to screen the ionic repulsions between the surfactant heads and thereby induce a molecular geometry that is optimal for packing into cylinders. Note that in these "normal" worms, the polar surfactant heads are in contact with the solvent water, while the nonpolar tails are buried in the interior of the micelle. "Reverse" or "inverted" worms formed in oils have the opposite structure, with the nonpolar tails extending into the oil and the polar heads sequestered in the interior of the micelle. A typical recipe for reverse worms requires adding the phospholipid, lecithin into an organic solvent together with a small amount of water.[10,12] The added water is believed to serve a similar purpose as the salts do in the aqueous system, in that it alters the geometry of the amphiphile to favor the formation of cylinders.

Normal and reverse worms are generally considered to be analogous.[59] Indeed, many theoretical considerations originally formulated to describe charge-screened worms in water have been shown to apply to reverse worms in oil as well.[10,12] Furthermore, experimental studies have also confirmed the similar rheological behavior of normal and reverse worms – for example, the characteristic Maxwellian response can be observed with both kinds of structures.[12,59] Also, key rheological parameters such as the zero-shear viscosity η_0 or the relaxation time t_R often exhibit a maximum as a function of a compositional variable in both types of systems.[10,12,23,59] Such viscosity maxima have been attributed to the branching of worms in both cases.

In this Chapter, we report a key difference between normal and reverse worms with respect to how their rheological properties change upon heating. While both types of micelles show an exponential decrease in their viscosity with temperature, the decrease is more pronounced for reverse worms. We show that the rapid viscosity decrease of reverse worms is associated with an *exponential reduction in their plateau modulus* with temperature. This result is established for two different types of reverse worms, one being a lecithin/water mixture in oil[10,12] and the other a newer system based on mixtures of lecithin and bile salt in oil.[60] In contrast, the plateau modulus of normal worms remains constant with temperature, as shown here for a typical aqueous sample based on the cationic surfactant, cetylpyridinium chloride (CPyCl) in combination with the aromatic salt, sodium salicylate (NaSal). This distinction in rheological behavior has not been highlighted so far to our knowledge. We believe that the drop in plateau modulus with temperature for reverse worms gives crucial insights into the mechanism for their formation – specifically, it underscores the importance of hydrogen-bonding as the driving force for the uniaxial growth of these micelles.

4.2. EXPERIMENTAL SECTION

Materials. The cationic surfactant, CPyCl (99% purity), the aromatic salt, NaSal (99%), the bile salt, sodium deoxycholate (SDC) (97%) and *n*-decane (99%) were purchased from Sigma-Aldrich. The zwitterionic lipid, soybean lecithin (95%) was purchased from Avanti Polar Lipids, Inc. All chemicals were used as received.

Sample Preparation. Normal worms of CPyCl/NaSal were prepared by adding ultra-pure deionized water from a Millipore water-purification system into weighed quantities of CPyCl and NaSal. The samples were heated to ~ 65°C under continuous stirring for approximately an hour till the solutions became homogeneous.

Lecithin/water reverse worms were prepared in *n*-decane by adding the organic solvent into dry lecithin (dried in a vacuum oven at room temperature for 48 hours), followed by stirring till the lecithin was completely dissolved. Water was then added to the lecithin solutions, followed by heating and stirring till the sample became homogeneous.

Lecithin/bile salt (SDC) reverse worms in *n*-decane were prepared by a procedure similar to that described in Chapter 3. First, lecithin and SDC were dissolved separately in methanol to form 200 mM and 100 mM stock solutions, respectively. Samples of desired composition were prepared by mixing the stock solutions. Methanol was removed by drying the samples in a vacuum oven at room temperature for 48 hours. The final samples with desired concentrations were obtained by adding *n*-decane, followed by stirring till the solutions became transparent and homogeneous. The above procedure ensured the removal of any residual water from the sample, and thereby facilitated reproducibile sample preparation. All samples were equilibrated at room temperature at least three days prior to conducting experiments.

Rheology. Steady and dynamic rheological experiments were performed on a AR2000 stress-controlled rheometer (TA Instruments) using either parallel-plate or couette geometries, which were equipped with Peltier-based temperature control. A solvent trap was used to minimize sample evaporation. The samples were equilibrated for at least 10 min at each temperature prior to conducing experiments. Frequency spectra were conducted in the linear viscoelastic regime of the samples, as determined from dynamic strain sweep measurements. For the steady shear experiments, sufficient time was allowed before data collection at each shear rate so as to ensure that the viscosity reached its steady-state value.

4.3. RESULTS AND DISCUSSION

4.3.1 Rheological Data as *f*(T) for Normal Worms

We now describe the rheology of normal worms in water as a function of temperature, and we will subsequently contrast this behavior with that of reverse worms. Temperature effects on normal worms have been studied by a number of authors.[24,61,62] To illustrate the typical response, we show data for a cationic wormlike micellar fluid in Figure 4.1. The recipe we have used is a classic one involving the C_{16}-tailed cationic surfactant, CPyCl combined with the aromatic salt, NaSal.[23] Figure 4.1a shows dynamic rheological data (elastic modulus G' and viscous modulus G'' as functions of frequency ω) for a sample of 235 mM CPyCl and 125 mM NaSal in water at 22°C, 28°C, 34°C, and 40°C. The data are typical of viscoelastic wormlike micelles, with a plateau in G' at high frequencies, and terminal behavior of G' and G'' (slopes of 2 and 1 respectively) at low

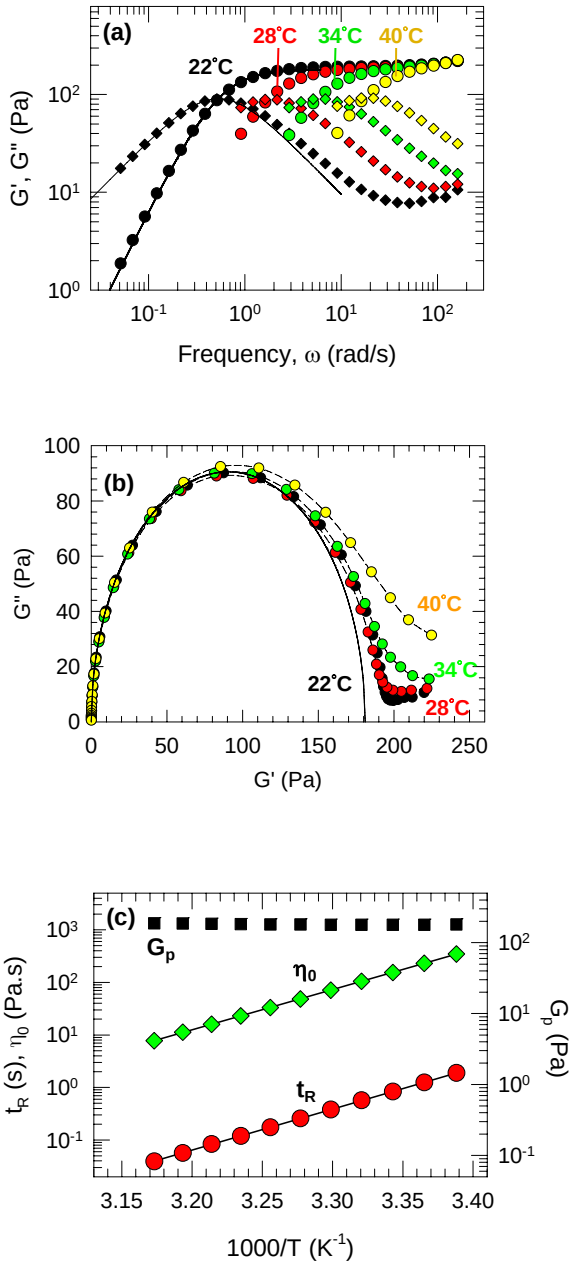

Figure 4.1. (a) Dynamic rheology of a normal worm sample (235 mM CPyCl + 125 mM NaSal in water) at different temperatures. Data are shown for the elastic modulus G' (circles) and the viscous modulus G'' (diamonds) as functions of frequency ω. The solid lines are fits to a single-relaxation-time Maxwell model. (b) The same data in a Cole-Cole plot. (c) Arrhenius (semilog) plot of the plateau modulus G_p, relaxation time t_R and zero-shear viscosity η_0 as functions of $1/T$.

frequencies. Moreover, the sample is nearly a Maxwell fluid over the range of temperatures – fits are shown at 22°C to a single-relaxation-time Maxwell model, given by the equations below:[59]

$$G'(\omega) = \frac{G_p \omega^2 t_R^2}{1+\omega^2 t_R^2};\ G''(\omega) = \frac{G_p \omega t_R}{1+\omega^2 t_R^2} \tag{4.1}$$

Here G_p is the plateau modulus and t_R is the relaxation time corresponding to $1/\omega_c$, where ω_c is the crossover frequency at which G' and G'' intersect. We note that the Maxwell model fits the data well, especially at low and intermediate frequencies, as has been shown for normal worms.[23,59]

Turning to the effect of temperature on the rheological data, we can note several trends from Figure 4.1a. As temperature increases, the entire frequency spectrum moves to the right (i.e., to higher frequencies or shorter timescales), but the plateau modulus G_p remains constant.[24,61,62] G_p values can be estimated equivalently from Cole-Cole plots (Figure 4.1b). The Cole-Cole equation is expressed by:

$$\left(G' - G_p/2\right)^2 + G''^2 = \left(G_p/2\right)^2 \tag{4.2}$$

At the midpoint of the semicircle, $G' = G'' = G_p/2$. Note that the semicircle radius in the Cole-Cole plot is independent of temperature, which implies that the value of G_p is also independent of temperature. The shift in crossover frequency ω_c to higher values means that the relaxation time t_R decreases with temperature. The variation of G_p and t_R with temperature are shown in Figure 4.1c on an Arrhenius plot, i.e., a semilog plot of the quantities vs. $1/T$. We find that the t_R values fall on a straight line, indicating an exponential decrease that can be represented by the following equation:[24,27]

$$t_R = A\exp\left(E_a / RT\right) \tag{4.3}$$

where E_a is the flow activation energy, R the gas constant, T the absolute temperature and A the pre-exponential factor. Figure 4.1c also plots the zero-shear viscosity η_0 as a function of $1/T$. The η_0 values are the viscosities in the Newtonian plateau at low shear-rates from steady-shear rheological experiments. We obtain nearly the same values of η_0 from the dynamic data using the Maxwell fluid relation $\eta_0 = G_p t_R$. Significantly, the η_0 data in Figure 4.1c also fall on a straight line with approximately the *same slope* as the t_R line. This result can be understood by combining the above Maxwell relation with eq 4.3:[24]

$$\eta_0 = G_p A\exp\left(E_a / RT\right) \tag{4.4}$$

Eq 4.4 shows that, when G_p is constant with temperature, η_0 will decrease exponentially with the same flow activation energy E_a. In other words, for a sample of normal worms, we can obtain E_a from the temperature dependence of either η_0 or t_R. For the present sample, we obtain E_a to be ca. 147 kJ/mol, which is comparable to reported values.[24,61,62]

The above trends for G_p, η_0 and t_R as functions of temperature have been observed for numerous kinds of normal worms.[24,27,61,62] It is worth reviewing the mechanistic underpinnings for these results. As mentioned earlier, the average worm length $\bar{L}$ is a thermodynamic quantity and it is predicted to decrease exponentially with temperature according to the equation:[27]

$$\bar{L} \simeq \phi^{1/2}\exp\left[E_c / 2k_B T\right] \tag{4.5}$$

Here, ϕ is the volume fraction of worms, E_c is the end-cap energy (i.e., the excess energy associated with the hemispherical caps compared to the cylindrical body of the worm), and k_B is Boltzmann's constant. A decrease in $\bar{L}$ will affect the dynamics of micellar stress relaxation. The relaxation time t_R is determined by a competition between micellar breaking and chain reptation, and Maxwellian behavior is generally observed when the breaking time τ_B is much lower than the reptation time τ_{rep}.[27] In this fast-breaking regime, the relaxation time $t_R = (\tau_{rep}\tau_B)^{1/2}$. Because $\tau_{rep} \sim \bar{L}^3$, a decrease in $\bar{L}$ will cause a drastic reduction in τ_{rep}, and this is the dominant effect on t_R.[27] Thus, as the worms grow exponentially shorter, they will relax exponentially faster, and this is indeed what is found empirically. The decrease in worm length will have no effect on the plateau modulus G_p, however. This is because G_p is primarily related to the mesh size ξ of the entangled network, and in the semidilute regime, ξ is a function only of the volume fraction ϕ of entangled worms:[27]

$$G_p = \frac{k_B T}{\xi^3} \quad ; \quad \xi \sim \phi^{-0.75} \tag{4.6}$$

Thus, with increasing temperature, as long as the volume fraction ϕ remains the same, the network mesh size will be independent of worm length and G_p will remain constant.

4.3.2. Rheological Data as *f*(T) for Reverse Worms

We now describe the temperature dependence of the rheology of reverse worms. Again, we have chosen a classic recipe for forming these worms, involving 125 mM soy-bean lecithin and 250 mM deionized water added to the nonpolar solvent, *n*-decane.[10,12]

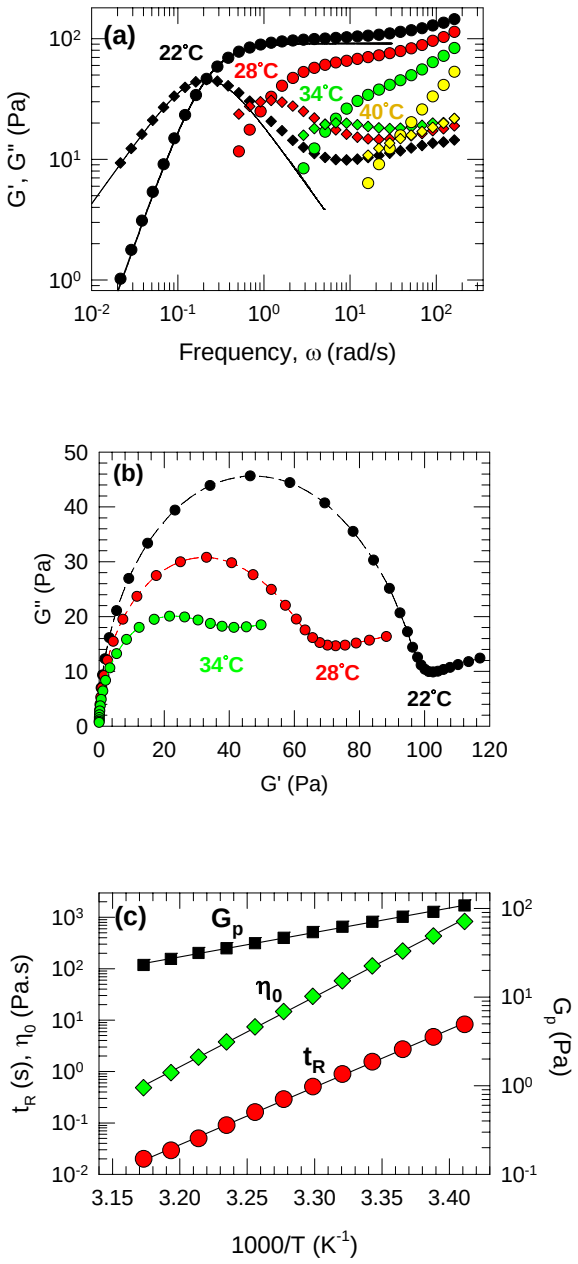

Figure 4.2. (a) Dynamic rheology at different temperatures of a water-induced reverse worm sample (125 mM lecithin + 250 mM water in *n*-decane). The elastic modulus G' (circles) and the viscous modulus G'' (diamonds) are shown as functions of frequency ω. The solid lines are fits to a single-relaxation-time Maxwell model. (b) The same data in a Cole-Cole plot. (c) Arrhenius (semilog) plot of the plateau modulus G_p, relaxation time t_R and zero-shear viscosity η_0 as functions of $1/T$.

Figure 4.2a shows the dynamic rheological data for this sample at 22°C, 28°C, 34°C, and 40°C. Here again, we observe the viscoelastic behavior typical of entangled networks. Maxwell model fits (eq 4.1) are shown at 22°C, and the fit is again reasonable at low to moderate frequencies (deviations at high frequencies can be attributed to alternate "breathing" modes of stress relaxation).[12] As temperature is raised, the entire frequency spectrum moves both downwards and to the right (i.e., towards decreasing moduli and increasing frequency). Specifically, note the behavior of the plateau modulus G_p. In contrast to the constant G_p observed for normal worms (Figure 4.1a), G_p for the reverse worms is seen to decrease upon heating (Figure 4.2a and 4.2b). Figure 4.2c plots the variation of G_p, η_0 and t_R vs. $1/T$ and we find that all three quantities decrease exponentially with temperature. Note that the G_p values have been estimated from Maxwell model fits or from Cole-Cole plots (Figure 4.2b).[12] Figure 4.2c also shows the slope of the Arrhenius plot for η_0 to be greater than that for t_R, indicating that the viscosity decreases more rapidly with temperature than the relaxation time.

Figure 4.2 thus indicates a qualitatively different rheological variation with temperature for reverse worms compared to normal worms. We have observed similar results for *all* reverse worm samples in the lecithin/water/*n*-decane system as well as with other non-polar solvents. One might wonder if the same pattern occurs for reverse worms that do not involve water as an additive. Recently, we have reported that *bile salts*, which are naturally-occurring "facial" amphiphiles, act just like water and induce reverse worms of lecithin in organic solvents.[60] It is therefore useful to examine temperature effects for these bile salt-based reverse worms. We show results in Figure 4.3 for a reverse worm

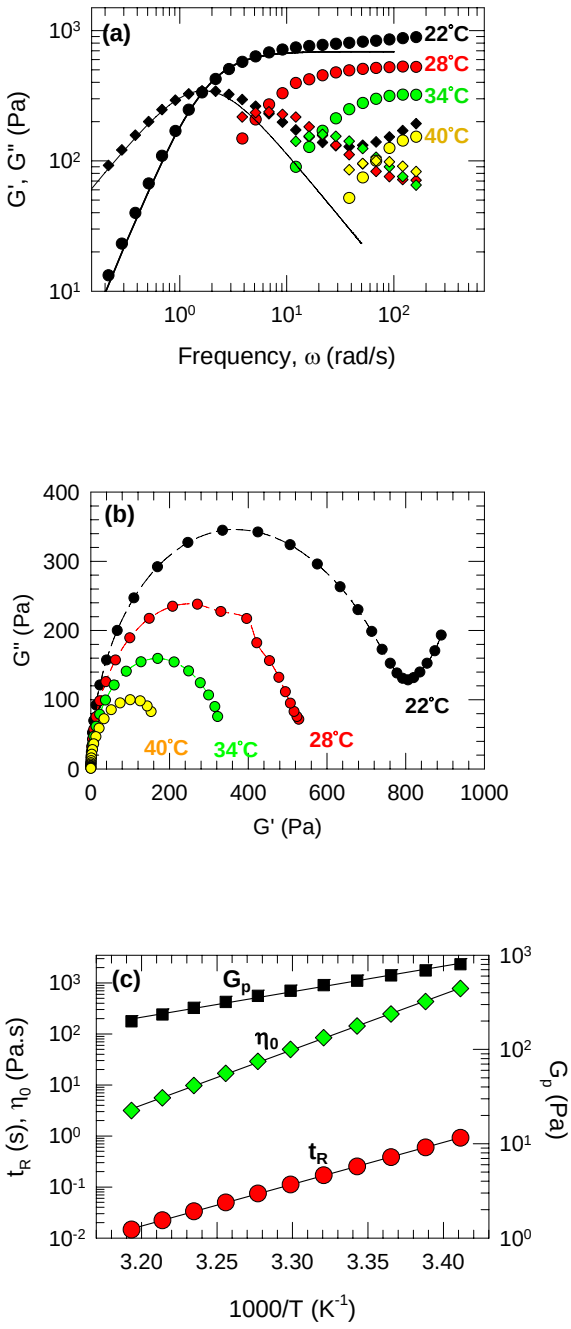

Figure 4.3. (a) Dynamic rheology at different temperatures of a bile salt-induced reverse worm sample (125 mM lecithin + 18.75 mM SDC in *n*-decane). The elastic modulus G' (circles) and the viscous modulus G'' (diamonds) are shown as functions of frequency ω. The solid lines are fits to a single-relaxation-time Maxwell model. (b) The same data in a Cole-Cole plot. (c) Arrhenius (semilog) plot of the plateau modulus G_p, relaxation time t_R and zero-shear viscosity η_0 as functions of $1/T$.

sample obtained by combining 125 mM lecithin and 18.75 mM of the bile salt, sodium deoxycholate (SDC) in *n*-decane. This sample also shows a viscoelastic response characteristic of entangled micelles (Figure 4.3a), and once again, the entire frequency spectrum moves to lower moduli and higher frequencies as temperature is increased. Thus, for bile salt-induced reverse worms also, the plateau modulus G_p decreases upon heating (Figure 4.3b). Figure 4.3c confirms the exponential drop in G_p, η_0 and t_R with temperature, as was seen in Figure 4.2c. Note that, here again, the zero-shear viscosity decreases more rapidly with temperature than does the relaxation time.

A notable feature exists in regard to the variation of G_p, η_0 and t_R for the two reverse worm samples (Figures 4.2c and 4.3c). Both these samples are sufficiently close to being Maxwell fluids such that the relation $\eta_0 = G_p t_R$ holds to a good approximation (the η_0 from steady-shear rheology and the η_0 calculated by the above relation match to within 6%). As a result, the slopes of the straight lines in Figures 4.2c and 4.3c obey the rule of exponents, i.e., $E_a[\eta_0] = E_a[G_p] + E_a[t_R]$, where we have assigned activation energies for each rheological parameter. In particular, for lecithin/water/*n*-decane reverse worms (Figure 4.2c), we find $E_a[G_p]$ = 53 kJ/mol, $E_a[t_R]$ = 215 kJ/mol, and the sum of these quantities is close to the empirical value of $E_a[\eta_0]$, which is 261 kJ/mol. Similarly, for lecithin/SDC/*n*-decane reverse worms (Figure 4.3c), we find $E_a[G_p]$ = 52 kJ/mol, $E_a[t_R]$ = 157 kJ/mol, and their sum matches almost exactly with the empirical $E_a[\eta_0]$ of 208 kJ/mol. Note that the quality of Arrhenius fits in Figures 4.1-4.3 is uniformly very good, so that the error in E_a is low (< 1%). It is interesting that the activation energies for G_p are nearly identical for the two reverse worm samples. Also, note that the activation

energies for η_0 are higher for the reverse worms than for the normal worms in Figure 4.1 (implying a more rapid decrease in viscosity with temperature for the reverse worms).

4.3.3. Mechanistic Differences Between Normal and Reverse Worms

We now put forward a plausible explanation for the observed contrast in behavior between normal and reverse worms. For normal worms, the derivation of eq. 4.5 for their contour length assumes that they have a constant end-cap energy E_c.[27] In other words, the driving force for forming worms is assumed to be independent of temperature. The dominant driving force for micellization in general arises from the hydrophobic effect.[29] For CPyCl/NaSal micelles to grow from spheres to worms in water, a strong electrostatic binding of the salicylate anions to the cationic pyridinium headgroups is also necessary.[23] But neither the hydrophobic interaction nor the electrostatic binding is expected to be strongly temperature dependent,[29] which is why it is indeed reasonable to assume a *constant E_c as a function of temperature for normal worms* (indeed, this conclusion has been validated by both theoretical[27] and experimental[24] studies). The predominant effect of temperature on the micelles is thus to simply accelerate the dynamics of surfactant exchange between them.[27] This rapid exchange of surfactant unimers weakens the impact of having unfavorable end-caps (i.e., individual surfactant molecules spend less time in their end-caps at a higher temperature). As a result, more end-caps can be formed, and this implies shorter worms. Although the worms get shorter upon heating, they are presumably still long enough to entangle so that the volume fraction of entangled worms remains constant, and this in turn explains why G_p is constant with temperature for normal worms.

In the case of reverse micelles, for spheres to grow into worms, the area per headgroup has to increase. In both the lecithin/water[12] and lecithin/bile salt[60] systems, the binding of water or bile salt to the lecithin headgroups is postulated to cause this increase. The binding in each case is believed to occur by hydrogen bonding between pairs of hydroxyl moieties on the headgroups and the additives.[12,60] In contrast to electrostatic or hydrophobic interactions, hydrogen bonds are expected to be *temperature sensitive*. Indeed, both theoretical and experimental studies show that hydrogen-bonding interactions decay exponentially with temperature.[63,64] A weakening of hydrogen bonds would, in turn, reduce the driving force for growth of long reverse worms. Thus, there are two factors at play for reverse worms as temperature is increased: first, the accelerated dynamics of surfactant exchange (same as in normal worms), and second, a reduced driving force for micellar growth (unique to reverse worms, since they are dependent on hydrogen-bonding interactions). In other words, while the end-cap energy E_c is approximately constant for normal worms, it may be a decreasing function of temperature for reverse worms (and this decrease could be related to $E_a[G_p]$). The net result would be to cause a rapid decrease in contour length for reverse worms upon heating (Figure 4.4). Moreover, since a population of worms is always highly polydisperse,[27] we believe that the worms at the tail of the distribution quickly fall below a length that is sufficient for entanglement, as shown in Figure 4.4. If this is true, the volume fraction of *entangled* reverse worms would drop, which (by eq 4.6) can explain the drop in plateau modulus G_p with temperature for these samples.

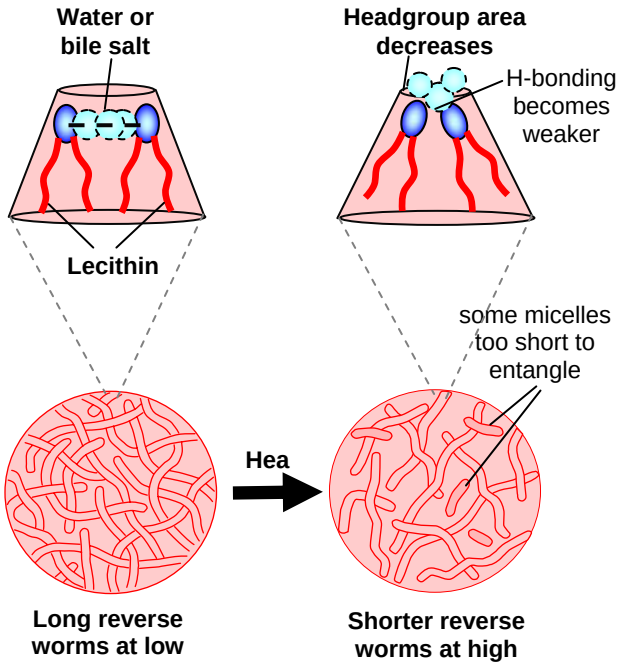

Figure 4.4. Schematic depiction of structural changes in lecithin-based reverse worms as a function of temperature. At low temperatures, the worms are very long and entangled. At higher temperatures, the worms are much shorter, and some of them are so short that they are not entangled with the rest (i.e., the volume fraction of entangled worms drops with temperature). A contributing factor to the decrease in worm length is the weakening of H-bonding interactions between lecithin and the polar additive (water or bile salt). In turn, the effective geometry of the amphiphile is altered in such a way as to disfavor the growth of reverse worms.

4.4. CONCLUSIONS

In conclusion, we have presented rheological data to show that normal and reverse worms respond differently to temperature. For normal worms, the plateau modulus G_p remains constant with temperature, while the relaxation time t_R and zero-shear viscosity η_0 drop exponentially. For reverse worms, in addition to t_R and η_0, G_p also

decreases exponentially with temperature. This result has been confirmed for two different reverse worm samples (lecithin/water/n-decane and lecithin/bile-salt/n-decane). We suggest that the decrease in G_p for reverse worms is due to a weakening of the hydrogen-bonding interactions that control the effective amphiphile geometry in these systems. The results presented here emphasize the importance of hydrogen-bonding as the key factor that dictates the self-assembly and growth of reverse micelles.

Chapter 5

STRAIN-STIFFENING BEHAVIOR OF REVERSE WORMLIKE MICELLES

5.1. INTRODUCTION

In this chapter, we describe an unusual strain-stiffening behavior in transient networks formed by reverse wormlike micelles. Strain-stiffening is a nonlinear rheological response closely associated with biological materials such as blood clots, cornea, and cytoskeletal networks.[65] The phenomenon refers to an increase in modulus (stiffness) when the material is strained above its linear regime of deformations. Such behavior is unusual because most classes of soft matter (polymeric or colloidal) tend to soften monotonically when deformed under non-linear conditions. Although there are a few examples of strain-stiffening in synthetic materials such as in colloidal gels or associating polymer solutions, the effects in these cases tend to be quite weak.[66-71] Currently, model studies on strain-stiffening are almost always conducted with biopolymer gels, such as those of actin, keratin, or fibrin.[65,72-74] Indeed, the ubiquity of strain-stiffening in biology has led researchers to speculate if this property may have physiological relevance since it prevents biological materials from experiencing high deformations.

Two different theories have recently been offered for strain-stiffening. The first is based on the non-linear stretching of semiflexible filaments.[65] A filament is considered

semiflexible when its persistence length l_p and contour length L_c are comparable. For such filaments, the force required to stretch out the thermal bending fluctuations diverges dramatically at large deformations, which is believed to cause the stiffening behavior. An alternative explanation has also been suggested, which attributes strain-stiffening to a transition from a bending-dominated response to a stretch-dominated response as strain is increased.[72] Both these theories, however, apply only to networks with permanent crosslinks – the bending or stretching is associated with chain segments between adjacent crosslink points.

In this study, we report the occurrence of strain-stiffening for *viscoelastic* solutions containing reverse wormlike micelles. The term "reverse" refers to the fact that the micelles are formed in nonpolar solvents, unlike "normal" micelles in water. Reverse worms are long, cylindrical filaments and their entanglement leads to a *transient* network.[60] That is, unlike the model biopolymer networks in which strain-stiffening is generally studied, the crosslink points in reverse worm networks are not permanent. Moreover, we will show that the reverse worms studied here probably have a low persistence length, i.e., they are quite *flexible* compared to the rigid or semiflexible biopolymer filaments. In other words, neither a permanent network nor the presence of rigid filaments may be necessary conditions for strain-stiffening to occur. An alternate model to explain this phenomenon will be proposed later in this paper.

The reverse worm samples in which we find strain-stiffening are mixtures of the phospholipid, lecithin with a small amount of the bile salt, sodium deoxycholate (SDC) in

a nonpolar organic solvent such as cyclohexane or *n*-decane.[60] The lecithin/SDC system represents a new class of reverse worms, and we have recently characterized these samples using rheology and small-angle neutron scattering (SANS). For comparison, the original and widely studied recipe for making reverse worms is to combine lecithin with a small amount of water in organic solvents.[8] Both water and SDC are believed to induce growth of reverse spherical micelles into reverse worms by a similar mechanism, which involves the formation of hydrogen bonds with the headgroups of lecithin.[75] However, a significant finding from the present study is that lecithin/water reverse worm samples do not exhibit strain-stiffening, while lecithin/SDC ones do.

5.2. EXPERIMENTAL SECTION

Materials and Sample Preparation. Materials and sample preparation were similar to those described in Chapter 3.

Rheology. Steady and dynamic rheological experiments were performed on a Rheometrics RDA-III strain-controlled rheometer. A couette geometry was used for all samples, which was equipped with water bath temperature control and all samples were studied at 25 $\pm$ 0.1°C. A solvent trap was used to minimize cyclohexane evaporation. For the steady shear experiments, sufficient time was allowed before data collection at each shear rate so as to ensure that the viscosity reached its steady-state value.

Small Angle Neutron Scattering (SANS). SANS measurements were made on the NG-7 (30 m) beamline at NIST in Gaithersburg, MD. Neutrons with a wavelength of 6 Å were

selected. Three distances of 1m, 4m and 13.25m between sample and detector were used, so as to yield a range of scattering vector q from 0.003 to 0.5 $Å^{-1}$. Samples for SANS studies were prepared with deuterated cyclohexane and were measured in 1 mm quartz cells at 25°C. The scattering spectra were corrected and placed on an absolute scale using calibration standards provided by NIST. The data presented here are for the radially averaged intensity I versus the scattering vector $q = (4\pi/\lambda) \sin(\theta/2)$, where λ is the wavelength of incident neutrons and θ is the scattering angle. Modeling of SANS data was done using software modules provided by NIST to be used with the IGOR graphing package.[53] Details of these models have been discussed earlier in Section 2.6.2.

5.3. RESULTS AND DISCUSSION

5.3.1. Non-Linear Rheology of Reverse Wormlike Micelles

Figure 5.1 depicts the contrast in non-linear rheological behavior between lecithin/water and lecithin/SDC based reverse worms. The data are for the elastic (G') and viscous (G'') moduli as functions of the strain-amplitude γ (in %). All lecithin/water samples show a strain-softening response at high strains, as typified by Figure 5.1a. Here, both G' and viscous G'' decrease at high γ relative to their values in the linear regime at low γ (below 30%). The data in Figure 5.1a correspond to a frequency $\omega = 10$ rad/s where the reverse worm sample shows elastic behavior due to its transient network (note that $G' >> G''$ in the linear regime). Similar strain-softening behavior was observed at all frequencies, however.

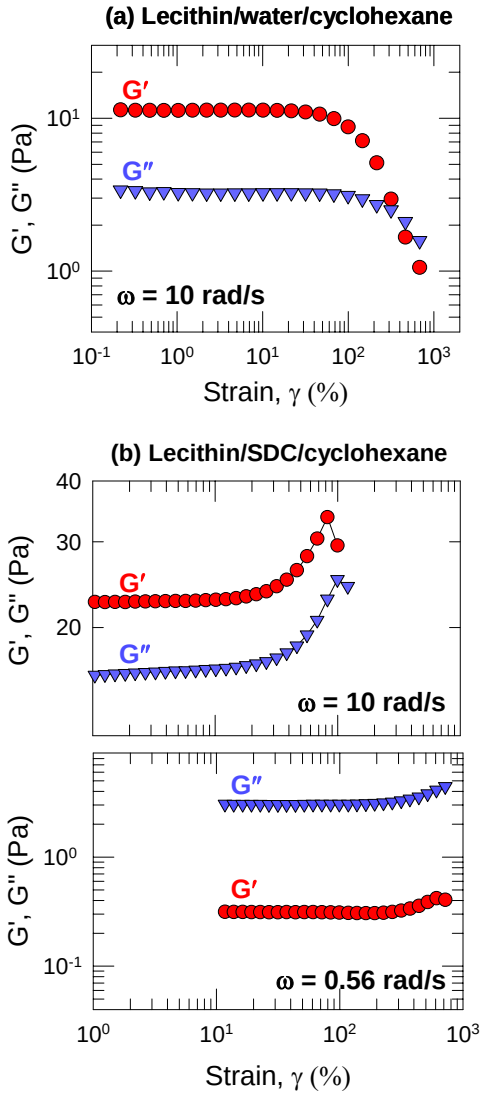

Figure 5.1. Strain sweeps at 25°C for samples of (a) 40 mM lecithin + 360 mM water in cyclohexane, and (b) 35 mM lecithin + 15 mM SDC in cyclohexane.

Figure 5.1b shows typical strain sweeps for a lecithin/SDC reverse worm sample at 10 rad/s and 0.56 rad/s. This sample again exhibits a viscoelastic linear response with a crossover of G' and G'' at 6.6 rad/s (see Figure 5.4 for the frequency spectrum). Thus, at 10 rad/s the behavior is elastic ($G' >> G''$) due to the reverse worm network, whereas at 0.56 rad/s the reverse worms have relaxed and the behavior is viscous ($G'' >> G'$). As seen in Figure 5.1b, the sample shows strain-stiffening at both these frequencies, i.e., the moduli increase over a range of strains. The increase is more pronounced at 10 rad/s: here, G' and G'' are constant until $\gamma \approx 20\%$ whereupon they show a sharp increase up to a maximum. The highest value reached by G', i.e., G_{max} is about 50% higher than its linear value G_0. Strain-stiffening is also observed at the lower frequency of 0.56 rad/s: in this case, the onset occurs at a higher γ (~ 300%). Note again that strain-stiffening occurs despite the viscous nature of the sample at this frequency (i.e., G'' being greater than G' in the linear regime).

Based on our studies, strain-stiffening is ubiquitous for lecithin/SDC reverse worms regardless of the experimental conditions. To verify that the stiffening is real and not an artifact, we have reproduced the same behavior on different rheometer geometries as well as on a stress-controlled rheometer (TA Instruments AR 2000). A few systematic trends are evident from our data. As suggested by Figure 5.1b, the critical strain at the onset of stiffening γ_{crit} is a monotonically decreasing function of frequency. The extent of stiffening, i.e. the ratio G_{max}/G_0, weakly increases with increasing frequency. We have also studied variations in the stiffening response as a function of the total amphiphile (lecithin + SDC) concentration. Results for G' vs. strain (at $\omega = 10$ rad/s) are shown in

Figure 5.2 for samples at different lecithin concentrations and a constant molar ratio of SDC:lecithin of 0.4. All samples show strain-stiffening, and the data clearly show three regimes: first G' is constant at low γ, next, it increases to a maximum over a range of γ, and finally, it decreases. The onset strain γ_{crit} and the strain γ_{max} at which G' shows a maximum both shift to lower values with increasing concentration. Also, the stiffening ratio G_{max}/G_0 slightly decreases with increasing concentration.

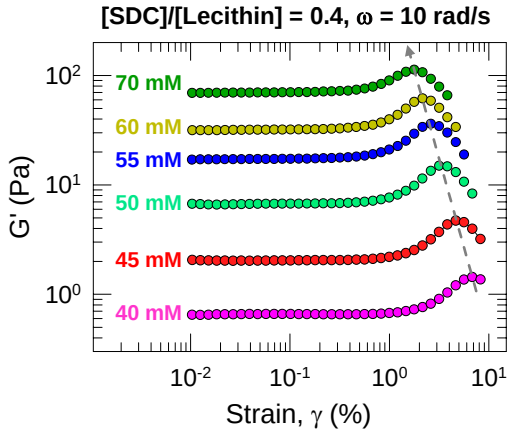

Figure 5.2. Strain sweeps at 25°C for lecithin/SDC cyclohexane samples over a range of lecithin concentrations.

5.3.2. Strain-Stiffening and the Rigidity of Reverse Worms

Why does strain-stiffening occur for lecithin/SDC reverse worms and not for lecithin/water reverse worms? If this phenomenon is indeed associated with stiff filaments as suggested by theory, one might expect the SDC-based worms to be stiffer (i.e., have higher persistence lengths l_p) than the water-based ones. To test this hypothesis, we have used SANS to extract l_p for the two types of reverse worms. Figure 5.3 shows typical SANS data (intensity I vs. wave vector q) for reverse worms based on 10 mM

lecithin in deuterated cyclohexane with 90 mM water and 4 mM SDC, respectively. We used a modified flexible cylinder model (eq 2.11 and 2.12), detailed in Section 2.6.2 and reference [49], to analyze the SANS data, and the corresponding fits are shown as solid lines through the data. From the fits, we obtain a shorter l_p of 91 Å for SDC-induced worms compared with 378 Å for water-induced worms. This suggests that the SDC-based worms are the more flexible structures. To corroborate this result, we also replot the $I(q)$ data in a plot of $qI(q)$ vs. q (called a Holtzer or bending rod plot)[76] that is shown as the inset of Figure 5.3. Here, each curve goes through a maximum at low q and then transitions to a flat region (indicating the $I \sim q^{-1}$ scaling that is typical of cylinders). This transition to the flat portion is expected to occur at $ql_p \sim 1.9$ for semiflexible chains.[77] Clearly, the transition is broader and shifted to higher q for the SDC-based worms, indicating that they have a lower value of l_p.

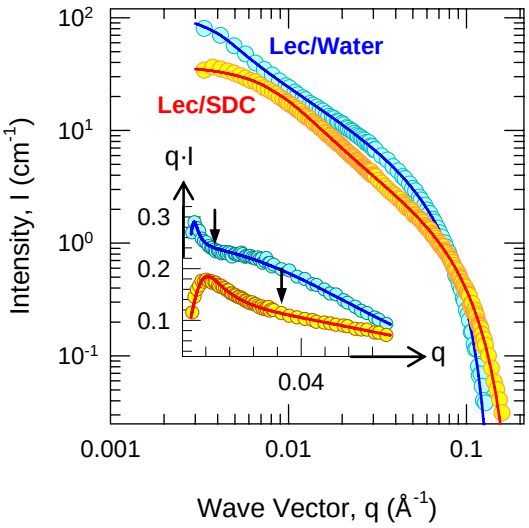

Figure 5.3. SANS data at 25°C for lecithin/water and lecithin/SDC reverse worms in deuterated cyclohexane, based on 10 mM lecithin with 90 mM water and 4 mM SDC, respectively. The solid lines are fits to a flexible cylinder model. The inset shows the same data in a plot of $(I{\cdot}q)$ vs. q.

The above results and analysis imply that neither a permanent network nor rigid filaments are necessary for strain-stiffening. How then can we account for this unusual phenomenon? One suggestive point is shown by a comparison of the dynamic frequency spectra of lecithin/SDC and lecithin/water samples at the same lecithin concentration 35 mM (Figure 5.4a), for which the molar ratio of SDC:lecithin = 0.425 and water:lecithin = 9, giving the highest viscosity respectively. Note that the plateau modulus G_p (i.e.,the high-frequency value of G') is significantly higher for the SDC-based worms. This difference is seen over the entire range of lecithin concentrations, as shown also by Figure 5.4b which plots G_p vs. overall volume fraction ϕ for water- and SDC-based worms. Both the G_p values as well as the power-law slopes are higher for the lecithin/SDC system. Generally, a higher G_p implies that the filaments in the network are more rigid: for example, actin solutions have much higher G_p values than polystyrene

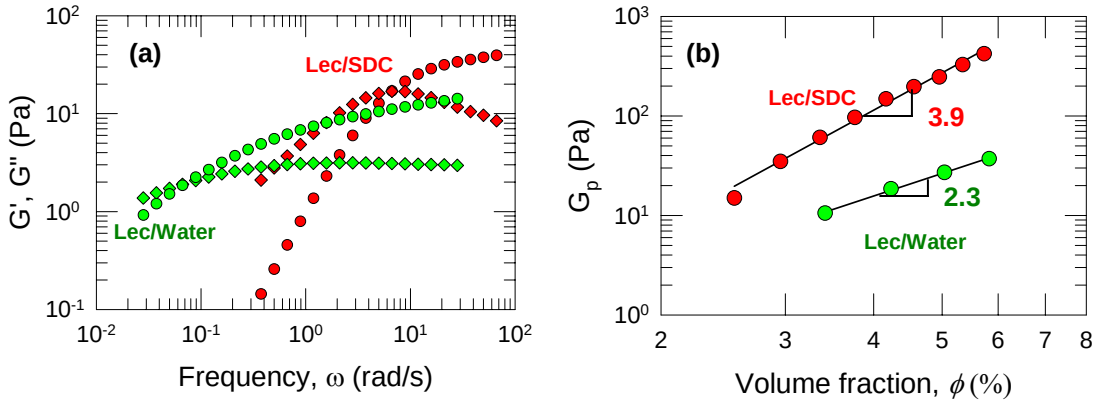

Figure 5.4. (a) Dynamic frequency spectra of lecithin/SDC and lecithin/water samples at the same lecithin concentration 35 mM, with 15 mM SDC and 315 mM water, corresponding to the highest viscosity respectively. Data is shown for the elastic modulus G' (circles) and the viscous modulus G'' (diamonds). (b) Plateau modulus vs. overall volume fraction ϕ for water- and SDC-based worms. The molar ratio of SDC:lecithin = 0.425 and water:lecithin = 9.

solutions at the same concentration.[78] However, a higher rigidity of lecithin/SDC filaments would be inconsistent with our SANS data. While this aspect needs resolution, the fact remains that, based on their G_p values, lecithin/SDC *networks* are stiffer than those of lecithin/water. It is therefore plausible that the previous theories for strain-stiffening might still apply to the transient, but stiff, networks of lecithin/SDC worms.

5.3.3. Alternate Mechanism for Strain-Stiffening

An alternate mechanism for strain-stiffening is also worth considering, and in this scenario, filament stiffness does not play a central role. Instead, strain-stiffening is attributed to a strain-induced aggregation of worms, or equivalently an increase in the volume fraction of entangled worms. Similar ideas have been proposed previously to explain shear-thickening (i.e., an increase in viscosity η at high shear-rates) in aqueous solutions of wormlike micelles[79] or associating polymers.[80] In this context, it is significant that lecithin/SDC samples also exhibit shear-thickening, as shown by Figure 5.5. Shear-thickening is very unusual for entangled networks of wormlike micelles – typically, this phenomenon occurs only for unentangled worms.[79] Also, importantly, entangled reverse worms of lecithin/water do not show shear-thickening (data not shown).

The occurrence of both strain-stiffening and shear-thickening for lecithin/SDC networks suggests a common origin based on shear/strain-induced aggregation. It is known that a population of worms is always highly polydisperse, with an exponential distribution of filament lengths.[27] Thus, some worms will be too short to fully entangle with the rest of the chains in the transient network. We speculate that at high

deformations, these "free" worms become incorporated into the network, leading to an increase in moduli (strain-stiffening). The free worms may connect either with other free worms and thus increase their overall length, or they might connect with worms that are already part of the entangled network. In either case, the entanglements in the network will be enhanced at high strains.

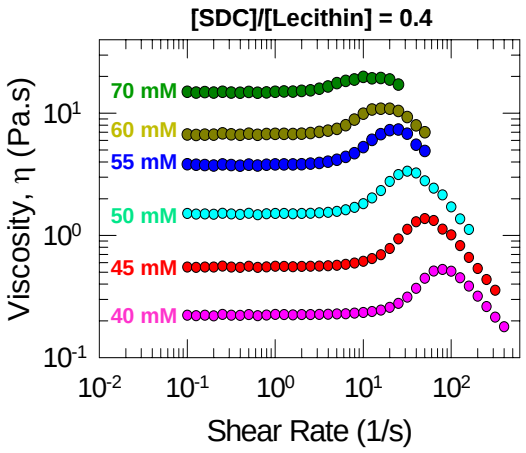

Figure 5.5. Strain sweeps at 25°C for lecithin/SDC cyclohexane samples over a range of lecithin concentrations.

How can this second mechanism explain the differences between lecithin/SDC and lecithin/water samples. Note that high strains can, not only connect free worms, but also break up existing entanglements between worms. If the dominant effect is to break up connections, the result is strain-softening – as is the case for lecithin/water worms. On the other hand, if the balance is tilted in favor of aggregating free worms, the result is strain-stiffening (and likewise, shear-thickening). It is possible that a greater fraction of free worms exists in lecithin/SDC samples, thus favoring their aggregation. Alternately,

the higher stiffness of the lecithin/SDC network may help to ensure that existing connections are maintained, and thereby to tilt the balance towards strain-stiffening.

5.4. CONCLUSIONS

In conclusion, we have described the unusual nonlinear rheology exhibited by viscoelastic solutions of lecithin/SDC reverse worms. The samples show strain-stiffening in dynamic rheology (increase in G' and G'' with strain) as well as shear-thickening (increase in η with shear-rate) in steady-shear rheology. We suggest that these phenomena are caused by increases in connectivity of the micelles at high strain amplitudes or shear-rates. Since lecithin/SDC samples can be easily prepared from widely available and inexpensive precursors, they may serve as a convenient model system for future studies into these unusual phenomena.

Chapter 6

REVERSE VESICLES IN MIXTURES OF LIPIDS

6.1. INTRODUCTION

In this chapter, we present a new route for forming stable unilamellar reverse vesicles by mixing short- and long-chain lipids (lecithins) in nonpolar organic liquids. Vesicles are spherical containers formed in aqueous solution by the self-assembly of amphiphilic molecules. While the core of the vesicle contains water, its outer shell is composed of a bilayer of the amphiphiles, with these molecules oriented in such a way that their hydrophobic portions are inside the bilayer and thereby shielded from water (Figure 2.3). The amphiphiles that form vesicles roughly have the shapes of cylinders, i.e., their "packing parameter" is close to 1.[81] Such a shape can generally be achieved by two-tailed surfactant (lipids)[21] or by mixtures of cationic and anionic single-tailed surfactants.[28] Vesicles have long held a fascination for scientists because of their structural resemblance to primitive biological cells. More importantly, vesicles are of technological interest for applications ranging from drug delivery and controlled release to bioseparations and sensing.[21] In particular, vesicles can encapsulate a variety of water-soluble solutes such as drugs, cosmetic ingredients or agrochemicals in their aqueous core. These solutes could subsequently be released slowly and in a controlled manner through the vesicle bilayer.

Much like the above "normal" vesicles in water, one can also find their counterparts in organic non-polar solvents ("oils"), and these are termed "reverse" vesicles. These reverse vesicles will have a "reverse" bilayer shell, where the hydrophobic portions of the precursor amphiphiles are exposed to the oily medium both in the core and outside (Figure 2.3b). Reverse vesicles are more rare than normal vesicles, but one might imagine that they too could find numerous applications much like the normal vesicles, e.g., for encapsulation and controlled delivery of hydrophobic solutes. A few attempts to assemble reverse vesicles have been reported, based on polyoxyethylene ethers,[30] phospholipids,[31] amino acid derivatives,[32] sucrose esters,[33] and metallosurfactants[34]. However, questions remain about the stability, robustness and ease of preparation of reverse vesicles by these methods, and as a result, these structures are not being widely exploited at the moment for applications. From a scientific standpoint, no clear rules or guidelines have been laid out for the systematic tuning of reverse aggregate geometry, in contrast to the extensive knowledge of normal aggregates.

In this chapter, we report a new route for forming stable unilamellar reverse vesicles in nonpolar organic liquids such as cyclohexane. Our method also offers a general framework for tuning reverse aggregate geometry from reverse spherical micelles to reverse cylindrical micelles and finally to reverse vesicles. The key ingredients in our samples are a combination of long- and short-chain phospholipids. The long-chain lipid is L-α-phosphatidylcholine (lecithin), a natural two-tailed lipid with an average tail length of 17 carbons and an unsaturation in one of the tails (Figure 1.1). The short-chain lipid

we have used is 1,2-dibutyroyl-*sn*-glycero-3-phosphocholine (C_4-lecithin) with two four-carbon saturated tails (Figure 1.1).

Let us consider what is known regarding the behavior of each of the above lipids, both in water and in oil. When added to water, lecithin alone forms large unstable mutilamellar vesicles while C_4-lecithin alone tends to form micelles.[21] Mixtures of short and long-chain lecithins have also been studied in water, and they assemble into disk-like micelles (bicelles)[82] or unilamellar vesicles.[83] In oil, C_4-lecithin is insoluble, presumably because its tails are too short to compensate for the hydrophilic head. The longer-tailed lecithin, however, does dissolve in oil and assembles into reverse spherical micelles. Also, lecithin reverse spheres can be made to grow into reverse cylinders by adding trace quantities of water or bile salts to the sample. The growth of long, flexible cylinders (reverse worms) imparts a strong viscoelastic character to these samples.

Now, let us consider a mixture of lecithin and C_4-lecithin in an oil such as cyclohexane. In the presence of the longer-tailed lecithin, the C_4-lecithin does dissolve. To obtain vesicles, it is critical that we also include a small amount of a salt, such as sodium chloride (NaCl), in the formulation. As we will show, in the above mixtures, the type of aggregate can be tuned by varying the ratio of C_4-lecithin to lecithin. When this ratio is high, the solutions develop a bluish tinge, and we find that they contain reverse unilamellar vesicles. The vesicles are very stable and robust, retaining their size and structure over a period of many months. We use dynamic light scattering (DLS), small-

angle neutron scattering (SANS) and transmission electron microscopy (TEM) to study the vesicles in these samples.

6.2. EXPERIMENTAL SECTION

Materials. Lecithin) (95%) and C_4-lecithin (> 99%) were purchased from Avanti Polar Lipids. The C_4-lecithin was supplied as a solution in chloroform. Cyclohexane and NaCl were purchased from J. T. Baker. Deuterated cyclohexane (99.5%D) was purchased from Cambridge Isotopes. All chemicals were used as received

Sample Preparation. Mixed solutions containing short- and long-chain lecithin were prepared as follows. Lecithin and NaCl were dissolved in methanol to form 100 mM and 85 mM stock solutions, respectively. The desired amount of C_4-lecithin was dried by evaporation in a vacuum oven for at least 12 h. Samples of desired compositions were prepared by mixing the lecithin and NaCl stock solutions with the dried C_4-lecithin. Methanol was removed by evaporation in a vacuum oven for 48 h. The final samples with desired concentrations were obtained by adding cyclohexane or deuterated cyclohexane, followed by stirring at 60°C till the solutions became homogeneous. The samples were then sonicated by a water-bath type sonicator (Branson 1510) for 30 min.

Dynamic Light Scattering (DLS). A Photocor-FC light scattering instrument with a 5 mW laser light source at 633 nm was used at 25°C, with the scattering angle being 90°. A logarithmic correlator was used to obtain the autocorrelation function, which was analyzed by the method of cumulants to yield a diffusion coefficient. The apparent

hydrodynamic size was obtained from the diffusion coefficient through the Stokes-Einstein relationship.

Small-Angle Neutron Scattering (SANS). SANS measurements were made on the NG-3 (30 m) beamline at NIST in Gaithersburg, MD. Neutrons with a wavelength of 6 Å were selected. The distances between sample chamber and detector were 1.35 m and 13.18 m. The range of scattering vector q was 0.004~0.4 $Å^{-1}$. Samples were prepared with deuterated cyclohexane and measured in 1 mm quartz cells at 25°C. The scattering spectra were corrected and placed on an absolute scale using calibration standards provided by NIST. The data are shown for the radially averaged intensity I versus the scattering vector $q = (4\pi/\lambda) \sin(\theta/2)$, where λ is the wavelength of incident neutrons and θ is the scattering angle. Modeling of SANS data was done using software modules provided by NIST to be used with the IGOR graphing package.[53] Details of these models have been discussed earlier in Section 2.6.2.

Transmission Electron Microscope (TEM). TEM was conducted on a Jeol JEM 2100 microscope at 80 KeV. The positive staining agent, ammonium molybdate (from Sigma-Aldrich), was dissolved in methanol to form a 13 mM stock solution. Desired amounts of this compound were combined with the stock solutions during sample preparation, as described above. The final reverse vesicle samples were diluted to 1 mM and a 1 μL drop was applied on a carbon-coated copper grid, which was then air-dried before imaging was conducted.

6.3. RESULTS

6.3.1. Phase Behavior

In cyclohexane, lecithin forms reverse spherical or ellipsoidal micelles and the resulting solutions are transparent and have a low viscosity essentially identical to that of the solvent.[60] To study the effect of adding C_4-lecithin, we conducted DLS at an overall lipid concentration of 20 mM in d-cyclohexane and as a function of the molar ratio R_0 of C_4-lecithin to lecithin. In addition to the two lipids, all the samples also contained 3.5 mM of NaCl, the role of which is discussed below. Figure 6.1 shows the scattering intensity measured at 90° as a function of R_0. We note that the intensity increases dramatically at $R_0 \sim 0.7$ and then reaches a plateau. The corresponding samples had a clear, bluish tinge, as shown by the photograph of the $R_0 = 2.6$ sample in Figure 6.1. The bluish color is a manifestation of the Tyndall effect, indicating the presence of large scatterers in solution, and it is generally seen for vesicle solutions.[29] Note that the bluish samples still had a low viscosity, comparable to the solvent. The average hydrodynamic radius R_h from DLS of the vesicles increases from 300 to 1300 Å with increasing R_0 (Table 6.1). The above data provide preliminary evidence for a phase transition from reverse micelles to vesicles with increasing R_0. With further increase in R_0, the mixtures phase-separate into a turbid liquid phase and a solid precipitate.

Table 6.1. Hydrodynamic radii (R_h) from DLS for C_4-lecithin + lecithin in d-cyclohexane

C_{lipids} = 20 mM, C_{NaCl} = 3.5 mM, Temp = 25°C				
R_0	0.7	1.0	1.6	2.6
R_h (Å)	294.2 ± 3.8	394.8 ± 3.6	687.8 ± 4.1	1301.7 ± 12.9

R_0: Molar ratio of C_4-lecithin to lecithin

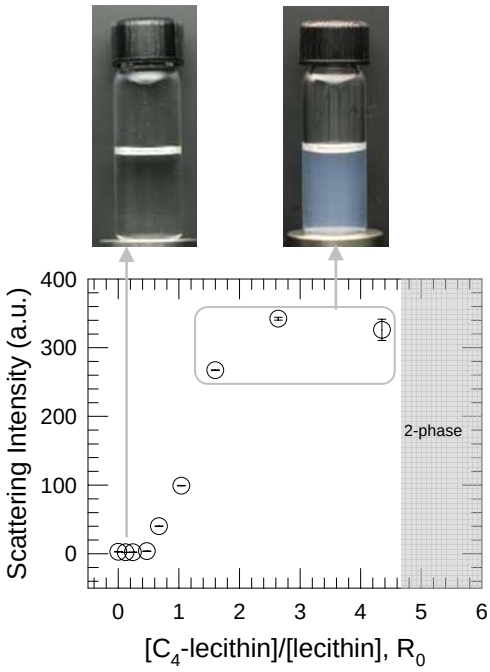

Figure 6.1. Light scattering intensity for C_4-lecithin + lecithin in d-cyclohexane as a function of R_0, the molar ratio of bile salt to lecithin, with the total lipid concentration held constant at 20 mM and 3.5 mM NaCl. The detector angle is 90° and the temperature is 25°C. Photographs of two samples corresponding to different R_0 values are also shown. At low R_0, the sample is transparent and colorless while at an R_0 of 2.6, the sample is bluish and scatters strongly. Finally, when R_0 exceeds ca. 4.5, the sample phase-separates.

We have found that the addition of an appropriate amount of salt, NaCl, is necessary to stabilize the vesicles. Otherwise, the vesicle samples are bluish and homogeneous initially, but within a few hours they tend to phase-separate into co-existing liquid phases. Note that NaCl itself is insoluble in cyclohexane and can be solubilized only when the lipids are present, and that too only at low concentrations. Thus, the amount of NaCl to be added has to be chosen carefully. For example, at a lipid molar ratio R_0 = 2.6 and an overall lipid content of 20 mM, if less than 3 mM of NaCl is present,

the vesicles are not stable, but if the salt concentration exceeds 8 mM, not all the salt can be dissolved within the amphiphilic aggregates (i.e., excess NaCl will precipitate from solution). However, with the right amount of salt, the reverse vesicles remain indefinitely stable and their size also remains unchanged with time.

6.3.2. Small-Angle Neutron Scattering (SANS)

To further elucidate the microstructures in these samples, we resorted to SANS. For these experiments, samples were made in deuterated cyclohexane to achieve the needed contrast between scatterers and solvent. SANS spectra (I vs. q) for 20 mM lipid solutions containing 3.5 mM NaCl are shown in Figure 6.2 at varying R_0. The data for $R_0 = 0$ asymptotes to a plateau at low q and essentially corresponds to micelles. In contrast, there is no plateau at the higher R_0, with the $R_0 = 0.7$ and 2.6 samples showing a q^{-2} decay of the intensity at low q. Such a decay is a signature of scattering from vesicle bilayers (eq 2.15). Importantly, the q^{-2} decay occurs only for samples within the vesicle region in Figure 6.1 (i.e., the region of bluish, low-viscosity samples). Thus, the SANS data support our hypothesis of a phase transition from micelles to vesicles with increasing R_0.

To obtain a more quantitative picture of micellar and vesicular sizes, we model the SANS data using appropriate form factors. The fits are shown as solid curves through the data in Figure 6.2. First, for the case of lecithin in cyclohexane ($R_0 = 0$), the micelles are modeled as ellipsoids of revolution (eq 2.9 and 2.10), and we obtain radii of 21.5 ± 0.1 Å and 29.8 ± 0.1 Å, respectively, for the minor and major axes. Upon the addition of

low amounts of C_4-lecithin, the micelles grow axially, and for R_0 = 0.5, they can be modeled as rigid cylinders (eq 2.6 and 2.7). The cylinder radius is found to be 22.6 ± 0.1 Å, while the contour length is about 197.6 ± 0.6 Å. At higher R_0, the data are fit to the polydisperse unilamellar vesicle model (eq 2.13-2.18). For R_0 = 2.6, an average vesicle radius of 1172.2 ± 10.1 Å is obtained, along with a bilayer thickness of ca. 37 ± 0.1 Å, and a polydispersity of 0.22. This value of the average vesicle radius is consistent with the hydrodynamic radius obtained from DLS (Table 6.1). In sum, the SANS data confirms the evolution of self-assembled reverse structures from spherical micelles to cylindrical micelles to vesicles, in mixtures of C_4-lecithin and lecithin.

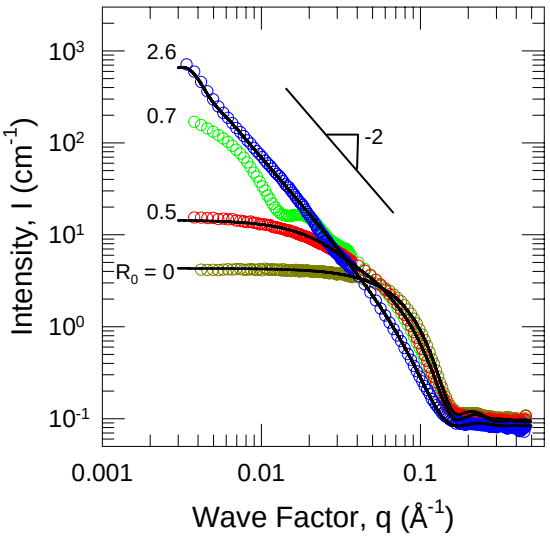

Figure 6.2. SANS data from samples in deuterated cyclohexane containing 20 mM total lipids and 3.5 mM NaCl with different C_4-lecithin:lecithin molar ratios R_0 at 25°C. The solid curves through the data are fits to appropriate models (see text for details).

6.3.3. Transmission Electron Microscope (TEM)

Figure 6.3 shows micrographs of the sample with R_0 = 2.6, which has been shown to contain vesicles by DLS, SANS, and visual observations. Here, 0.8 mM of ammonium molybdate was added as a positive stain that would bind with the headgroups of lipids and thus clearly reveal the bilayers. The TEM images reveal a number of spherical structures with distinct shells, much like conventional micrographs of unilamellar vesicles. The diameters of these structures range from less than 100 nm to 1 μm. Note that these sizes are larger than those obtained from SANS and DLS. We believe this disagreement is due to the collapse of vesicles as the solvent, cyclohexane, is evaporated from the TEM grid. Also, during the evaporation process, vesicles may come into contact

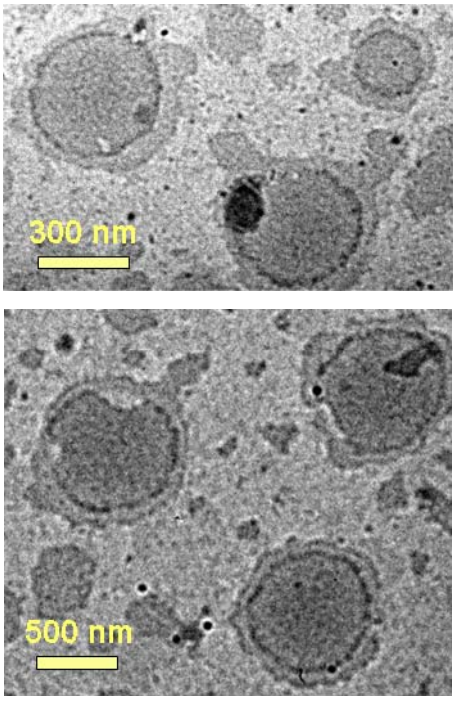

Figure 6.3. TEM image of C4-lecithin + lecithin in cyclohexane at R_0 = 2.6. The image was taken after cyclohexane has been air-dried.

by diffusion, and possibly fuse. Generally conventional TEM (with or without staining) is not as reliable as the technique of cryo-TEM in deducing the structures present in solutions. However, the sample preparation steps in cryo-TEM are optimized only for aqueous solutions, and we have therefore not been able to successfully use this technique for our samples. Despite the limitations of conventional TEM, we stress out that our results using this technique are quite consistent and reproducible. Importantly, the spherical shell-like structures indicated in Figure 6.3 are only seen in the vesicle samples, i.e., they were not observed in the control (micellar) samples.

6.4. DISCUSSION

We will now address the mechanism by which C_4-lecithin transforms lecithin reverse micelles to reverse vesicles. Additionally, we will also address the role of NaCl in this process. It is known that the shape of self-assembled structures formed by amphiphiles is governed by their geometry. This connection is usually expressed in terms of the critical packing parameter $p = a_{tail}/a_{hg}$ where a_{tail} and a_{hg} are the cross-sectional areas of the amphiphile's tail and headgroup respectively.[81] In water, ionic surfactants in the absence of salt have a p around 1/3 (i.e., a "cone" shape), and thus form spherical micelles. When salt is added, the effective headgroup area is reduced due to a decrease in the electrostatic screening length.[27] The packing parameter p then increases to around 1/2 ("truncated cone" shape) and the micelles, in turn, transform from spheres to cylinders. A further increase of p to around 1 ("cylinder" shape) leads to the formation of bilayers and

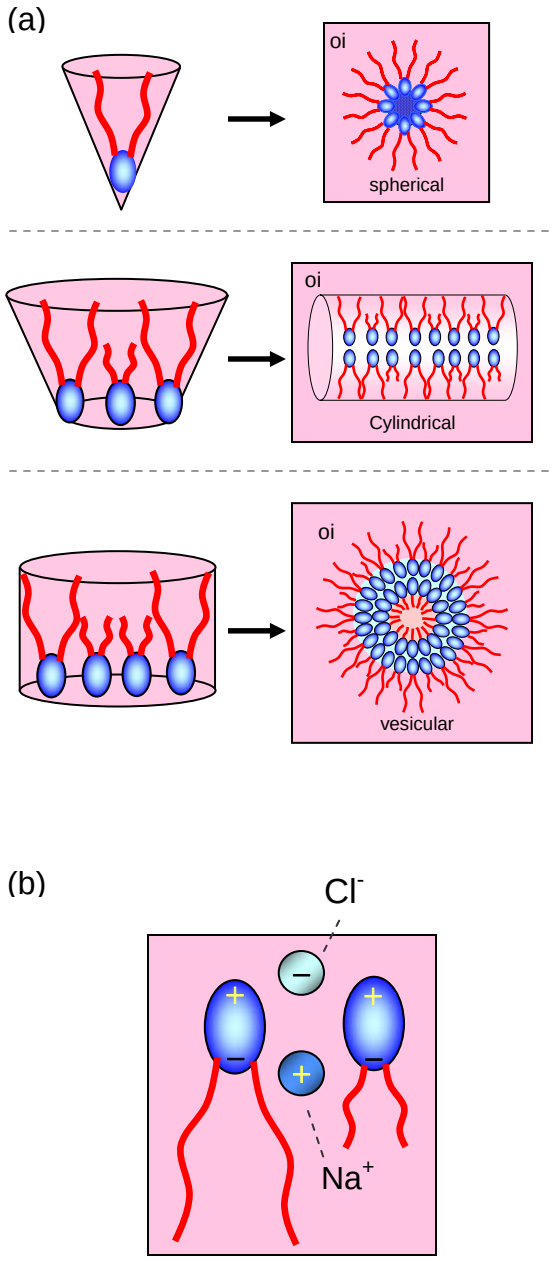

Figure 6.4. (a) Schematic of the reverse self-assembled structures formed by lecithin with increasing C_4-lecithin. Lecithin is shown as a molecule with a blue head and two long red tails, while the C_4-lecithin with two short tails. Lecithin alone tends to form approximately spherical reverse micelles in a nonpolar solvent (oil). When C_4-lecithin is added, the zwitterionic headgroups of C_4-lecithin and lecithin bind each other through electrostatic interactions with NaCl (b), thus expanding the headgroup area. This alters the net geometry from a cone to a truncated cone to cylinder, and thereby induces the spherical micelles to grow into cylinders and then to vesicles.

vesicles. Lipids form vesicles in water because their two hydrophobic tails give them a packing parameter close to 1.

In the case of organic solvents, the shapes of self-assembled structures are still regulated by p but in an opposite way.[60] The formation of reverse micelles requires a packing parameter p much larger than 1, and spherical reverse micelles evidently correspond to an inverse cone shape (Figure 6.4a). For these spheres to transform into cylinders or vesicles, the packing parameter p should *decrease*. Such a decrease can be caused, for instance, by the binding of C_4-lecithin to the lecithin headgroups. In other words, since C_4-lecithin has the same headgroup as lecithin but much shorter tails, it increases the headgroup area a_{hg} while maintaining about the same tail area. The net effect is to decrease p, and at low R_0, the effective geometry resembles an inverse truncated cone (Figure 6.4a), inducing a growth of reverse spheres into cylinders. As R_0 further increases, p keeps decreasing to around 1, thereby driving a second transition to vesicles. Note that in the proposed scenario, the C_4-lecithin orients its hydrophobic tails outward into the organic solvent while its hydrophilic head is directed towards the interior of the cylindrical micelles or vesicle bilayers.

An important aspect in the context of reverse aggregates is the driving force for reverse self-assembly. In water, the dominant driving forces for micellization are hydrophobic interactions.[29] For some cases, such as in mixtures of cationic and anionic surfactants, a strong electrostatic interaction between the headgroups is also necessary.[23] In organic solvents, hydrogen bonding has been suggested to be the driving force for the

growth of reverse spheres to cylinders in lecithin/water and lecithin/bile-salt systems.[60] However, C_4-lecithin and lecithin have the same zwitterionic headgroups, and thus it is unlikely that hydrogen bonding plays a role in the co-assembly of these headgroups. In this regard, it is interesting that solutions containing only C_4-lecithin and lecithin become unstable and phase-separate. Presumably, the interactions between the two lipids are quite weak and are insufficient to stabilize the aggregates. The role of NaCl in imparting stability suggests that it might mediate the interactions between the lipids. Specifically, we hypothesize that the Na^+ and Cl^- ions bind with the negative and positive charges on the lipid headgroups through short-range electrostatic interactions, and thereby serve as a bridge between the C_4-lecithin and lecithin (Figure 6.4b). Note that, while salt-lipid interactions (especially for metal salts) have been widely studied in aqueous solution,[84] such interactions in oils have not been investigated due to the low solubility of the salt in nonpolar media. Further studies are required to clarify the nature of these interactions and their connection with reverse vesicle stability.

6.5. CONCLUSIONS

In conclusion, we have shown that mixing short- and long-chain lecithins in cyclohexane along with a small amount of NaCl gives rise to reverse vesicles. The presence of reverse vesicles has been verified by DLS, SANS, and TEM and the structures have been shown to be unilamellar, with diameters ranging from 60 to 300 nm. Moreover, our preparation technique provides a general framework for systematically tuning reverse aggregate morphology from reverse spheres to cylinders to vesicles, simply by controlling the molar ratio of the two lipids. We suggest that electrostatic

interactions may be important in reverse vesicle formation and stabilization; in particular, NaCl is believed to act like a “glue” in binding lipid headgroups together and in stabilizing the vesicles in solution.

Chapter 7

ORGANOGELS OF BILE SALT AND AOT

7.1. INTRODUCTION

In this chapter, we report that trace amounts of the dihydroxy bile salt (< 1mM) can transform dilute micellar solutions into self-supporting, transparent organogels. Molecular gels are spontaneous assemblies of small molecules into three-dimensional networks that can entrap the solvent via surface tension and capillary forces.[35,85] In recent years, the importance of molecular gels in the chemical and biological sciences has become widely recognized. Numerous kinds of gelator molecules have been reported, some that are capable of gelling organic solvents,[35] and others that can gel water.[85] The gelling ability of these molecules is often associated with their ability to form filamentous structures (chains, tubes, tapes, or fibers).[35,85] Individual filaments, in turn, tend to get connected into a network at junction points through physical bonds. A wide range of physical interaction forces have been implicated in gel formation, including hydrogen bonds, metal coordination bonds, electrostatic bonds, van der Waals forces, and hydrophobic interactions.[35]

An important motivation for the study of synthetic molecular gels has been their structural resemblance to gels found in nature. Indeed, the gel state characterizes much of biology; in particular, the cytoplasm in eukaryotic cells is a gel formed from filaments of cytoskeletal proteins such as actin and tubulin.[86] Numerous biophysical studies have been

conducted on the aqueous assembly of small, globular proteins such as G-actin into filaments (F-actin) and thereby into gel networks.[73,87-89] Synthetic hydrogel mimics of actin have recently been reported from *de novo*-synthesized peptides.[90] However, most of the literature on gels has focused on those formed by organic molecules in non-polar solvents, i.e., "organogels".[35] While such organogels are broadly analogous to actin hydrogels, it is generally believed that their structures are fundamentally different. For example, the junctions in many organogels consist of pseudo-crystalline microdomains, which is not the case for actin gels.[35] The latter do not have specific links or bonds between their filaments; rather, the filaments are so long (~ 20 μm) that they become tightly entangled and interpenetrated, leading to gel-like behavior.[87]

In this chapter, we report a new two-component organogel system formed by the synergistic assembly of two amphiphilic molecules. We will highlight some of the unusual features of these gels, including their formation at very low precursor concentrations. More importantly, we will show that these organogels are structurally and rheologically similar to actin hydrogels. In particular, both types of gels show the property of *strain-stiffening*, i.e., an increase in stiffness (gel modulus) with the amplitude of the deformation. This property has been closely associated with biological gels and tissues, and its origin is very much in debate.[65,72] We believe that the biomimetic properties of our organogels may make them attractive models system for future studies.

The amphiphilic constituents of our organogel are each well-known molecules that have been studied in detail. The major component is the twin-tailed anionic

surfactant, sodium bis(2-ethylhexyl) sulfo-succinate (AOT) (Figure 1.1). It is widely known that AOT forms spherical reverse micelles in a range of organic solvents and over a range of concentrations.[91] The second component of our organogel system is the bile salt, sodium deoxycholate (SDC) (Figure 1.1). Bile salts are physiological surfactants that have been studied extensively in water.[92] In organic solvents, on the other hand, most bile salts, including SDC, are insoluble. Thus, neither the AOT nor the SDC alone can act as an organogelator. However, when a dilute (e.g., 5 mM or 0.2 wt%) reverse micellar solution of AOT in *n*-decane is combined with trace amounts (e.g., 1 mM or 0.04 wt%) of SDC, the result is a transparent organogel that can hold its weight in the inverted vial (Figure 1.1). Note that these samples are gels in the strict rheological sense, i.e., in that they have a finite (non-zero) value of the elastic modulus G' at low frequencies. The less rigorous "tube inversion" test for gelation can be satisfied by AOT/SDC samples at even lower total concentrations.

It is useful to place our investigation in the context of some previous studies with AOT that have dealt with reverse micellization and gelation. John and co-workers have shown that certain phenol and naphthalene derivatives can also transform AOT reverse micelles into organogels.[37,38] Thus, AOT organogels can apparently be induced by a variety of molecules, although the gel structure seems to differ from one gelator to the other. For instance, many of the earlier AOT gels were opaque, indicating that they were composed of larger-scale, hierarchical structures rather than nanoscale filaments.[93] Significantly, our studies with SDC show that it is by far the most efficient gelator for AOT, i.e., it induces AOT organogels at much lower concentrations than the earlier

gelators. Further comparison between the AOT-SDC and earlier organogel systems is provided in subsequent sections of this paper.

Finally, we should clarify our motivation for studying bile salts, which might seem an unusual choice for a gelator, especially in organic solvents. Our interest in bile salts arose out of our earlier study on mixtures of these molecules with the phospholipid, lecithin in organic solvents – these mixtures formed viscoelastic solutions that were shown to contain reverse wormlike micelles.[60] We should reiterate that lecithin-bile salt mixtures were viscoelastic organosols, not gels, i.e., their elastic moduli G' fell to zero at low frequencies. Moreover, a variety of bile salts (not just SDC) could induce lecithin to form viscoelastic organosols. Here, on the other hand, we find that only SDC can induce AOT to form organogels, and furthermore, AOT/SDC gels are formed at much lower concentrations compared to lecithin/SDC solutions. Further discussion on the unique nature of SDC as a gel inducer will be provided later in this paper.

7.2. EXPERIMENTAL SECTION

Materials. The bile salts, SDC (> 97% purity) and AOT (> 98%) were purchased from Sigma-Aldrich. Cyclohexane, deuterated cyclohexane (99.5% D) and *n*-decane were purchased from J. T. Baker, Cambridge Isotopes and Sigma-Aldrich, respectively. All chemicals and solvents were used as received.

Sample Preparation. Mixed solutions containing AOT and bile salts were prepared as follows. First, 100 mM stock solutions of AOT in ethanol and bile salts in methanol were

prepared. Samples of desired composition were prepared by mixing the stock solutions. The ethanol and methanol were then removed by evaporation in a fume hood for 24 h, and the resulting AOT-bile salt film was further dried in a vacuum oven at room temperature for 72 h. The organic solvent (cyclohexane, deuterated cyclohexane or *n*-decane) was then added to this dried film and the sample was stirred until it became transparent and homogeneous. The above procedure ensured the removal of any residual water from the sample, and thereby facilitated reproducibile sample preparation. The samples were equilibrated for at least 3 days at room temperature prior to conducting experiments.

Rheology. Dynamic rheological experiments were performed on an AR2000 stress-controlled rheometer (TA Instruments) using either parallel-plate or couette geometries, which were equipped with Peltier-based temperature control. A solvent trap was used to minimize sample evaporation. Frequency spectra were conducted in the linear regime of the samples, as determined from dynamic strain sweep measurements. To prevent the absorption of moisture by the samples during rheological experimentation, it was found to be advantageous to work under conditions when the relative humidity in the laboratory was low (below 20%).

Small Angle Neutron Scattering (SANS). SANS measurements were made on the NG-7 (30 m) beamline at NIST in Gaithersburg, MD. Neutrons with a wavelength of 6 Å were selected. Two distances of 1.2 m and 15 m between sample and detector were used, so as to yield a range of scattering vector q from 0.004 to 0.4 $Å^{-1}$. Samples for SANS studies

were prepared with deuterated cyclohexane and were measured in 1 mm quartz cells at 20°C. The scattering spectra were corrected and placed on an absolute scale using calibration standards provided by NIST. The data presented here are for the radially averaged intensity I versus the scattering vector $q = (4\pi/\lambda)\sin(\theta/2)$, where λ is the wavelength of incident neutrons and θ is the scattering angle. Modeling of SANS data was done using software modules provided by NIST to be used with the IGOR graphing package.[53] Details of these models have been discussed earlier in Section 2.6.2.

7.3. RESULTS

7.3.1. Visual Observations, Birefringence

Photographs of AOT/SDC organogels in cyclohexane are shown in Figure 1.1. The gels contain 10 mM of AOT and 2 mM of SDC. The gels are shown in inverted vials to indicate that they are rigid enough to support their own weight. Note that the gels are transparent, indicating that their internal structures are in the nanoscale size range. This is in contrast to many organogel systems that tend to be cloudy or opaque – in those cases, the inherent structures are either thick (microscale) fibrils[93] or spherulitic crystallites.[94] The gels do become cloudy as the SDC:AOT molar ratio (X_{SDC}) is increased above 0.25 – however, these samples tend to become unstable with time and are not the focus of our investigation. All gels at low X_{SDC}, however, remain transparent and stable for more than one year when stored in sealed containers.

From a structural standpoint, it is also useful to examine the gels under crossed polarized light. Such a photograph is shown in Figure 7.1 for a series of AOT/SDC samples (20 mM AOT, varying SDC). The figure shows that samples above a SDC concentration of 3 mM (X_{SDC} = 0.15) exhibit pronounced birefringence (all these samples are gels). Note that the samples are being examined at rest, i.e., in the absence of any shear. Birefringence at rest in organogels is usually indicative of spherulites;[94] however, no such structures could be observed by optical microscopy. An alternate source of static birefringence can arise from the alignment of filamentous structures in solution. In particular, it is known that a dispersion of rodlike particles can undergo a transition from isotropic to nematic (1-dimensional order) as the size and/or volume fraction of the particles is increased. Such a transition is driven by entropy and is referred to as an Onsager transition.[95] Thus the birefringence in Figure 7.1 could be indicating that AOT and SDC self-assemble together into rather rigid filaments, and that these filaments spontaneously align to produce nematic gels.

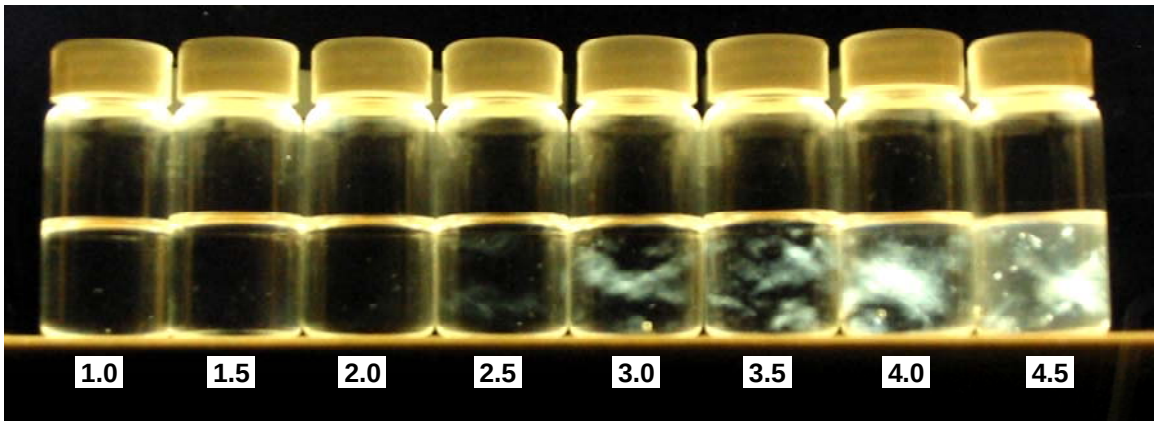

Figure 7.1. Photographs under crossed polarizers of AOT/SDC gels in cyclohexane. The AOT concentration is 20 mM, and the SDC concentrations (in mM) are indicated below each vial. The gels at higher SDC concentrations show birefringence.

We believe that AOT/SDC gels do indeed contain filaments, and we will corroborate this aspect using SANS later in the paper. However, these gels are not true nematics, i.e., there is no Onsager transition in these systems. In this context, the thermal behavior of these gels is revealing. As the birefringent gels are heated to about 80°C, the gels undergo "melting", i.e., they are transformed from self-supporting solids to thin liquids (see below). This melting transition is thermoreversible, i.e., the gel reforms when the sample is cooled. However, the cooled gels no longer exhibit birefringence. If the gel is now shaken vigorously, the birefringence reappears and it does not go away (samples are still strongly birefringent after more than a year). The interpretation here is that the filaments in AOT/SDC gels become aligned by shear, but this alignment is locked in by the volume-filling network. Interestingly, gels of F-actin also have similar properties: they show a persistent birefringence that was initially believed to be indicative of an Onsager transition, but more recently has been correlated with the shear-alignment of F-actin filaments.[96] The similarities with actin gels will be a recurring theme in this paper.

7.3.2. Effects of Temperature, Humidity

As mentioned above, gels of AOT/SDC melt when heated above a characteristic melting temperature T_m. This melting is abrupt, i.e., the sample remains a self-supporting gel up to T_m, but then it rapidly melts at T_m. Such abrupt melting is characteristic of organogels, whereas viscoelastic organosols show a steady, exponential drop in viscosity with temperature. We have studied the variation of T_m with gel composition – these experiments were done for AOT/SDC gels in *n*-decane. T_m was determined by a combination of visual and rheological methods. We found that T_m occurred at ca. 80°C

independent of the SDC:AOT ratio and increased only slightly with AOT concentration (from ca. 79°C to 83°C over an AOT concentration range from 25 to 100 mM). Another point to be addressed is the thermoreversibility – as mentioned, melted gels could be re-solidified upon cooling back to room temperature. However, if a gel were heated well beyond T_m (e.g., to about 90°C), then a precipitate formed in the sample and the gel did not reform upon cooling. This irreversibile precipitation could be due to the thermal degradation or hydrolysis of the precursor molecules (AOT or SDC) at these high temperatures.

Another interesting property of AOT/SDC organogels is that they are very sensitive to water, and thereby to humidity. The addition of trace quantities of water is enough to liquefy the gel. Similarly, if a sample vial is left open and thereby exposed to atmospheric humidity for a few hours, the gel will often melt. Such sensitivity to moisture has been noted before by John and co-workers for their AOT organogels induced by phenolic compounds.[97] This behavior strongly implies that hydrogen-bonding is the driving force for self-assembly and gel formation – the action of water in disrupting the gel can then be attributed to the disruption of hydrogen bonds by water molecules.

7.3.3. Linear Rheology

We use dynamic rheological techniques to study the onset and evolution of AOT/SDC gels as a function of composition. Our main focus is on the linear sample response at low strain amplitudes and as a function of frequency. First, we consider trends as a function of SDC content at fixed AOT – typical data are shown in Figure 7.2

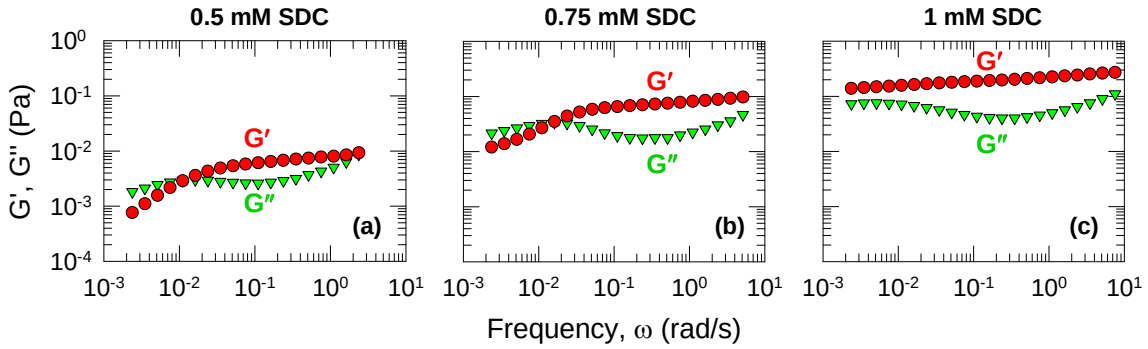

Figure 7.2. Dynamic rheology at 20°C of three AOT-SDC mixtures in cyclohexane, each containing 10 mM AOT and with varying SDC concentrations (as indicated on the plots). Each plot shows the elastic modulus G' (circles) and the viscous modulus G'' (triangles) as functions of frequency ω.

for 10 mM AOT samples in cyclohexane at 20°C. Note that a 10 mM solution of AOT in cyclohexane contains spherical reverse micelles and its viscosity is close to that of the solvent. Figure 7.2a shows that adding just 0.5 mM of SDC (X_{SDC} = 0.05) converts the AOT micellar solution into a viscoelastic fluid. In this case, the elastic modulus G' exceeds the viscous modulus G''at high frequencies, indicating elastic behavior, whereas G'' exceeds G' at low frequencies, indicating viscous behavior. The crossover of G' and G'' occurs at a frequency ω = 0.01 rad/s and the inverse of this frequency gives a characteristic relaxation time of 100 s for this sample. Note that this kind of dynamic spectrum is typical of transient entangled networks (e.g., of polymer chains or wormlike micelles in solution). Increasing the SDC content to 0.75 mM does not change the nature of the response, but the entire frequency spectrum shifts upward to higher moduli. Also,

at low frequencies below the crossover point, the slopes of G' and G'' become closer to each other, which indicates the onset of gel formation. As the SDC concentration is increased to 1 mM (X_{SDC} = 0.1), the dynamic rheological response becomes characteristic of an organogel (Figure 7.2c). Here G' is nearly independent of frequency and exceeds G'' over the entire range of frequencies, indicating that the gel is an elastic material with an infinite relaxation time (and thereby an infinite viscosity). The level of G' characterizes the strength and stiffness of the gel, and can be termed the gel modulus.

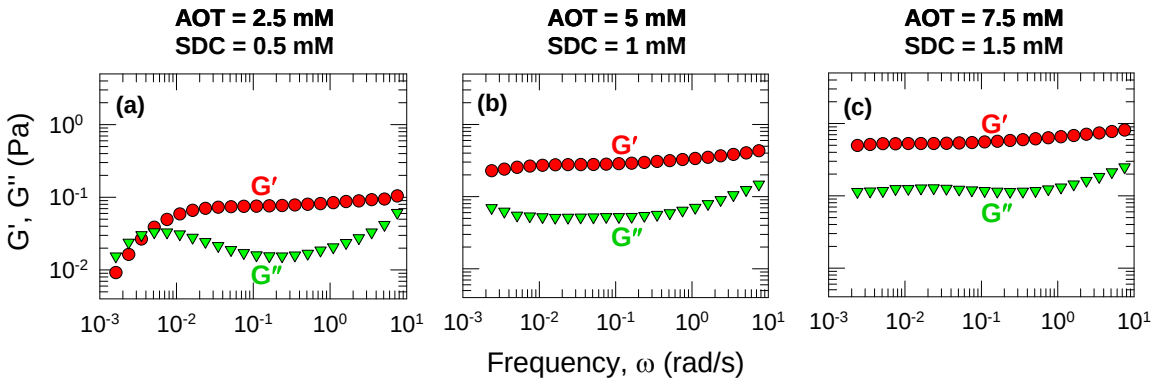

Figure 7.3. Dynamic rheology at 20°C of three AOT-SDC mixtures in cyclohexane with a constant molar ratio of SDC:AOT = 0.2 and with varying overall concentration. The composition of each sample is indicated on the corresponding plot. Each plot shows the elastic modulus G' (circles) and the viscous modulus G'' (triangles) as functions of frequency ω.

Next, we consider trends in rheology as a function of the overall (AOT + SDC) concentration. These experiments were done at a constant SDC:AOT ratio, X_{SDC} = 0.2. Data at 20°C for a series of these samples in cyclohexane are shown in Figure 7.3. We observe that combining just 2.5 mM AOT with 0.5 mM SDC gives rise to a strongly

viscoelastic solution (Figure 7.3a). Here, G' and G'' cross at a frequency $\omega = 0.004$ rad/s, indicating a relaxation time of 250 s for the sample. As the concentration is increased to 5 mM AOT and 1 mM SDC (Figure 7.3b), we find the onset of a gel-like response. Note again that G' is frequency-independent and exceeds G'' over the frequency range, i.e., the sample satisfies the strict rheological definition of a gel. Increasing the concentration to 7.5 mM AOT and 2.5 mM SDC makes the gel stronger, i.e., the value of G' becomes higher (Figure 7.3c). The above rheological data thus show that very low concentrations of AOT and SDC are enough to produce organogels. Figure 7.4 shows the scaling of gel modulus G' with overall volume fraction ϕ of the amphiphiles (AOT + SDC) for a molar ratio $X_{SDC} = 0.15$. G' increases with ϕ according to a power law with an exponent of 2.1. This exponent is close to that found for gels of semiflexible biopolymers such as actin, where the values range from 2.0 to 2.2.[78,98]

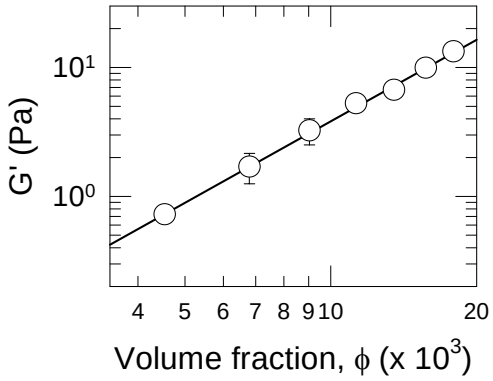

Figure 7.4. Elastic modulus at 20°C of AOT-SDC mixtures in cyclohexane as a function of the total amphiphile volume fraction ϕ. The SDC:AOT molar ratio is 0.15 in all these samples. The solid line through the data corresponds to a scaling of $G' \sim \phi^{2.1}$.

7.3.4. Non-Linear Rheology (Strain-Stiffening)

We now briefly discuss the non-linear rheology of AOT/SDC organogels, i.e., their response at high deformations exceeding the linear viscoelastic regime. Figure 7.5 shows the dependence of elastic modulus G' on strain-amplitude γ at a constant frequency of 10 rad/s. Data are shown for gels with different (AOT+SDC) concentrations and a constant X_{SDC} = 0.15. In the low-strain regime (γ < 0.3), G' is a constant (= G_0), representing the linear response. As the strain-amplitude of the deformation is increased, there is an increase in G' to a maximum value (= G_{max}) followed by an abrupt decrease. This increase in G' vs. γ is termed strain-stiffening or strain-hardening or strain-thickening by different researchers. Note that an increase with strain-amplitude is also seen for G'', but the focus is usually on G' since it is the parameter that most correlates with the network structure. Similar behavior is also seen at other frequencies as well. Figure 7.5 also shows that the strain γ_{max} at which G' shows a maximum and the magnitude of the strain-stiffening effect (i.e., the ratio G_{max}/G_0) are higher at lower amphiphile concentrations. As the AOT/SDC network becomes more dense (e.g., at overall concentrations exceeding 25 mM), strain-stiffening becomes negligible.

To put strain-stiffening in perspective, it is worth noting that most polymeric or colloidal networks generally show strain-thinning, where G' decreases with γ beyond the linear regime. Strain-thinning can be understood to occur due to the deformation-induced rupture of the physical bonds in the network. Strain-stiffening, on the other hand, is unusual because it implies that the network becomes stiffer when it is deformed compared to its stiffness at rest. In effect, the tendency to stiffen makes the network

becomes more resistant to rupture. Interestingly, strain-stiffening has been seen in a range of soft biological materials (e.g., blood clots, cornea, blood vessels) and biopolymer networks, leading some researchers to speculate that the added resistance at large deformations is a material property that has useful biological relevance.[65] A model system for laboratory studies on strain-stiffening has been gels of F-actin.[65,72] Significantly, actin gels show the same trends as a function of concentration as seen in Figure 7.5, i.e., γ_{max} in these gels drops with increasing actin concentration.[73]

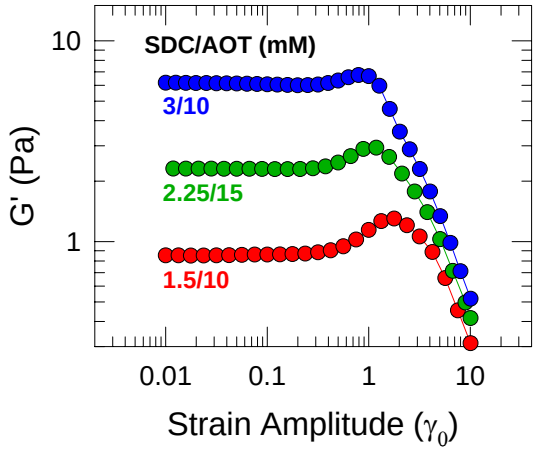

Figure 7.5. Strain-stiffening response at 20°C of AOT-SDC samples in cyclohexane (SDC:AOT molar ratio = 0.15 in all cases). All samples show an increase in their elastic modulus G' over a range of strain amplitudes, i.e., they exhibit strain-stiffening.

7.3.5. Small-Angle Neutron Scattering (SANS)

Finally, we turn to SANS to elucidate the microstructure of AOT/SDC gels. For these experiments, samples were made in deuterated cyclohexane (these samples were identical to those in cyclohexane). The AOT concentration was fixed at a relatively low

value of 20 mM so as to minimize interactions (structure factor effects) between the assemblies. SANS spectra (I vs. q) for 20 mM AOT solutions containing varying amounts of SDC (from 0 to 5 mM) are shown in Figure 7.6. It is clear that the addition of SDC causes a dramatic increase in the low-q scattering, while there are slight (but important) changes at higher q as well. The increase in low-q scattering is consistent with a transformation of spherical AOT micelles into elongated structures (note also the asymptotic slope of –1 at low q, which is indicative of cylinders).[47] Thus, SANS confirms the growth of filamentous structures upon addition of SDC to AOT solutions.

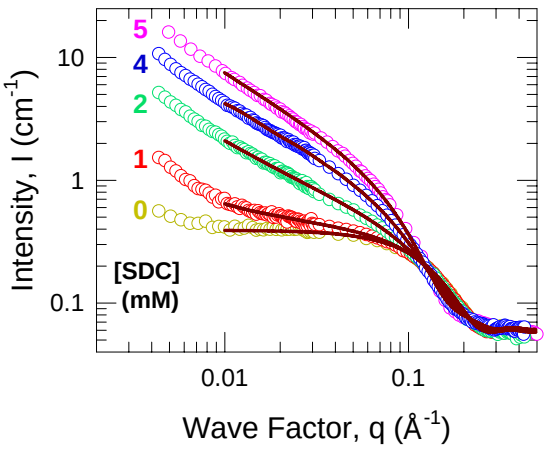

Figure 7.6. SANS data from samples in deuterated cyclohexane containing 20 mM AOT and different SDC concentrations. The solid curves through the data are fits to appropriate models (see text for details).

Further insight can be obtained by modeling the SANS data using appropriate form factors (eq 2.5-2.8). Model fits are shown as solid lines through the data in Figure 7.6, and we focus on the data at $q > 0.01$. First, for the case of AOT alone in cyclohexane,

we can adequately model the micelles as spheres (eq 2.5) with radii of 16.1 ± 0.1 Å, in agreement with other studies.[36,91] As SDC is added, we expect the spheres to grow into cylinders; however, we cannot fit the SANS data for AOT/SDC samples assuming cylinders alone to be present (eq 2.6 and 2.7) (in particular, the fits break down at high q, where SANS mainly probes the cross-section of the micelles). We therefore hypothesize that the AOT/SDC samples contain co-existing populations of spherical micelles and cylindrical filaments. This can be rationalized if we assume that at these low molar ratios of SDC:AOT, the SDC collects in only some of the AOT spherical micelles, which in turn grow while the rest remain intact. Accordingly, we use eq 2.8 to model the data, and this yields excellent fits. From the fit parameters (Table 7.1), we infer that all samples contain co-existing spheres with radii of 16 Å (consistent with pure AOT micelles) and cylinders of radii 22 Å. With increasing SDC, the key parameter that changes is the fraction of cylinders, which increases from 0 (no SDC) to 60% (at SDC = 5 mM). In turn, an increasing fraction of cylindrical filaments correlates with the onset of gel-like behavior in the sample.

Table 7.1. Parameters of SANS modeling for AOT + SDC in d-cyclohexane

Concentration of AOT = 20 mM				
[SDC] (mM)	R_s (Å)	R_c (Å)	ϕ_s*	ϕ_c
0	16	-	1	0
1	16	22	0.97	0.03
2	16	22	0.81	0.19
4	16	22	0.57	0.43
5	16	22	0.40	0.60

R_s: radius of sphere ϕ_s: volume fraction of sphere
R_c: radius of cylinder ϕ_c: volume fraction of cylinder
*The errors for volume fractions are within ± 1%

7.3.6. Indirect Fourier Transform (IFT)

The notion of co-existing spherical micelles and cylindrical filaments might appear unusual, although a similar idea has been proposed earlier for other AOT-based organogels.[99] To further substantiate this claim, we have resorted to modeling the SANS data in a different way, using the IFT technique. This method allows SANS data to be analyzed without assuming *a priori* if spheres or cylinders are present. Pair distance distribution functions $p(r)$ from IFT are shown in Figure 7.7 for the $I(q)$ data from Figure 7.6. For the pure AOT solution, $p(r)$ is symmetrical, and this is typical of spherical micelles. The point where $p(r)$ meets the x-axis gives the micelle diameter, which is 33 Å in this case, in good agreement with the value obtained above. Next, we examine how $p(r)$ changes upon addition of SDC. Note that if only cylinders are present, $p(r)$ should show an inflection point followed by a linear decrease to zero at a value of r equal to the cylinder length.[100] However, the $p(r)$ curves for AOT/SDC mixtures are not consistent with either spherical or cylindrical structures alone. For example, the $p(r)$ for 1 mM SDC initially tracks the symmetrical curve of pure AOT, but then it has a further tail that extends up to 270 Å. The $p(r)$ curves for 2 and 4 mM SDC have inflection points at 36 and 45Å, respectively, followed by shoulders at higher values of r and eventual drops to zero above 400 Å. These complicated $p(r)$ curves imply a co-existence of spheres and cylinders, although it is difficult to deconvolute their individual sizes. Nevertheless, IFT does offer model-independent confirmation for the presence of two distinct types of structures in AOT/SDC samples, in agreement with our direct SANS modeling. Why do only some AOT spherical micelles grow into cylindrical filaments? The answer is

discussed in the next section, where we also explain why the value of cylinder radius of 22 Å is significant.

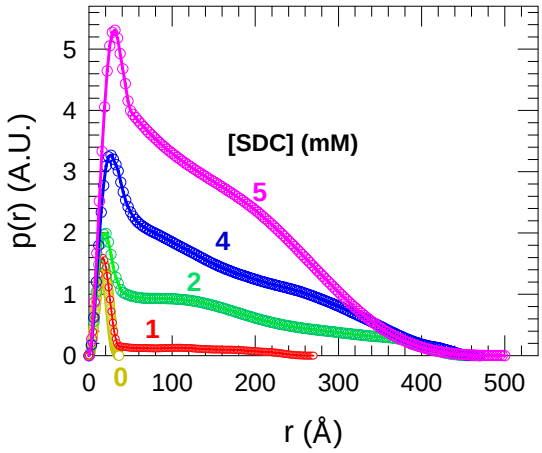

Figure 7.7. Pair distance distribution functions $p(r)$ obtained by IFT analysis of the SANS data shown in Figure 7.6 for 20 mM AOT + SDC samples in deuterated cyclohexane.

7.4. DISCUSSION

We have shown using SANS that the bile salt, SDC transforms spherical AOT micelles into cylindrical filaments. As the SDC:AOT ratio is increased, the number density of these filaments increases and so does their length. When the filaments are sufficiently numerous and long, we believe they form a highly interpenetrated and entangled network, leading to gel-like behavior of the sample. Note that there is no evidence for any other types of physical or chemical crosslinks in AOT/SDC networks. Such gel formation simply by entanglement of long, semi-flexible filaments is directly analogous to that occurring with biopolymers such as actin.[87] One might argue that the filaments in both AOT/SDC and actin networks will indeed relax by reptation at

extremely long times since they are not constrained by crosslinks. However, for all practical purposes the samples behave as gels, i.e., as permanent networks, and they also satisfy the rheological definition of a gel (Figures 7.2, 7.3).

7.4.1. Structure of AOT/SDC Filaments

Given that AOT/SDC samples behave as gels due to the presence of filaments, we still need to explain why SDC induces these filaments to form. Also, why do filaments co-exist with spherical micelles, as suggested by SANS? To answer these questions, we need to know how SDC molecules are distributed within the filaments. Being insoluble in non-polar solvents, SDC can either orient next to the AOT molecules at the interface, or it could arrange in the core of the filament. If the SDC were oriented at the interface, the radius of the filament would be identical to that of AOT spherical micelles (i.e., 16 Å). However, from SANS, we estimated a larger filament radius of 22 Å (i.e., diameter of 44 Å). We suggest that this larger radius can be explained only by assuming that the SDC molecules are stacked in the filament core and surrounded by AOT molecules (as depicted in Figure 7.8).

The above model for AOT/SDC filaments can explain several aspects. First, we mentioned earlier that among all the bile salts we have studied, SDC is the only one that induces AOT to form organogels.[101,102] Significantly, SDC is also the only bile salt that can directly form a hydrogel in water – this gel has been shown to consist of helical SDC fibrils with a radius of 9 Å, as determined by X-ray diffraction.[103] If we combine the above fibril radius with the length of a fully extended AOT molecule (13 Å),[91] we obtain

a net figure of 22 Å, which nicely matches with the filament radius from SANS modeling. Also, our model suggests that the binding of SDC to AOT must be a *highly co-operative* process, i.e., for a filament to form, there has to be a sufficient number of SDC molecules in the core. This readily explains why filaments must co-exist with native AOT micelles; in other words, only a few spherical micelles can grow into filaments when only a few SDC molecules are present (i.e., at low SDC:AOT molar ratios). In summary, we believe the unique ability of SDC to stack and form fibrils also explains its action as an organogel-inducer. The core of AOT micelles provides a hydrophilic environment in which SDC can stack, and this must be facilitated by strong hydrogen-bonding between the AOT headgroups and the hydroxyl groups on the outer face of SDC.

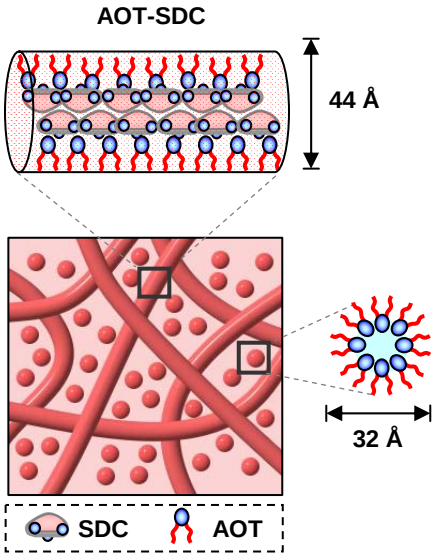

Figure 7.8. Schematic of the structures formed when AOT and SDC are added to nonpolar liquids (oils). AOT is represented as a molecule with a blue head and two red tails, while SDC is represented as a facial amphiphile, following Figure 1.1. AOT alone tends to form spherical reverse micelles in oil. When small amounts of SDC are added, the SDC preferentially segregates in some of these spheres, causing their transformation into long cylinders. The remaining AOT spheres remain intact and coexist with the cylinders. Based on their radii from SANS, the cylinders are expected to comprise stacks of SDC surrounded by AOT molecules.

7.4.2. Similarities with Actin Gels

Finally, it is worth summarizing all the features that are shared between AOT/SDC organogels and actin hydrogels. Structurally, both materials are gels simply due to the entanglement of long, semiflexible filaments. No other crosslinking agents are necessary to yield a gel, although in the case of actin, the addition of crosslinking proteins can further strengthen the gel. Both gels are formed at very low concentrations of precursor molecules (less than 1 wt% or 0.1 mg/mL). In both cases, the initial structures present are spheres (AOT micelles and G-actin monomers) that transform into filaments upon appropriate conditions. Interestingly, in the case of actin also, a co-existence of filaments and spheres is known to occur, quite similar to that shown in Figure 7.8.[104,105] Actin filaments are also known to be semiflexible, i.e., their persistence length l_p is comparable to their contour length.[106] Although, we have not measured l_p for AOT/SDC filaments, our hypothesis for their structure (with the planar and rigid steroidal rings of SDC in the core, Figure 7.8), suggests that these filaments should also be quite rigid.

Actin and AOT/SDC gels have similar properties as well. Both gels show a persistent birefringence, reminiscent of a nematic fluid, although it is more likely to reflect the shear-induced creation of aligned domains that are trapped within the network. Both actin and AOT/SDC gels also exhibit similar rheological response in the linear regime, and their gel moduli scale with concentration in similar ways. Lastly, both types of gels exhibit strain-stiffening, i.e., their gel moduli increase with strain amplitude. Even the variation in γ_{max} with concentration (Figure 7.5) is similar for the two classes of gels.

Currently, the origin of strain-stiffening is a matter of debate. One mechanism attributes strain-stiffening to the intrinsic rigidity of network filaments.[65] If this is correct, it reiterates that AOT/SDC filaments are quite rigid, much like actin filaments. Indeed, the rigidity imparted by steroidal bile salt to AOT filaments is analogous to the rigidification of lipid bilayers by addition of steroidal cholesterol.[107]

7.5. CONCLUSIONS

We have shown that the addition of the bile salt, sodium deoxycholate (SDC), to AOT reverse micellar solutions induces a transition from a low-viscosity liquid to a solid-like organogels. Remarkably, organogels can be induced by very small (submillimolar) amounts of SDC. SANS measurements show that the spherical AOT micelles are progressively transformed into long, semiflexible filaments by addition of SDC. The gel is believed to form by the entanglement and interpenetration of these filaments into a volume-filling network. Based on SANS data, we suggest that the filaments consist of an AOT shell surrounding a core of planar and rigid SDC molecules, with the AOT and SDC connected by hydrogen bonds. AOT/SDC gels share many properties with gels of biopolymers such as actin, including their birefringence, gel-like linear rheology, and strain-stiffening in non-linear rheology.

Chapter 8

CONCLUSIONS AND RECOMMENDATIONS

8.1. CONCLUSIONS

Unlike conventional studies on the self-assembly of amphiphiles in aqueous solution, we have focused on the reverse self-assembly of lecithin and AOT in nonpolar solvents in conjunction with other additives. Previous studies that dealt with reverse aggregates have only used water as an additive to tune aggregate morphology. However, other additives such as salts or short lipids that are generally insoluble in nonpolar solvents have not been considered. In this dissertation, we have reported three new classes of reverse aggregates: reverse wormlike micelles, reverse vesicles and organogels. We have made connections between these new reverse systems with existing reverse systems and even with existing aqueous self-assembled systems. These connections can be described by simple rules that are summarized below.

Firstly, we have shown that, apart from water, the addition of bile salt, a biological amphiphile, to lecithin organosols also induces a transition from discrete spherical reverse micelles to entangled networks of wormlike reverse micelles (Chapter 3). Bile salts and water are very different in chemical structure; however, both of them are capable of hydrogen-bonding with lecithin. In turn, both can alter the effective geometry of lecithin to that of a truncated cone, thus favoring cylinders. This explains the analogous effects of bile salt and water on reverse micellar growth.

In addition to reverse wormlike micelles, we have extended our studies to a different and rare form of reverse aggregate, i.e., reverse vesicles (Chapter 6). Based on the geometric theory of self-assembly, if the effective molecular geometry is reduced to a cylindrical shape, reverse vesicles may be formed. We accomplished this by combining a short-chain C_4-lecithin with conventional lecithin (C_{17}) in cyclohexane. C_4-lecithin has the same hydrophilic headgroup as lecithin but much shorter tails. When the two lipids pack together, the headgroup area expands while the tail area remains about the same, thus bringing the critical packing parameter close to 1 (i.e., a cylinder shape). Coincidentally, mixing short- and long-chain lipids in aqueous solution has been shown to produce stable unilamellar normal vesicles.[83] Also, we showed that to stabilize the reverse vesicles, we need to add a trace of sodium chloride to help the lipids to bind together via electrostatic interactions.

The third reverse structure we have discovered is a self-assembled organogel (Chapter 7). The addition of bile salt, SDC into AOT reverse micellar solution induces a solid-like organogel. Unlike wormlike micellar solutions that flow very slowly, the organogel can support its own weight when the sample is inverted. This is because a network that comprises long and rigid filaments can hold the solvent through capillarity. We believe the cores of the filaments are filled with stacks of SDC molecules with the AOT molecules surrounding them. Interestingly, SDC is a "dual" gelator that can both gel water and nonpolar liquids. In water, SDC is the only bile salt that can form a gel at neutral pH. We believe that the hydrophilic cores of AOT micelles can provide an

environment where SDC can self-assemble into fibrillar structures in a manner very similar to that in water.

From the above instances, we see that, although water and nonpolar liquids are on opposite sides in terms of polarity, there are many analogous effects in these two systems. For example, the interactions in water between bile salt-lecithin and metal ion-lecithin also take place in nonpolar liquids. Moreover, certain self-assembly phenomena can occur in both water and nonpolar liquids, such as the self-assembly of SDC into fibrils. More generally, the regulation of amphiphile geometry through the critical packing parameter can not only guide self-assembly in water but also in nonpolar liquids. In underscoring the fact that only a thin line separates water and nonpolar liquids, it is worth noting the phenomenon of enzymatic catalysis in organic solvents. It has been shown that enzymes that are normally active in water can also act as catalysts in organic solvents and they can even have a higher stability.[108]

Apart from the studies of the self-assembled structures, we have also presented interesting and unusual rheological properties of reverse wormlike micelles. First, we have shown that normal and reverse worms respond differently to temperature. For normal worms, the plateau modulus remains constant with temperature, while for reverse worms, it decreases exponentially with temperature. The results emphasize the different driving forces for the formation of normal and reverse worms. Specifically, it confirms hydrogen-bonding as the key factor that drives the self-assembly and growth of reverse worms. Also, we have reported a strain-stiffening behavior in reverse worms formed by

mixing bile salt and lecithin. Unlike the response of conventional gels or viscoelastic solutions, the elastic modulus of this system increases with strain amplitude in the non-linear regime. Our study highlights the importance of the polydisperse population and the "living" character of the worms in dictating the stiffening behavior. More importantly, this system provides a simple and inexpensive model to further investigate the phenomenon of strain-stiffening, which until now has been mainly studied by biophysicists in complicated model biopolymer systems.

8.2. RECOMMENDATIONS FOR FUTURE WORK

Based on the systems we have reported, it is highly possible to explore new reverse systems following the hypotheses and ideas we have provided. Moreover, although this dissertation focuses on the fundamental aspects of reverse self-assembly, certain promising applications exist for some of the new systems we have discovered. We suggest three feasible projects for future work, and these are briefly described below.

8.2.1. Reverse Aggregates Induced by Multivalent Ions

The hypothesis of formation of reverse worms in Chapter 3 was that the addition of bile salts alters the net geometry of lecithin from one that favors spheres to one favoring cylinders. Based on this hypothesis, we have sought to identify other molecules that can also induce the formation of cylinders when added to lecithin. These kinds of molecules must have the ability to bind with lecithin so that they can alter the effective geometry. We have presented in Chapter 7 that NaCl plays an important role in

stabilizing reverse vesicles. In fact, studies have shown that monovalent ions have weaker binding strength with phosphocholine headgroups than di- and trivalent ions.[84,109] Thus, multivalent ions, such as Ca^{2+} and La^{3+} may be good candidates for inducing reverse aggregates. Nobody has studied the effects of these ions in organic media because salts are known to be insoluble in nonpolar liquids. Our experiments, however, have shown that if lecithin is present in the organosol, salts can indeed be dissolved in the sample. What is more, salts of multivalent ions, such as $CaCl_2$, do increase the viscosity of the solution and ultimately lead to a strong organogel (Figure 8.1), whereas NaCl does not. More importantly, this organogel can be formed in biocompatible solvents, such as ethyl myristate and butyl laurate, thus offering a potential candidate for drug delivery applications. We again conjecture that this effect is due to the binding of Ca^{2+} to lecithin headgroups and the resulting alteration of the molecular geometry. As part of future work, the effects of salt type and concentration on reverse self-assembly can be systematically studied.

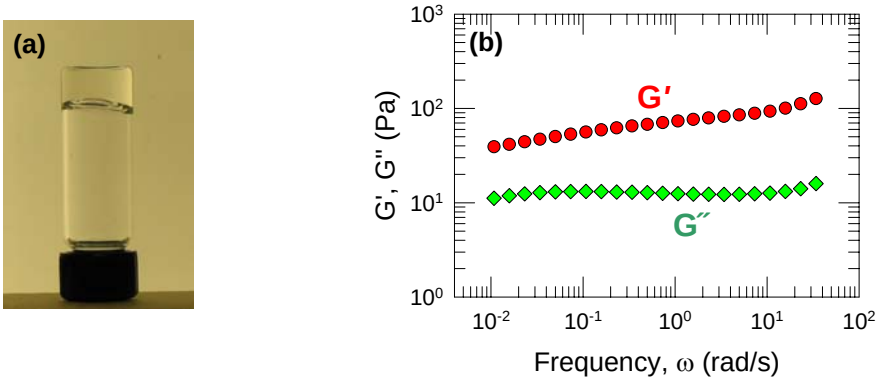

Figure 8.1. (a) Photograph of a sample containing 40 mM lecithin and 13 mM $CaCl_2$ in *n*-decane. The sample supports its own weight in the overturned vial. (b) Dynamic rheology at 25°C of this sample, showing a response typical of gels.

8.2.2. Encapsulation of Model Compounds by Reverse Vesicles

Since vesicles are containers that have an interior liquid core, they can encapsulate a variety of solutes such as drugs, cosmetic ingredients or agrochemicals. These solutes could then be released slowly and in a controlled manner through the vesicle bilayer. Since many drugs and other commercially relevant molecules are hydrophobic, it is quite possible that reverse vesicles could prove to be a useful structure and could form the basis for new applications. But first we need to measure the encapsulation ability of reverse vesicles for different hydrophobic solutes. Oil-soluble dyes such as nile red, or oil-soluble biological molecules such as cholesterol, can be ideal model compounds for encapsulation experiments. The encapsulation efficiency of vesicles for a given solute is usually determined by passing the vesicle-solute mixtures through a chromatography column.[110] Here, since the density difference between lipids and organic solvents is relatively large, an even simpler way is to use a centrifuge to separate the vesicles with encapsulated solute from free, unencapsulated solute. Preliminary experiments show that reverse vesicles can indeed be separated from solutions by centrifugation, and they remain stable during this process.

8.2.3. Drug Delivery Using Lecithin/Bile Salt Reverse Worms

Wormlike micelles offer several advantages for drug delivery. Take normal worms as an example: hydrophilic drugs can be suspended in these viscoelastic solutions, while hydrophobic drugs can be intercalated into hydrophobic core of worms. Moreover, the flexibility of worms allows them to penetrate through nanoporous membranes,

whereas vesicles may be blocked. In fact, wormlike micelles have been shown to be capable of tissue permeation and controlled release.[111]

Interestingly, reverse worms of lecithin/water/oil have been used as a vehicle for dermal and transdermal drug delivery.[6] These worms are biocompatible and have been proven to be safe for dermal treatment. The micelles can enhance skin penetration and are effective for the treatment of muscle spasm as well as in the management of peripheral or neuropathic pain. Much like the lecithin/water/oil system, the new reverse worms of lecithin/bile salts that we have reported are also biocompatible. The bile-salt-based worms also have a higher elastic modulus at the same concentration, i.e., the samples are stiffer. Also, they are more stable, as they are able to maintain a high viscosity for several months while lecithin/water worms tend to soften gradually with time. More importantly, this system is water-free, which may be advantageous to retain the stability and activity of some drugs. From these standpoints, we believe that lecithin/bile salt reverse worms may be promising for drug delivery applications.

REFERENCES

1. Knezevic, Z. D.; Siler-Marinkovic, S. S.; Mojovic, L. V., Kinetics of lipase-catalyzed hydrolysis of palm oil in lecithin/izooctane reversed micellles. *Applied Microbiology and Biotechnology* **1998,** 49, (3), 267-271.

2. Madamwar, D.; Thakar, A., Entrapment of enzyme in water-restricted microenvironment for enzyme-mediated catalysis under microemulsion-based organogels. *Applied Biochemistry and Biotechnology* **2004,** 118, (1-3), 361-369.

3. Van Horn, W. D.; Simorellis, A. K.; Flynn, P. F., Low-temperature studies of encapsulated proteins. *Journal of the American Chemical Society* **2005,** 127, (39), 13553-13560.

4. Dreher, F.; Walde, P.; Walther, P.; Wehrli, E., Interaction of a lecithin microemulsion gel with human stratum corneum and its effect on transdermal transport. *Journal of Controlled Release* **1997,** 45, (2), 131-140.

5. Kreilgaard, M., Influence of microemulsions on cutaneous drug delivery. *Advanced Drug Delivery Reviews* **2002,** 54, S77-S98.

6. Kumar, R.; Katare, O. P., Lecithin organogels as a potential phospholipid-structured system for topical drug delivery: A review. *AAPS Pharmscitech* **2005,** 6, (2).

7. Luisi, P. L.; Scartazzini, R.; Haering, G.; Schurtenberger, P., Organogels from water-in-oil microemulsions. *Colloid and Polymer Science* **1990,** 268, (4), 356-374.

8. Scartazzini, R.; Luisi, P. L., Organogels from lecithins. *Journal of Physical Chemistry* **1988,** 92, (3), 829-833.

9. Schurtenberger, P.; Magid, L. J.; King, S. M.; Lindner, P., Cylindrical structure and flexibility of polymer-like lecithin reverse micelles. *Journal of Physical Chemistry* **1991,** 95, (11), 4173-4176.

10. Schurtenberger, P.; Scartazzini, R.; Luisi, P. L., Viscoelastic properties of polymer-like reverse micelles. *Rheologica Acta* **1989,** 28, (5), 372-381.

11. Schurtenberger, P.; Scartazzini, R.; Magid, L. J.; Leser, M. E.; Luisi, P. L., Structural and dynamic properties of polymer-like reverse micelles. *Journal of Physical Chemistry* **1990,** 94, (9), 3695-3701.

12. Shchipunov, Y. A., Lecithin organogel - A micellar system with unique properties. *Colloids and Surfaces A-Physicochemical and Engineering Aspects* **2001,** 183, 541-554.

13. Simorellis, A. K.; Van Horn, W. D.; Flynn, P. F., Dynamics of low temperature induced water shedding from AOT reverse micelles. *Journal of the American Chemical Society* **2006,** 128, (15), 5082-5090.

14. De, T. K.; Maitra, A., Solution behavior of aerosol-OT in nonpolar-solvents. *Advances in Colloid and Interface Science* **1995,** 59, 95-193.

15. Zulauf, M.; Eicke, H. F., Inverted micelles and microemulsions in the ternary-system H_2O-aerosol-OT-isooctane as studied by photon correlation spectroscopy. *Journal of Physical Chemistry* **1979,** 83, (4), 480-486.

16. Harrison, W. J.; McDonald, M. P.; Tiddy, G. J. T., Phase-Behavior and mesophase formation in the lithium phenylstearate + 1-phenylheptane system. *Journal of Physical Chemistry* **1991,** 95, (10), 4136-4140.

17. Hellweg, T.; Eimer, W., The micro-structures formed by Ni^{2+}-AOT/cyclohexane/water microemulsions: a light scattering study. *Colloids and Surfaces A-Physicochemical and Engineering Aspects* **1998,** 136, (1-2), 97-107.

18. Steytler, D. C.; Jenta, T. R.; Robinson, B. H.; Eastoe, J.; Heenan, R. K., Structure of reversed micelles formed by metal salts of bis(ethylhexyl) phosphoric acid. *Langmuir* **1996,** 12, (6), 1483-1489.

19. Yu, Z. J.; Neuman, R. D., Giant Rodlike Reversed micelles formed by sodium bis(2-Ethylhexyl) phosphate in *n*-heptane. *Langmuir* **1994,** 10, (8), 2553-2558.

20. Hofmann, A. F.; Small, D. M., Detergent Properties of Bile Salts - Correlation with Physiological Function. *Annual Review of Medicine* **1967,** 18, 333-&.

21. Lasic, D. D., *Liposomes: From Physics to Applications*. Elsevier: Amsterdam, 1993.

22. Israelachvili, J. N., *Intermolecular and Surface Forces*. Academic Press: New York, 1992.

23. Hoffmann, H., Viscoelastic surfactant solutions. In *Structure and Flow in Surfactant Solutions*, Herb, C. A.; Prud'homme, R. K., Eds. American Chemical Society: Washington, DC, 1994; pp 2-31.

24. Raghavan, S. R.; Kaler, E. W., Highly viscoelastic wormlike micellar solutions formed by cationic surfactants with long unsaturated tails. *Langmuir* **2001,** 17, (2), 300-306.

25. Shchipunov, Y. A.; Shumilina, E. V., Lecithin bridging by hydrogen-bonds in the organogel. *Materials Science & Engineering C-Biomimetic Materials Sensors and Systems* **1995,** 3, (1), 43-50.

26. Willard, D. M.; Riter, R. E.; Levinger, N. E., Dynamics of polar solvation in lecithin/water/cyclohexane reverse micelles. *Journal of the American Chemical Society* **1998,** 120, (17), 4151-4160.

27. Cates, M. E.; Candau, S. J., Statics and dynamics of worm-like surfactant micelles. *Journal of Physics-Condensed Matter* **1990,** 2, (33), 6869-6892.

28. Kaler, E. W.; Murthy, A. K.; Rodriguez, B. E.; Zasadzinski, J. A. N., Spontaneous vesicle formation in aqueous mixtures of single-tailed surfactants. *Science* **1989,** 245, (4924), 1371-1374.

29. Evans, D. F.; Wennerstrom, H., *The Colloidal Domain: Where Physics, Chemistry, Biology, and Technology Meet*. Wiley-VCH: New York, 2001.

30. Kunieda, H.; Nakamura, K.; Evans, D. F., Formation of reversed vesicles. *Journal of the American Chemical Society* **1991,** 113, (3), 1051-1052.

31. Kunieda, H.; Nakamura, K.; Infante, M. R.; Solans, C., Reversed vesicles from biocompatible surfactants. *Advanced Materials* **1992,** 4, (4), 291-293.

32. Boettcher, C.; Schade, B.; Fuhrhop, J. H., Comparative cryo-electron microscopy of noncovalent N-dodecanoyl- (D- and L-) serine assemblies in vitreous toluene and water. *Langmuir* **2001,** 17, (3), 873-877.

33. Mollee, H.; De Vrind, J.; De Vringer, T., Stable reversed vesicles in oil: Characterization studies and encapsulation of model compounds. *Journal of Pharmaceutical Sciences* **2000,** 89, (7), 930-939.

34. Dominguez-Gutierrez, D.; Surtchev, M.; Eiser, E.; Elsevier, C. J., Ru(II)-based metallosurfactant inverted aggregates. *Nano Letters* **2006,** 6, (2), 145-147.

35. Terech, P.; Weiss, R. G., Low molecular mass gelators of organic liquids and the properties of their gels. *Chemical Reviews* **1997,** 97, (8), 3133-3159.

36. Singh, M.; Tan, G.; Agarwal, V.; Fritz, G.; Maskos, K.; Bose, A.; John, V.; McPherson, G., Structural evolution of a two-component organogel. *Langmuir* **2004,** 20, (18), 7392-7398.

37. Waguespack, Y. Y.; Banerjee, S.; Ramannair, P.; Irvin, G. C.; John, V. T.; McPherson, G. L., An organogel formed by the addition of selected dihydroxynaphthalenes to AOT inverse micelles. *Langmuir* **2000,** 16, (7), 3036-3041.

38. Xu, X. D.; Ayyagari, M.; Tata, M.; John, V. T.; McPherson, G. L., Formation of novel organogels by the addition of phenols to AOT micelles in isooctane. *Journal of Physical Chemistry* **1993,** 97, (43), 11350-11353.

39. Carey, M. C.; Small, D. M., Characteristics of mixed micellar solutions with particular reference to bile. *American Journal of Medicine* **1970,** 49, (5), 590-&.

40. Coello, A.; Meijide, F.; Nunez, E. R.; Tato, J. V., Aggregation behavior of bile salts in aqueous solution. *Journal of Pharmaceutical Sciences* **1996,** 85, (1), 9-15.

41. Cohen, D. E.; Thurston, G. M.; Chamberlin, R. A.; Benedek, G. B.; Carey, M. C., Laser light scattering evidence for a common wormlike growth structure of mixed micelles in bile salt- and straight-chain detergent-phosphatidylcholine aqueous systems: Relevance to the micellar structure of bile. *Biochemistry* **1998,** 37, (42), 14798-14814.

42. Hjelm, R. P.; Thiyagarajan, P.; Alkanonyuksel, H., Organization of phosphatidylcholine and bile-salt in rodlike mixed micelles. *Journal of Physical Chemistry* **1992,** 96, (21), 8653-8661.

43. Nichols, J. W.; Ozarowski, J., Sizing of lecithin-bile salt mixed micelles by size-exclusion high-performance liquid-chromatography. *Biochemistry* **1990,** 29, (19), 4600-4606.

44. Macosko, C. W., *Rheology: Principles, Measurements and Applications*. VCH Publishers: New York, 1994.

45. Zemb, T.; Lindner, P., *Neutron, X-Ray and Light Scattering: Introduction to an Investigative Tool for Colloidal and Polymeric Systems*. Elsevier: Amsterdam, 1991.

46. Feigin, L. A.; Svergun, D. I., *Structure Analysis by Small-Angle X-Ray and Neutron Scattering*. Plenum Press: New York, 1987.

47. Pedersen, J. S., Analysis of small-angle scattering data from colloids and polymer solutions: modeling and least-squares fitting. *Advances in Colloid and Interface Science* **1997,** 70, 171-210.

48. Pedersen, J. S.; Schurtenberger, P., Scattering functions of semiflexible polymers with and without excluded volume effects. *Macromolecules* **1996,** 29, (23), 7602-7612.

49. Chen, W. R.; Butler, P. D.; Magid, L. J., Incorporating intermicellar interactions in the fitting of SANS data from cationic wormlike micelles. *Langmuir* **2006,** 22, (15), 6539-6548.

50. Glatter, O.; Kratky, O., *Small-Angle X-Ray Scattering*. Academic Press: New York, 1982.

51. Glatter, O., New method for evaluation of small-angle scattering data. *Journal of Applied Crystallography* **1977,** 10, (OCT1), 415-421.

52. Brown, W., *Dynamic Light Scattering: The Method and some Applications*. Clarendon Press: Oxford, 1993.

53. Kline, S. R., Reduction and analysis of SANS and USANS data using IGOR Pro. *Journal of Applied Crystallography* **2006,** 39, 895-900.

54. De Gennes, P. G., *Scaling Concepts in Polymer Physics*. Cornell University Press: Ithaca, NY, 1979.

55. Israelachvili, J., *Intermolecular and Surface Forces*. Academic Press: San Diego, 1991.

56. Arleth, L.; Bauer, R.; Ogendal, L. H.; Egelhaaf, S. U.; Schurtenberger, P.; Pedersen, J. S., Growth behavior of mixed wormlike micelles: a small-angle scattering study of the lecithin-bile salt system. *Langmuir* **2003,** 19, (10), 4096-4104.

57. Schurtenberger, P.; Mazer, N.; Kanzig, W., Micelle to vesicle transition in aqueous-solutions of bile-salt and lecithin. *Journal of Physical Chemistry* **1985,** 89, (6), 1042-1049.

58. Egelhaaf, S. U.; Schurtenberger, P., Shape transformations in the lecithin bile-salt system - from cylinders to vesicles. *Journal of Physical Chemistry* **1994,** 98, (34), 8560-8573.

59. Berret, J. F.; Appell, J.; Porte, G., Linear rheology of entangled wormlike micelles. *Langmuir* **1993,** 9, (11), 2851-2854.

60. Tung, S. H.; Huang, Y. E.; Raghavan, S. R., A new reverse wormlike micellar system: Mixtures of bile salt and lecithin in organic liquids. *Journal of the American Chemical Society* **2006,** 128, (17), 5751-5756.

61. Kern, F.; Zana, R.; Candau, S. J., Rheological properties of semidilute and concentrated aqueous-solutions of cetyltrimethylammonium chloride in the presence of sodium-salicylate and sodium-chloride. *Langmuir* **1991,** 7, (7), 1344-1351.

62. Fischer, P.; Rehage, H., Rheological master curves of viscoelastic surfactant solutions by varying the solvent viscosity and temperature. *Langmuir* **1997,** 13, (26), 7012-7020.

63. Nucci, N. V.; Vanderkooi, J. M., Temperature dependence of hydrogen bonding and freezing behavior of water in reverse micelles. *Journal of Physical Chemistry B* **2005,** 109, (39), 18301-18309.

64. Sun, L.; Wick, C. D.; Siepmann, J. I.; Schure, M. R., Temperature dependence of hydrogen bonding: An investigation of the retention of primary and secondary alcohols in gas-liquid chromatography. *Journal of Physical Chemistry B* **2005,** 109, (31), 15118-15125.

65. Storm, C.; Pastore, J. J.; MacKintosh, F. C.; Lubensky, T. C.; Janmey, P. A., Nonlinear elasticity in biological gels. *Nature* **2005,** 435, (7039), 191-194.

66. Bhatia, S. R.; Mourchid, A.; Joanicot, M., Block copolymer assembly to control fluid rheology. *Current Opinion in Colloid & Interface Science* **2001,** 6, (5-6), 471-478.

67. Pellens, L.; Corrales, R. G.; Mewis, J., General nonlinear rheological behavior of associative polymers. *Journal of Rheology* **2004,** 48, (2), 379-393.

68. Tirtaatmadja, V.; Tam, K. C.; Jenkins, R. D., Superposition of oscillations on steady shear flow as a technique for investigating the structure of associative polymers. *Macromolecules* **1997,** 30, (5), 1426-1433.

69. Gisler, T.; Ball, R.; Weitz, D. A., Strain hardening of fractal colloidal gels. *Physical Review Letters* **1999,** 82, (5), 1064-1067.

70. Pouzot, M.; Benyahia, L.; Nicolai, T., Dynamic mechanical characterization of the heat-induced formation of fractal globular protein gels. *Journal of Rheology* **2004,** 48, (5), 1123-1134.

71. George, M.; Funkhouser, G. P.; Terech, P.; Weiss, R. G., Organogels with Fe(III) complexes of phosphorus-containing amphiphiles as two-component isothermal gelators. *Langmuir* **2006,** 22, (18), 7885-7893.

72. Onck, P. R.; Koeman, T.; van Dillen, T.; van der Giessen, E., Alternative explanation of stiffening in cross-linked semiflexible networks. *Physical Review Letters* **2005,** 95, (17).

73. Gardel, M. L.; Shin, J. H.; MacKintosh, F. C.; Mahadevan, L.; Matsudaira, P.; Weitz, D. A., Elastic behavior of cross-linked and bundled actin networks. *Science* **2004,** 304, (5675), 1301-1305.

74. Xu, J. Y.; Tseng, Y.; Wirtz, D., Strain hardening of actin filament networks - Regulation by the dynamic cross-linking protein alpha-actinin. *Journal of Biological Chemistry* **2000,** 275, (46), 35886-35892.

75. Tung, S. H.; Huang, Y. E.; Raghavan, S. R., Contrasting effects of temperature on the rheology of normal and reverse wormlike micelles. *Langmuir* **2007,** 23, (2), 372-376.

76. Holtzer, A., Interpretation of the angular distribution of the light scattered by a polydisperse system of rods. *Journal of Polymer Science* **1955,** 17, (85), 432-434.

77. Kirste, R. G.; Oberthur, R. C., *In Small-Angle X-ray Scattering*. Academic Press: London, 1982.

78. Mackintosh, F. C.; Kas, J.; Janmey, P. A., Elasticity of semiflexible biopolymer networks. *Physical Review Letters* **1995,** 75, (24), 4425-4428.

79. Rehage, H.; Hoffmann, H., Shear induced phase-transitions in highly dilute aqueous detergent solutions. *Rheologica Acta* **1982,** 21, (4-5), 561-563.

80. Annable, T.; Buscall, R.; Ettelaie, R.; Whittlestone, D., The rheology of solutions of associating polymers - Comparison of experimental behavior with transient network theory. *Journal of Rheology 4QE,Cheshire,England* **1993,** 37, (4), 695-726.

81. Israelachvili, J. N.; Mitchell, D. J.; Ninham, B. W., Theory of self-assembly of hydrocarbon amphiphiles into micelles and bilayers. *Journal of the Chemical Society-Faraday Transactions II* **1976,** 72, 1525-1568.

82. van Dam, L.; Karlsson, G.; Edwards, K., Direct observation and characterization of DMPC/DHPC aggregates under conditions relevant for biological solution NMR. *Biochimica Et Biophysica Acta-Biomembranes* **2004,** 1664, (2), 241-256.

83. Gabriel, N. E.; Roberts, M. F., Spontaneous formation of stable unilamellar vesicles. *Biochemistry* **1984,** 23, (18), 4011-4015.

84. Akutsu, H.; Seelig, J., Interaction of metal-ions with phosphatidylcholine bilayer-membranes. *Biochemistry* **1981,** 20, (26), 7366-7373.

85. Estroff, L. A.; Hamilton, A. D., Water gelation by small organic molecules. *Chemical Reviews* **2004,** 104, (3), 1201-1217.

86. Kreis, T.; Vale, R., *Cytoskeletal and Motor Proteins*. 2nd ed.; Oxford University Press: 1999.

87. Janmey, P. A.; Hvidt, S.; Peetermans, J.; Lamb, J.; Ferry, J. D.; Stossel, T. P., Viscoelasticity of F-actin and F-actin gelsolin complexes. *Biochemistry* **1988,** 27, (21), 8218-8227.

88. Chaudhuri, O.; Parekh, S. H.; Fletcher, D. A., Reversible stress softening of actin networks. *Nature* **2007,** 445, (7125), 295-298.

89. Buxbaum, R. E.; Dennerll, T.; Weiss, S.; Heidemann, S. R., F-actin and microtubule suspensions as indeterminate fluids. *Science* **1987,** 235, (4795), 1511-1514.

90. Menger, F. M.; Caran, K. L., Anatomy of a gel. Amino acid derivatives that rigidify water at submillimolar concentrations. *Journal of the American Chemical Society* **2000,** 122, (47), 11679-11691.

91. Kotlarchyk, M.; Huang, J. S.; Chen, S. H., Structure of AOT-reversed micelles determined by small-angle neutron-scattering. *Journal of Physical Chemistry* **1985,** 89, (20), 4382-4386.

92. Small, D. M., *The Bile Acids*. Plenum Press: New York, 1971; Vol. 1.

93. Simmons, B. A.; Taylor, C. E.; Landis, F. A.; John, V. T.; McPherson, G. L.; Schwartz, D. K.; Moore, R., Microstructure determination of AOT plus phenol organogels utilizing small-angle X-ray scattering and atomic force microscopy. *Journal of the American Chemical Society* **2001,** 123, (10), 2414-2421.

94. Huang, X.; Terech, P.; Raghavan, S. R.; Weiss, R. G., Kinetics of 5 alpha-cholestan-3 beta,6-yl N-(2-naphthyl)carbamate/n-alkane organogel formation and its influence on the fibrillar networks. *Journal of the American Chemical Society* **2005,** 127, (12), 4336-4344.

95. Onsager, L., The effects of shape on the interaction of colloidal particles. *Annals of the New York Academy of Sciences* **1949,** 51, 627-659.

96. Helfer, E.; Panine, P.; Carlier, M. F.; Davidson, P., The interplay between viscoelastic and thermodynamic properties determines the birefringence of F-actin gels. *Biophysical Journal* **2005,** 89, (1), 543-553.

97. Tata, M.; John, V. T.; Waguespack, Y. Y.; McPherson, G. L., Microstructural characterization of novel phenolic organogels through high-resolution NMR-spectroscopy. *Journal of Physical Chemistry* **1994,** 98, (14), 3809-3817.

98. Kroy, K.; Frey, E., Force-extension relation and plateau modulus for wormlike chains. *Physical Review Letters* **1996,** 77, (2), 306-309.

99. Atkinson, P. J.; Grimson, M. J.; Heenan, R. K.; Howe, A. M.; Robinson, B. H., Structure of microemulsion-based organo-gels. *Journal of the Chemical Society-Chemical Communications* **1989**, (23), 1807-1809.

100. Glatter, O., Interpretation of Real-Space Information from small-angle scattering experiments. *Journal of Applied Crystallography* **1979,** 12, (APR), 166-175.

101. Blow, D. M.; Rich, A., Studies on the formation of helical deoxycholate complexes. *Journal of the American Chemical Society* **1960,** 82, (14), 3566-3571.

102. Rich, A.; Blow, D. M., Formation of a helical steroid complex. *Nature* **1958,** 182, (4633), 423-426.

103. D'Archivio, A. A.; Galantini, L.; Giglio, E.; Jover, A., X-ray and quasi-elastic light-scattering studies of sodium deoxycholate. *Langmuir* **1998,** 14, (17), 4776-4781.

104. Ballestrem, C.; Wehrle-Haller, B.; Imhof, B. A., Actin dynamics in living mammalian cells. *Journal of Cell Science* **1998,** 111, 1649-1658.

105. Wegner, A., Head to tail polymerization of actin. *Journal of Molecular Biology* **1976,** 108, (1), 139-150.

106. Gittes, F.; Mickey, B.; Nettleton, J.; Howard, J., Flexural rigidity of microtubules and actin-filaments measured from thermal fluctuations in shape. *Journal of Cell Biology* **1993,** 120, (4), 923-934.

107. Simons, K.; Ikonen, E., Cell biology - How cells handle cholesterol. *Science* **2000,** 290, (5497), 1721-1726.

108. Zaks, A.; Klibanov, A. M., Enzymatic catalysis in organic media at 100°C. *Science* **1984,** 224, (4654), 1249-1251.

109. Tanaka, T.; Tamba, Y.; Masum, S. M.; Yamashita, Y.; Yamazaki, M., La^{3+} and Gd^{3+} induce shape change of giant unilamellar vesicles of phosphatidylcholine. *Biochimica Et Biophysica Acta-Biomembranes* **2002,** 1564, (1), 173-182.

110. Hagen, A. J.; Hatton, T. A.; Wang, D. I. C., Protein refolding in reversed micelles. *Biotechnology and Bioengineering* **2006,** 95, (2), 285-294.

111. Kim, Y.; Dalhaimer, P.; Christian, D. A.; Discher, D. E., Polymeric worm micelles as nano-carriers for drug delivery. *Nanotechnology* **2005,** 16, (7), S484-S491.